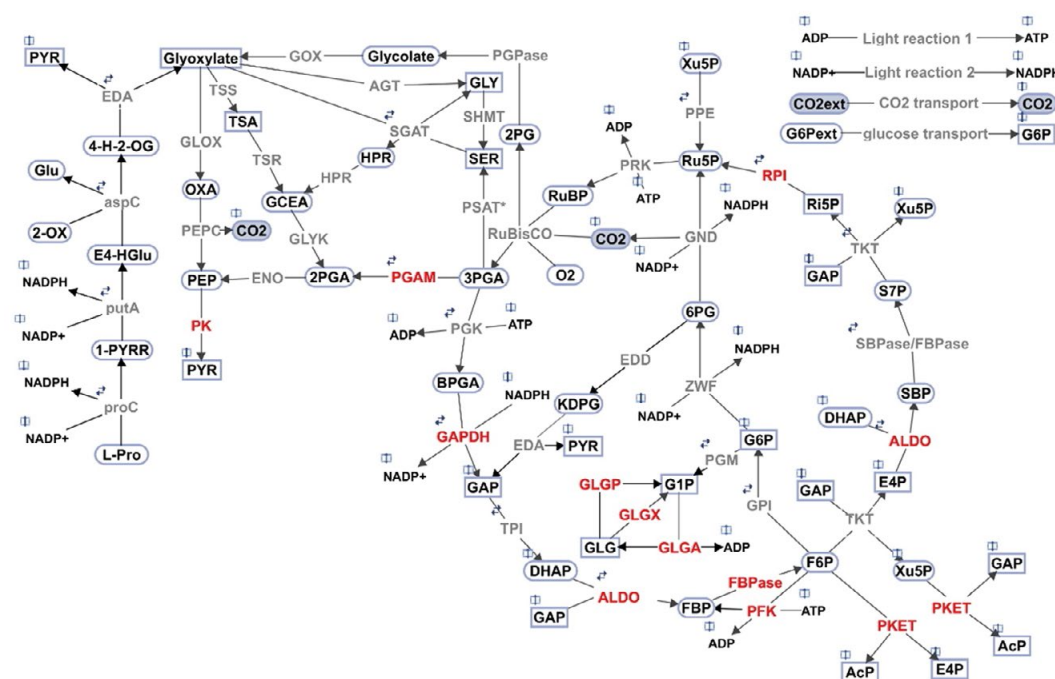


## Role of isoenzymes in metabolic regulation of cyanobacteria

### Úloha izoenzymů v regulaci metabolismu sinic



Doctoral thesis by  
Anushree Bachhar





Fakulta rybnářství  
a ochrany vod  
Faculty of Fisheries  
and Protection  
of Waters

Jihočeská univerzita  
v Českých Budějovicích  
University of South Bohemia  
in České Budějovice

# **Role of isoenzymes in metabolic regulation of cyanobacteria**

**Úloha izoenzymů v regulaci metabolismu sinic**

*Doctoral thesis by  
Anushree Bachhar*

*I, Anushree Bachhar, hereby declare that I wrote the Ph.D. thesis using results of my own research with the help of other publication resources which are properly cited.*

*I hereby declare that, in accordance with § 47b Act No. 111/1998 Coll., as amended, I agree with publicizing of my Ph.D. thesis in full version electronically in a publicly accessible part of the STAG database operated by the University of South Bohemia in České Budějovice on its web sites, with keeping my copyright to the submitted text of this Ph.D. thesis. I also agree so that the same electronic way, in accordance with above mentioned provision of the Act No. 111/1998 Coll., was used for publicizing reviews of supervisor and reviewers of the thesis as well as record about the progress and result of the thesis defence. I also agree with comparing the text of my Ph.D. thesis with a database of theses "Theses.cz" operated by National Register of university theses and system for detecting of plagiarism.*

*In Nové Hradky 25<sup>th</sup> January, 2023*

**Supervisor:**

Jiří Jablonský, Ph.D.  
University of South Bohemia in České Budějovice (USB)  
Faculty of Fisheries and Protection of Waters (FFPW)  
Institute of Complex Systems  
Zámek 136, 373 33 Nové Hradky, Czech Republic

**Head of Laboratory of Experimental Complex Systems:**

Prof. Dalibor Štys

**Dean of Faculty of Fisheries and Protection of Waters:**

Prof. Pavel Kozák

**Board of doctorate study defence with reviewers:**

Prof. Lukáš Kalous – head of the board  
Prof. Luděk Bláha – board member  
Assoc. Prof. Pavel Horký – board member  
Assoc. Prof. Hana Kocour Kroupová – board member  
Assoc. Prof. Vladimír Žlábek – board member  
Assoc. Prof. Zdeněk Adámek – board member

Prof. Dr. Martin Hagemann, University of Rostock, Germany – thesis reviewer  
Prof. Dušan Lazár, Palacký University, Olomouc, Czech Republic – thesis reviewer

**Date, hour, and place of Ph.D. defense:**

31. 3. 2023, 9 a.m., in USB, FFPW, RIFCH, Vodňany, Czech Republic

**Name:**

Anushree Bachhar

**Title of thesis:**

Role of isoenzymes in metabolic regulation of cyanobacteria  
Uloha izoenzymů v regulaci metabolismu sinic

**Doctoral study program:**

Protection of Aquatic Ecosystems, full-time

---

*Anushree Bachhar, 2023. Role of isoenzymes in metabolic regulation of cyanobacteria Doctoral thesis. University of South Bohemia in Ceske Budejovice, Faculty of Fisheries and Protection of Waters, Czech Republic, 71 pp.*

*ISBN 978-80-7514-183-5*

*Graphic design & technical realisation: JENA Šumperk, [www.jenasumperk.cz](http://www.jenasumperk.cz)*

## CONTENT

### CHAPTER 1

7

General introduction

### CHAPTER 2

27

A new insight into role of phosphoketolase pathway in *Synechocystis* sp. PCC 6803

### CHAPTER 3

39

Entner-Doudoroff pathway in *Synechocystis* PCC 6803: Proposed regulatory roles and enzyme multifunctionalities

### CHAPTER 4

53

General discussion

55

English summary

66

Czech summary

67

Acknowledgements

68

List of publications

69

Training and supervision plan during the study

70

*Curriculum vitae*

71

## **CHAPTER 1**

---

### **GENERAL INTRODUCTION**

---





## General introduction

### 1.1. A brief introduction to cyanobacteria

Cyanobacteria are unicellular photosynthetic prokaryotes that live in terrestrial as well as aquatic ecosystems (De los Ríos et al., 2007). As they live in diverse ecosystems, cyanobacteria have specialised growth habit and metabolism specific to ecosystems for survival. Though all cyanobacteria are photoautotrophs, some of them are found to be mixotrophic as well as facultatively heterotrophic in nature (Droop, 1974), but most of them are obligatory photoautotrophs. Heterotrophy enables cyanobacteria to use organic sources of carbon in dark phases through the oxidative pentose phosphate (OPP) pathway, glycolysis and tricarboxylic acid (TCA) cycle (Subashchandrabose et al., 2013). Mixotrophy gives cyanobacteria an advantage under limited light and changing carbon conditions (Stoecker et al., 2006) as it consists of both photoautotrophic and heterotrophic mechanisms (Heidorn et al., 2011), whereas light heterotrophy is a growth condition in which cyanobacterial culture is maintained with pulsed light (up to 5 minutes exposure to light) with glucose and further maintained in darkness (Tabei et al., 2009).

The circadian clock controls the simultaneous shift in gene expression in response to light and dark photosynthetic phases of cyanobacteria. Also, the biorhythm enables them to change growth styles under light and dark phases (Dong and Golden, 2008). As one of the most utilised green producers and model organism, cyanobacterium *Synechocystis* PCC 6803 is used as a host organism to synthesise a various number of products, e.g., mass production of ethanol (Yoshikawa et al., 2017) or (E)- $\alpha$ -bisabolene (Rodrigues and Lindberg, 2020).

### 1.2. Isoenzymes

Isoenzymes (isozymes) are variants of the enzyme with different amino acid structures but catalysing the same reaction. Hunter and Markert (1957) first proposed the term isoenzyme/isozyme to describe “the different molecular forms in which proteins may exist with the same enzymatic specificity”. Though they have the same substrate(s) and product(s), they have different kinetic properties. Isoenzymes are found in both in eukaryotic and prokaryotic organisms. An example of well-studied isozyme is phosphofructokinase (PFK), found in *E. coli* (PFK A and PFK B), and humans (organ specific PFK L, PFK M).

Isozymes differ in primary structure because they are encoded by different genes, either allelic or non-allelic. The primary structure could also be modified by different reactive groups or amino acid residues (Scandalios, 1969). Furthermore, the occurrence of isoenzymes in a species happens due to mutation in a gene – point mutations in genes create two or more copies of genes, post-translational modification (PTM), natural selection of multiple variants of the same enzyme, also they can be expressed in specific stage/phase of life (Huang, 2009).

Many isozymes originally active in prokaryotes are silenced in eukaryotic organisms as redundancies (Ononye et al., 2014). However, some of these redundancies are reactivated by cancer cells to satisfy the increased metabolic demand of cancer cells, and thus these isozymes may be targeted with new therapeutic strategies (Ononye et al., 2014). Isozymes are also commonly observed in cyanobacteria (Beck et al., 2012). However, many of them have been annotated based on in silico mRNA to protein translation and BLAST, some were shown to have different functions rather than the predicted one (Jablonsky et al., 2013) while the function of others, e.g., ribose phosphate isomerase B, are yet to be specified. Metabolic requirements for each organ or tissue are different therefore the requirement of tissue-specific variants of isoenzymes are understandable. However, for a prokaryotic cell

without having any membrane-bound organelles, requirements of several set of isoenzymes (e.g., PGM in *Synechocystis* PCC 6803; Table 1.1.) is rather interesting to study. In the following section, I have discussed more about different types of isoenzymes found in central carbon metabolism of *Synechocystis* PCC 6803.

### 1.3. Isoenzymes in carbon metabolism of cyanobacteria

Throughout the central carbon (Calvin-Benson-Bassham cycle, glycolysis and TCA cycle) metabolism of *Synechocystis* PCC 6803 (*Synechocystis*), a number of isoenzymes are distributed (Beck et al., 2012) in the metabolic network of cyanobacterium (Table 1.1.). It is a point to be noted that *Synechocystis* is one of those cyanobacteria that have highest number of isoenzymes coding genes in their genome. Though the whole genome sequencing and annotation for *Synechocystis* were done in 1996 (Kaneko et al., 1996), there is much confusion regarding the annotation of isoenzymes as many of the predicted proteins found to have similarities in amino acid sequences with enzymes from other species. Also, it is still not sure if a particular enzyme is having one or more than one copies of gene under specific cases with minor variations (point mutations). It is also unknown for some cases why isoenzymes are needed for a specific reaction, for instance, ribose phosphate isomerase (RPI) is in a position of the Calvin-Benson-Bassham cycle (Calvin cycle) which does not cross with other pathways and thus, the need for a second RPI is unclear. Finally, the question is about the function of these isoenzymes, do isoenzymes protect against the accumulation of toxic metabolites such as sugar phosphates (e.g., fructose-6-phosphate, dihydroxyacetone phosphate) through the system, or is it because of their survival in harsh environmental changes?

**Table 1.1.** Isoenzymes in central carbon metabolism of *Synechocystis* PCC 6803. List contains isoenzymes that are experimentally verified as well as predicted (putative). Data source: Uniprot.

| Name  | Isoenzyme         | Gene id         |
|---|-------------------|-----------------|
| Ribose phosphate isomerase                                | RPI A             | <i>slr 0194</i> |
|   | RPI B             | <i>ssl 2153</i> |
| Fructosebisphosphate aldolase                             | Class I FBA       | <i>slr 0943</i> |
|   | Class II FBA      | <i>sll 0018</i> |
| Fructose bisphosphatase/ sedoheptulose 1,7 bisphosphatase | Class I FB Pase   | <i>slr 0952</i> |
|   | Class II FB Pase  | <i>slr 2094</i> |
| Phosphofructokinase                                       | PFK A1            | <i>sll 1196</i> |
|   | PFK A2            | <i>sll 0745</i> |
| Glyceraldehyde-3-phosphate dehydrogenase                  | GAPDH 1           | <i>slr 0884</i> |
|   | GAPDH 2           | <i>Sll 1342</i> |
| Phosphoketolase   | PKET 1            | <i>slr 0453</i> |
|   | PKET 2 (putative) | <i>sll0529</i>  |
| Phosphoglycerate mutase                                   | PGAM A            | <i>slr 1945</i> |
|   | PGAM B            | <i>slr 1124</i> |
|   | PGAM 3 (putative) | <i>sll 0395</i> |
| Pyruvate kinase   | PK 1              | <i>Sll 0587</i> |
|   | PK 2              | <i>sll 1275</i> |
| Phosphoglucomutase  | PGM 1             | <i>sll0726</i>  |
|   | PGM 2 (putative)  | <i>slr 1334</i> |

|                             |                   |                 |
|-----------------------------|-------------------|-----------------|
| Glycogen synthase           | GLGA 1            | <i>slI 0945</i> |
|                             | GLGA 2 (putative) | <i>slI 1393</i> |
| Glycogen debranching enzyme | GLGX 1            | <i>slr 0237</i> |
|                             | GLGX 2            | <i>slr1857</i>  |
| Glycogen phosphorylase      | GLGP 1            | <i>slr 1356</i> |
|                             | GLGP 2            | <i>slr 1367</i> |

### 1.3.1. Ribose phosphate isomerase

---

#### ribose-5-phosphate ↔ ribulose-5-phosphate

Ribose phosphate isomerase catalyses the interconversion of ribose-5-phosphate to ribulose-5-phosphate within the Calvin cycle and pentose phosphate pathway. Beck et al. (2012) mentioned the presence of 2 isoenzymes, RPI A (*slr 0194*) and RPI B (*ssl 2153*). RPI A is annotated and reviewed (Uniprot), whereas RPI B is unreviewed. The sequences are showing only 37% similarity with each other, and the BLAST result indicates that RPI A is more similar to cyanobacterial RPI whereas RPI B is showing more similarity to bacterial RPI sugar phosphate isomerase (RPI B/LacA/LacB family) with the exception of *Gleobacter* genus (Figure 1.1.). Looking at the position of the enzyme in the metabolic network of *Synechocystis* (Figure 1.2.), the need for an isoenzyme for any specific scenario is still unclear.

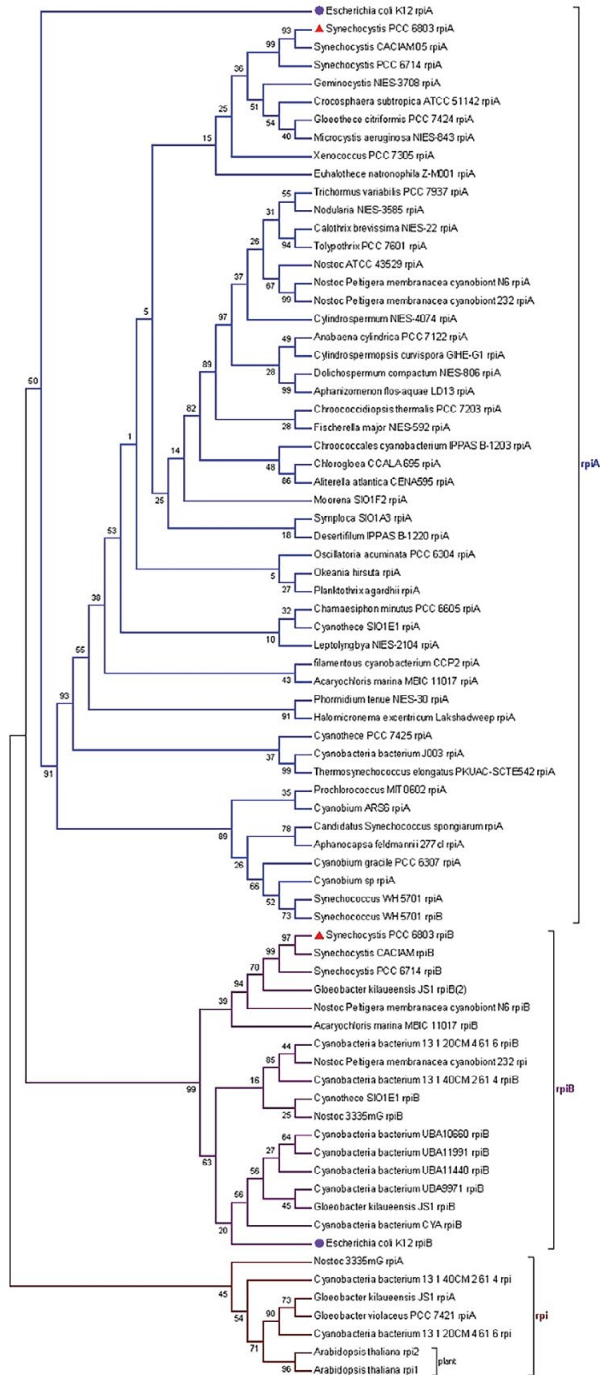


**Figure 1.1.** Phylogenetic analysis of RPI isoenzymes. From different species in reference to *Synechocystis* PCC 6803 (red triangle). The blue branch denotes rpi A whereas dark purple branch denotes rpi B, similar to bacterial rpi B. Brown branch denotes rpi from cyanobacteria which have clustered with plant *Arabidopsis* rpi 1 and 2. rpi A and B from *E. coli* is highlighted with a purple dot. The author of analysis is me.

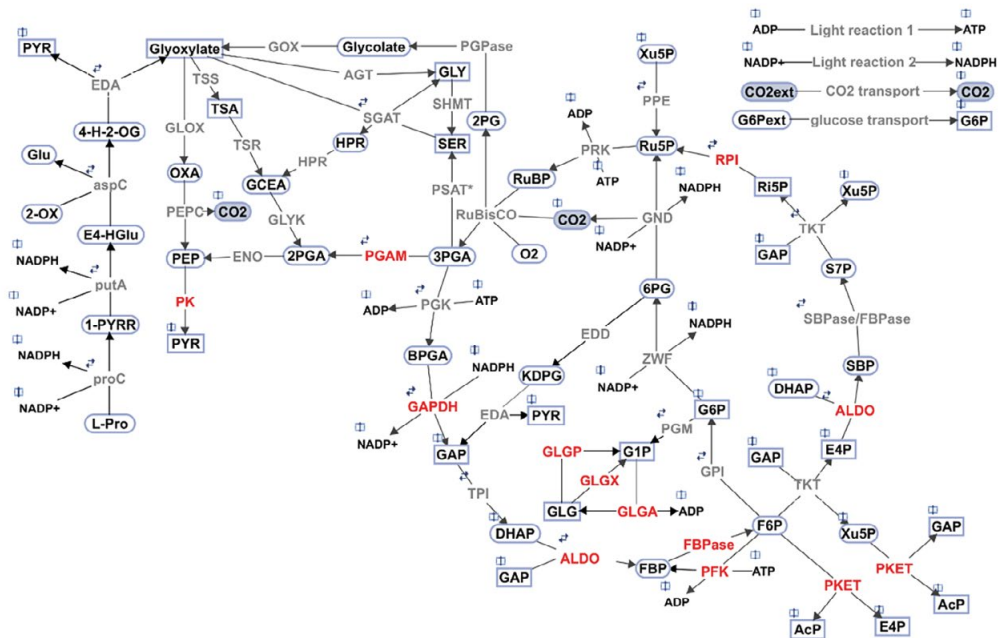
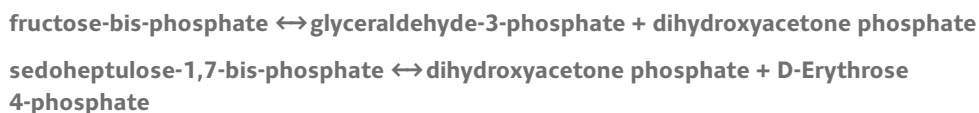


**Figure 1.2.** Schematic representation of the central carbon metabolism network of *Synechocystis* sp. PCC 6803. Red indicates the isozymes. The scheme includes the Calvin-Benson-Bassham cycle, photorespiratory pathways, phosphoketolase pathway, glycolysis, the oxidative pentose pathway, Entner-Doudoroff pathway, and sink reactions (representing the adjacent pathway and the calculation of biomass production, indicated by metabolites in rectangular shapes). The reversibility of a particular reaction is indicated by two small arrows. Grey indicates the involved enzymes: RuBisCO ribulose-1,5-bisphosphate carboxylase oxygenase, PGK phosphoglycerate kinase, GAP glyceraldehyde-3-phosphate dehydrogenase, TPI triose-phosphate isomerase, ALDO aldolase, FBPase fructose-1,6 bisphosphatase, PFK phosphofructokinase, TKT transketolase, SBPase sedoheptulose-1,7 bisphosphatase, RPI phosphopentose isomerase, PPE phosphopentose epimerase, PRK phosphoribulokinase, GPI glucose-6-phosphate isomerase, G6PD glucose-6-phosphate dehydrogenase, PGD phosphogluconate dehydrogenase, PGase phosphoglycolate phosphatase, PKET phosphoketolase, GOX glycolate oxidase, SGAT serineglyoxylate transaminase, HPR hydroxypyruvate reductase, GLYK glycerate kinase, AGT alanineglyoxylate transaminase, TSS tartronatesemialdehyde synthase, TSR tartronatesemialdehyde reductase, SHMT serine hydroxymethyltransferase, GLOX glyoxylate oxidase, PSAT\* phosphoserine transaminase, PPC - phosphoenolpyruvate carboxylase, PGAM phosphoglycerate mutase, ENO enolase, PK - pyruvate kinase, GND 6-phosphogluconate dehydrogenase, ZWF glucose-6-phosphate dehydrogenase, GLGA - glycogen synthase, GLGX - glycogen debranching enzyme, GLGP - glycogen phosphorylase, EDD 6P-gluconate dehydratase, EDA 2-keto-3-deoxygluconate-6- phosphate aldolase, aspC L-erythro-4-hydroxyglutamate:2-oxoglutarate aminotransferase (activity of aspartate aminotransferase), putA delta-1-pyrroline-5-carboxylate dehydrogenase, proC pyrroline-5-carboxylate reductase. Names of metabolites in the suggested (red) pathway: 4-H-2-OG 4-hydroxy-2-oxoglutarate, E4-HGlu L-erythro-4-hydroxyglutamate, 1-PYRR L-1-pyrroline-5-carboxylate. Open book symbol indicates involvement of metabolite in other reaction(s). The scheme was created in SimBiology toolbox of MATLAB 2021b (The MathWorks, Inc., Natick, Massachusetts, United States of America), <http://www.mathworks.com>.

### 1.3.2. Fructose bisphosphate aldolase



FBA catalyses 2 reversible reactions in the central carbon metabolism of *Synechocystis*, conversion of sedoheptulose-1,7-bisphosphate (SBP) to dihydroxyacetone phosphate (DHAP) and erythrose-4-phosphate (E4P) in Calvin cycle and conversion of fructose bisphosphate (FBP) to GAP and DHAP in glycolysis and Calvin cycle (Nakahara et al., 2003). Based on their reaction mechanism, the enzyme FBA is divided into two classes (Rutter, 1964). Of two types of aldolases, class I is mainly found in animals, plants and green algae, whereas the class II is primarily present in fungi. Both classes can be found in eukaryotes and bacteria (Siebers et al., 2001; Patron et al., 2004). The two classes of FBAs share non-homologous amino acid sequences; hence it can be assumed that the two classes have originated and evolved separately. *Synechocystis* has both classes of FBA, but most of the other strains of cyanobacteria have only class II of FBA present (Nakahara et al., 2003).

In case of *Synechocystis*, the class I FBA (slr 0943) does not require any divalent ion for its activity and forms Schiff base with its substrates whereas Class II FBA (sll 0018) is dependent on divalent ion as well as it can be inhibited by 1m Mol · liter<sup>-1</sup> EDTA (ethylenediaminetetraacetic acid). Though there are 2 FBAs present in *Synechocystis*, it is unknown which isoenzyme has more activity *in vivo* under autotrophic and mixotrophic conditions. While in *in vitro* condition, 90% of the FBA activity is contributed by the class II of FBA (FBA 2). It is already discussed by Tabei et al. (2007), that both FBAs are expressed in autotrophic conditions but can be completely suppressed under prolonged dark conditions. However, occasional light pulses and glucose supplementation can activate FBA 2 (Tabei et al., 2009, 2012). In contrast, FBA 1 can be suppressed by light pulses (Tabei et al., 2009), these findings suggest that FBA 2 has the key role in light induced heterotrophy in *Synechocystis* and belongs to the glycolytic gene set controlled by regulator sll 1330 (Okada et al., 2015). Though in some other species of cyanobacteria, e.g., *Halotheca* sp. PCC 7418, it is found that the class I FBA (FBA 1) is beneficial in protection against salt stress (Patipong et al., 2019). It is one of the most studied enzymes in cyanobacteria.

Bioinformatic analysis of the types of FBA revealed that FBA 1 of *Synechocystis* have more similarity to bacterial FBAs rather than cyanobacterial FBA whereas FBA 2 is 90–60% similar (homologous) in almost all species of cyanobacteria. This finding suggests that *Synechocystis* might have acquired the FBA 1 through horizontal gene transfer from some non-sister group of bacteria. Through BLAST and phylogenetic analysis (Fig. 1.3.), it was found that the FBA 1 from *Synechocystis* showed maximum similarity with the bacterial FBA from a marine bacteria *Blastopirellula marina* (Schlesner et al., 2004) and *Blastopirellula cremea*, first isolated from south coast of Korea (Lee et al., 2013), both species grow in salty environment.

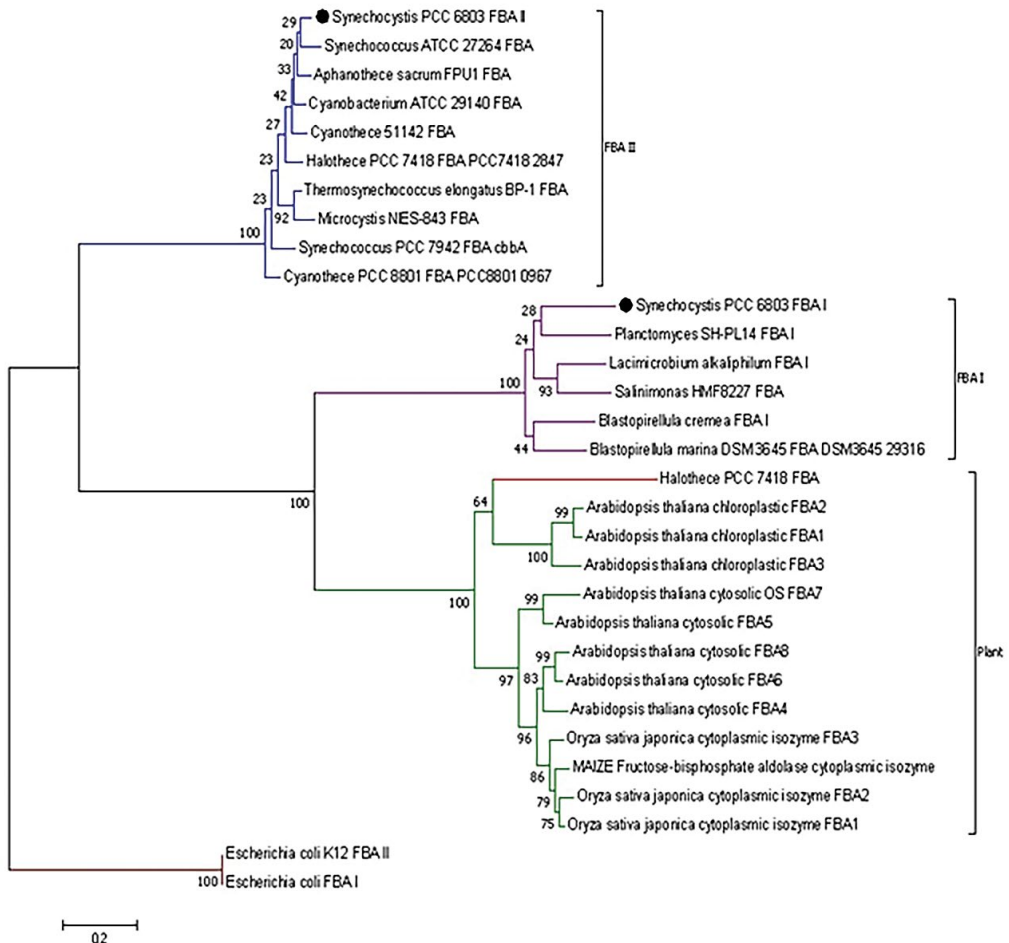


**Figure 1.3.** Phylogenetic analysis of FBA from different species in reference to *Synechocystis* PCC 6803 (black dot). The blue branch of FBA consists of FBA class 2 (FBA II) originated in cyanobacteria, whereas, the purple branch, FBA class 1 (FBA I), originated in bacteria. The green sub cluster of FBAs originated from Plants. Class 1 FBA from *Halotheca* 7418 (red line) clustered with plant-originated FBAs. Brown branch *E. coli* (Bacteria). The author of analysis is me.

### 1.3.3. Fructose biphosphatase

fructose-1,6- biphosphate → fructose-6-phosphate

sedoheptulose 1,7-biphosphate → sedoheptulose 7-phosphate (class II FB Pase)

FBPase converts Fructose-1,6- biphosphate (FBP) into the Fructose-6-phosphate (F6P). This enzyme has two distinct classes Class I FBPase (*slr 0952*) is substrate specific, whereas class II FBPase (*slr 2094*) have two substrates: FBP and sedoheptulose 1,7-biphosphate (SBP), see the second reaction above. From the analysis of primary amino acid sequences of class I and class II FBPases, it was found that these two isoenzymes share ~ 21% similarity (EMBOSS Matcher). The transcriptomic properties also vary significantly, FBPase class I is upregulated under autotrophic and light heterotrophic conditions compared to mixotrophic

conditions whereas for the gene of FBPase class II significant upregulation is found under mixotrophic condition compared to the other two growth conditions (Yoshikawa et al., 2013). The biochemical characterization of the class II FBPase is yet to be performed with both of its substrates in case of *Synechocystis*.

#### 1.3.4. Phosphofructokinase

##### fructose-6-phosphate +ATP → fructose-1,6- bisphosphate + ADP

PFK is one of the most important enzymes in glycolysis and probably the one with the highest number of isoenzymes identified across the species. In eukaryotes, it can be tissue-specific, has a major role in cancer metabolism as the cleaved PFK M found in human cancer cell facilitates the hyperactive glycolysis, enabling faster growth (Andrejc et al., 2017). Also, PFK B3 of human have multiple oncogenes like exon codes due to alternate splicing (PTM) they get activated (Shi et al., 2017).

In the case of *Synechocystis*, it has two annotated isoenzymes, PFK A1 (*sll 1196*) and PFK A2 (*sll 0745*), both are ATP dependent, similarity as PFK B of *E. coli* (Parducci et al., 2006). The expression of PFK A2 is induced by glucose in the dark while slightly suppressed by light (Tabei et al., 2007). In contrast to PFK A2, PFK A1 is not expressed in the dark (Tabei et al., 2007), and it belongs to light-glucose dependent set of glycolytic isozymes (FBA A, PFK A1, glucokinase, phosphoglycerate mutase and pyruvate kinase (Tabei et al., 2007)). These light-dependent isozymes are regulated by regulator gene *sll1330* (Marin et al., 2004; Wang et al., 2004; Tabei et al., 2007, and Okada et al., 2015), which is controlled by histidine kinases 8 (HIK 8), activated in the presence of glucose and light (light-induced heterotrophy) (Singh and Sherman, 2005) and high concentration CO<sub>2</sub> (Wang et al., 2004). The light-induced heterotrophy regime is based on light pulses insufficient to activate the photoautotrophy (Anderson and McIntosh, 1991).

Although there are two PFKs in *Synechocystis*, that is not the case for majority of cyanobacteria having only one PFK. With the aid of current bioinformatic tools (BLAST, MSA), I searched for the possible distribution of these 2 PFKs among the cyanobacterial species. Phylogenetic analysis (Fig. 1.4.) with retrieved amino acid sequences of PFK from various species/strains of cyanobacteria (sources: Cyanobase, GenBank, Uniprot) revealed the distributed in three sub-clusters under same branch of constructed tree. Clusters PFK A1 and PFK A2 and the third sub-cluster (named as PFK A 3) consist of PFKs from several strains of cyanobacteria (Fig. 1.4). PFKs from the cyanobacterial strains currently annotated as PFK A1 (Uniprot) came under same sub-cluster PFK B1 (Fig. 1.4.). Further, the 2nd cluster is further divided in 2 sub-clusters (PFK B2 and PFK B3). Sub-cluster PFK B3 is having PFKs annotated as PFK A2 as well as other PFKs generally annotated as 'PFK's in cyanobacteria. Most of the PFKs of sub-cluster PFK B3, e.g., *Synechococcus* PCC 7942, *Synechococcus* PCC 6301 and *Leptolyngbya* NIES 2135, were showing identity coverage between 40 to 50% with both PFKs.



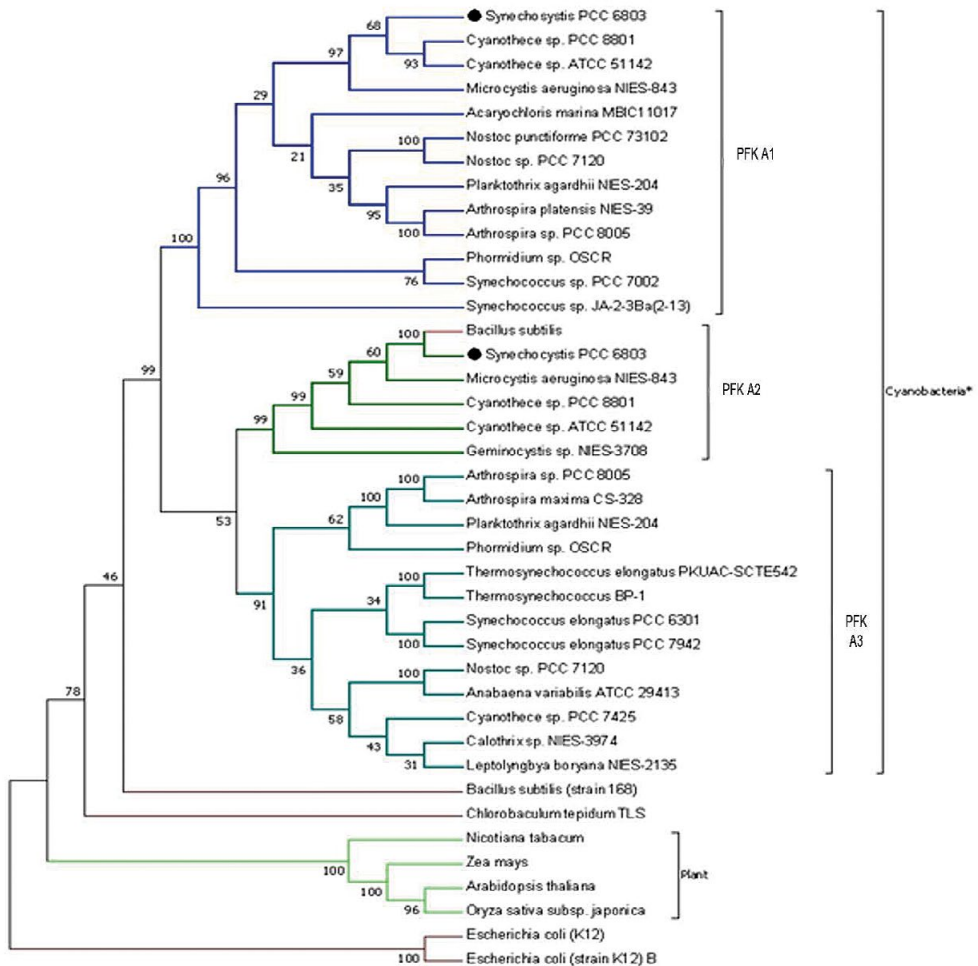


**Figure 1.4.** Phylogenetic analysis of phosphofructokinase from cyanobacteria and other reference model species (plants and bacteria) Blue branch – PFKs with similarity to the PFK A1 from our reference species *Synechocystis* (black dot). Dark green branch is similar to PFK A2 also highlighted as PFK A2. Turquoise coloured branch – PFK A3. Light green cluster consists of plants. Bacterial strains were highlighted with brown branches. The author of analysis is me.

### 1.3.5. Glyceraldehyde-3-phosphate dehydrogenase

#### glyceraldehyde 3-phosphate $\leftrightarrow$ D-glycerate 1,3-bisphosphate

Glyceraldehyde-3-phosphate dehydrogenase (GAPDH) is one of those enzymes which can be found in multiple metabolic pathways: Calvin cycle, glycolysis and gluconeogenesis (Koksharova et al., 1998). It catalyzes a reversible reaction, conversion of D-glycerate-1,3-bisphosphate (BPG) to glyceraldehyde-3-phosphate (GAP) and vice versa. Cyanobacterial species have number of GAPDH isoenzymes present it differs from species to species. It is found from the work of Beck et al. (2012) that several cyanobacterial species have 3 GAPDH isoenzymes, for instance, *Synechococcus* 7942, *Nostoc* 7120 and *Anabaena variabilis* (Martin et al., 1993), but most of them have two GAPDH isoenzymes.

*Synechocystis* encodes two GAPDH isoenzymes, GAPDH 2 (*sll 1342*) operates in all 3 above mentioned metabolic pathways of cyanobacteria whereas GAPDH 1 (*slr 0884*) is glycolysis specific. Results of experiments done by Gao et al. (2014) showed that GAPDH 2 expression is rapidly induced by light and photosynthesis, but GAPDH 1 is weakly expressed in the presence of light. Whereas in dark and low CO<sub>2</sub> condition both GAPDHs expression was lost but addition of glucose can partially recover GAPDH 2 and GAPDH 1. Addition of photosynthetic electron flow inhibitors can completely block the expression of GAPDH 2 but in case of GAPDH 1 it can happen only in the absence of glucose. Furthermore GAPDH 1 belongs to the cascade of glycolytic genes controlled by HIK 8 and *sll 1330* genes (Okada et al., 2015).

### 1.3.6. Phosphoketolase

---

**D-xylulose 5-phosphate + phosphate ↔ acetyl phosphate + D-glyceraldehyde 3-phosphate**

**D-fructose 6-phosphate + phosphate ↔ acetyl phosphate + D-erythrose 4-phosphate**

PKET catalyzes two reversible reactions, the conversion of fructose-6-phosphate in erythrose-4-phosphate and acetyl phosphate, xylulose-5-phosphate to GAP and acetyl phosphate (Jablonsky et al., 2016). In genomic and enzyme databases there is only one gene annotated as phosphoketolase (*slr 0453*), however, another predicted protein (*sll 0529*) gives similarity to phosphoketolases of other cyanobacteria, with identity match of 75% (BLAST). Though the function of this gene is still unknown, experiments done by Xiong et al. (2015) implied an important role in dark heterotrophy of cyanobacteria. Further, our own modelling work provide a support for the existence and functions of secondary PKET in *Synechocystis* (Bachhar and Jablonsky, 2020). Also, in absence of PKET 1 (*slr 0453*), the acetyl production gets disrupted, neither glucose nor xylulose supplementation can revive the acetyl phosphate production (Xiong et al., 2015).

### 1.3.7. Phosphoglycerate mutase

---

**3-phosphoglycerate ↔ 2,3-bisphosphoglycerate ↔ 2-phosphoglycerate**

PGAM is an enzyme with a major role in maintaining the carbon metabolism in cyanobacteria as it regulates the carbon flow towards TCA cycle from lower glycolysis, Calvin cycle, as well as from OPP pathway. Jablonsky et al. (2013) had analysed the four annotated PGAMs in *Synechococcus* PCC 7942, out of which only three were suggested to be beneficial for central carbon metabolism functions. PGAM 4 was predicted as phosphoserine phosphatase (PSP), providing an additional source for serine synthesis (Klemke et al., 2015). *Synechocystis* contains 2 annotated PGAMs (Okada et al., 2015), PGAM A (*slr 1945*) and PGAM B (*slr 1124*). Another gene annotated as hypothetical protein, *sll 0395*, has shown similarity with PGAMs from other cyanobacterial species such as *Microcystis aeruginosa* NIES-843 or *Cyanothece* sp. PCC 7822 with around 74% identity. To note, both mentioned *Microcystis aeruginosa* NIES 843, *Cyanothece* sp. PCC 7822 as well as *Synechocystis* belong to the category of cyanobacteria with higher count of isoenzyme within central carbon metabolism (Beck et al., 2012). They are mixotrophic and facultatively heterotrophic in nature. Thus, based on the similarities with other cyanobacteria, we might speculate that this so far unverified protein might be another PGAMs. Finally, out of two annotated PGAMs, PGAM A (*slr 1945*) belongs to the cascade of gene controlled by HIK 8 where as PGAM B is not dependent on HIK 8 but glucose can affect

the gene expression slightly (slightly upregulated) (Okada et al., 2015). PGAM A is essential for the survival of *Synechocystis* as it pushes 3-phosphoglycerate (PG) (organic carbon) produced by the activity of Rubisco towards glycolysis or Calvin cycle in form of 2,3- diphosphoglycerate, which further converts into GAP. The excess amount of GAP is used in gluconeogenesis which in turn feeds all the other glycolytic pathways (Orthwein et al., 2021).

### 1.3.8. Pyruvate kinase

---

#### phosphoenolpyruvate + ADP → pyruvate + ATP

PK catalyzes the non-reversible conversion of phosphoenolpyruvate to pyruvate. In *Synechocystis*, two PKs are annotated, PK 1 (*sll 0587*) and PK 2 (*sll 1275*). Knowels and Plaxton (2003) had discussed about both PKs activity together increased to 200–300% in heterotrophic condition compared to the photoautotrophic condition. PK 2 is controlled by HIK 8, whereas PK1 is not known to be co-regulated. Individual activity of PKs are still unknown as well as if the two PKs are essential for the survival of *Synechocystis* or if it can survive with only one PK like other obligatory photoautotrophic cyanobacteria.

### 1.3.9. Phosphoglucomutase

---

#### D-glucose 1-phosphate ↔ D-glucose 6-phosphate

Phosphoglucomutase (PGM) catalyzes the interconversion of glucose-1-phosphate to glucose-6-phosphate. To date, there are two known isoenzymes found for this reaction in *Synechocystis*: PGM 1 (*sll 0726*) and PGM 2 (*slr 1334*) (Doello et al., 2022). PGM 1 is well conserved in other organisms, whereas PGM 2 is a putative isoenzyme that belongs to phosphohexomutase family and shares around 50% amino acid sequence conservation with other cyanobacterial phosphoglucomutases.

### 1.3.10. Glycogen synthase

---

#### Glucose 1-phosphate → ADP + glycogen

Glycogen synthases (GLGA) have two known isoforms GLGA 1 (*sll 0945*) and GLGA 2 (*sll 1393*; probable). GLGA is known to be essential as multiple copy numbers for each isoenzyme are encoded in the *Synechocystis* genome and a complete double mutant of these pair of isoenzymes could never be achieved (Yoo et al., 2014). The experiments performed by Yoo et al. (2014) also suggested that in cases of GLGA single mutants, the activities of the remaining isoenzyme were increased to cover for the deleted isoenzyme, as well as the activity of GLGA 2 showed a comparative increase in activity in cases of GLGA 1 mutants compared the other way around.

### 1.3.11. Glycogen debranching enzyme

---

#### Glycogen + orthophosphate → glucose 1-phosphate

The Glycogen debranching enzyme (GLGX) is a part of glycogen metabolism (Fig. 1.2.) which converts glycogen back to glucose-1-phosphate (Romeo et al., 1988). The isoenzymes involved in this reaction are GLGX 1 (*slr 0237*) and GLGX 2 (*slr 1857*) (Neumann et al., 2022). The full extent of molecular functions is yet to be deciphered for this pair of enzymes.

### 1.3.12. Glycogen phosphorylase

#### Glycogen + orthophosphate → glucose 1-phosphate

Glycogen Phosphorylases (GLGP) takes part in glycogen degradation. The GLGP isoenzymes acts under different stress conditions. GLGP 1 (*slr 1356*) is actively involved in glycogen metabolism under high temperature conditions, whereas GLGP 2 (*slr 1367*) is mostly active under dark conditions and rejuvenation from chlorosis (Neumann et al., 2022).

### 1.4. Multifunctional enzymes

After a thorough analysis the enzymes, isoenzymes and their substrates in the central carbon metabolism of *Synechocystis*, it is clear that more than one enzymes or isoenzymes are capable of metabolizing different substrates, e.g., FBA, FB Pase and PKETs. On the other hand, many enzymes have regulatory roles and additional functions (Bachhar and Jablonsky, 2022). A simple study of fructose phosphate and its associated enzymes revealed that there are ten different enzymes capable of metabolising fructose as a primary or secondary substrate in *Synechocystis*. The robustness of fructose metabolism in *Synechocystis* (Fig. 1.5.) could be either due to the potential of fructose-mediated toxicity in *Synechocystis* (Ungerer et al., 2008) or to enable rapid growth under the ever-changing aquatic environment. However, it can be assumed that isoenzymes and multifunctional enzymes are key tools of *Synechocystis* that helps it to become one of the most efficient biomass producers in nature.

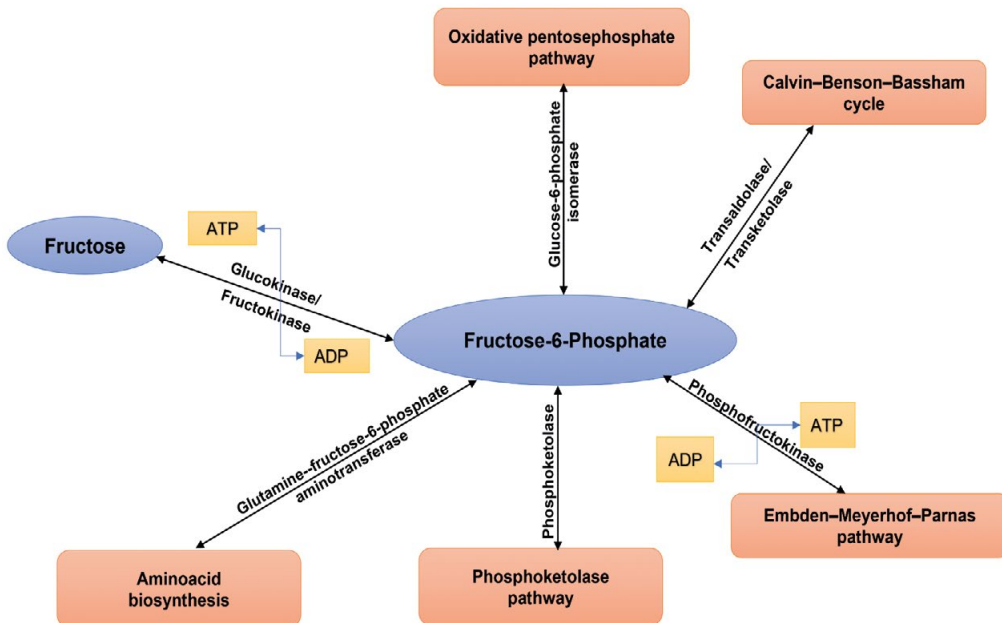


**Figure 1.5.** Scheme of fructose phosphate metabolism in cyanobacteria. Orange denotes the pathways. Blue denotes substrates.

## 1.5. Possible isoenzyme regulation mechanism in *Synechocystis* PCC 6803 via regulatory genes

### 1.5.1. HIK 8 and *sll* 1330

Histidine kinases (HIKs) are involved in the transduction of environmental signals in prokaryotes, as well as in plants, fungi, and protozoa (Marin et al., 2004; Koretke et al., 2000). Wang et al. (2004) described two-component response regulators, *rre32* (*slr0312*), *rre33* (*sll0797*), *rre37* (*sll1330*), and *rre38* (*slr1584*), were down-regulated by low inorganic carbon stress. Singh and Sherman (2005), In their paper they have suggested that HIK 8 has a major role in glucose metabolism under dark conditions also reported that supplementation of HIK 8 in  $\Delta$ hik 8 mutant strains of *Synechocystis* will recover photoheterotrophy/ heterotrophy in them under dark. Also, they have suggested that after four days, complete growth was suppressed in *Synechocystis* (Osanai et al., 2015). The transcript level of FBA II was enhanced by HIK 8 overexpression under light conditions, while those of GLGX (*slr0237*) and PFKA (*sll1196*) were repressed.

*sll1330* is gene code for another response regulator, induced by light and glucose, activating a cascade of genes (Tabei et al., 2007, 2009). Under heterotrophic conditions in the absence of light, the *sll1330* is down-regulated, however the expression is partially regulated by HIK 8, which can keep it expressed for a limited amount of time under dark (Singh and Sherman, 2005; Tabei et al., 2007, 2009).

### 1.5.2. Regulation by of *sll1334* gene on genes controlled by HIK 8

*sll1334* is a regulator gene that suppresses the upregulation of glycolytic genes. Whereas in the presence of glucose, HIK 8 protein is responsible for the upregulation of certain enzymes in the glycolytic pathway and OPP pathway (Table 1.2.). Experiments done by Okada et al., 2015 have showed the impact of the *sll1334* regulator gene on HIK 8. It is worth mentioning that *sll1334* mutant variants of *Synechocystis* have higher rate of HIK 8 expression compared to the wild type under dark supplemented glucose conditions.

**Table 1.2.** Enzyme coding genes controlled by HIK 8 and *sll1330* separately.

| HiK 8                                     | <i>sll1330</i>          |
|---|-------------------------|
| GLK                                       | GAP 1                   |
| PFK 1 ( <i>sll1196</i> )                  | PGK                     |
| FBA                                       | PGAM ( <i>slr1975</i> ) |
| PGAM B ( <i>slr1124</i> )                 | TKT A                   |
| PK <i>sll0587</i>                         | Enolase                 |
| TAL (tyrosine ammonia lyase)              | PK ( <i>sll1275</i> )   |
| CFXE (Ribulose phosphate-3-epimerase)     | FBA*                    |
| ZWF (glucose-6-phosphate-1-dehydrogenase) |                         |
| PGL (6-phosphogluconolactonase)           |                         |
| GND (6-phosphogluconate dehydrogenase)    |                         |

FBA\* also works independently of *sll1330* and HIK

## Reference

- Anderson, S.L., McIntosh, L., 1991. Light-activated heterotrophic growth of the cyanobacterium *Synechocystis* sp. Strain PCC 6803: a blue-light-requiring process. *J. Bacteriol.* 173, 2761–2767.
- Andrejc, D., Možir, A., Legiša, M., 2017. Effect of the cancer specific shorter form of human 6-phosphofructo-1-kinase on the metabolism of the yeast *Saccharomyces cerevisiae*. *BMC Biotechnol.* 17, 41.
- Bachhar, A., & Jablonsky, J., 2020. A new insight into role of phosphoketolase pathway in *Synechocystis* sp. PCC 6803. *Sci. Rep.* 10, 22018.
- Bachhar, A., Jablonsky, J., 2022. Entner-Doudoroff pathway in *Synechocystis* PCC 6803: Proposed regulatory roles and enzyme multifunctionalities. *Front. Microbiol.* 13, 967545.
- Beck, C., Knoop, H., Axmann, I.M., Steuer, R., 2012. The diversity of cyanobacterial metabolism: genome analysis of multiple phototrophic microorganisms. *BMC Genom.* 13, 56.
- De los Ríos, A., Grube, M., Sancho, L.G., Ascaso, C., 2007. Ultrastructural and genetic characteristics of endolithic cyanobacterial biofilms colonizing Antarctic granite rocks". *FEMS Microbiol. Ecology* 59, 386–95.
- Dong, G., Golden, S.S., 2008. How a cyanobacterium tells time. *Current Opinion Microbiol.* 11, 541–546.
- Doello, S., Neumann, N., Forchhammer, K., 2022. Regulatory phosphorylation event of phosphoglucosmutase 1 tunes its activity to regulate glycogen metabolism. *The. FEBS. J.* 289, 6005–6020.
- Droop, M.P., 1974. *Heterotrophy of carbon*. University of California Press, Los Angeles. pp. 530–559.
- Gao, L., Shen, C., Liao, L., Huang, X., Liu, K., Wang, W., Guo, L., Jin, W., Huang, F., Xu, W., Wang, Y. 2014. Functional proteomic discovery of *Slr0110* as a central regulator of carbohydrate metabolism in *Synechocystis* species PCC6803. *Molecular & cellular proteomics : MCP* 13, 204–219.
- Heidorn, T., Camsund, D., Huang, H., Lindberg, P., Oliveria, P., Stensjo, K., Lindblad, P., 2011. Chapter Twenty-Four – Synthetic Biology in Cyanobacteria: Engineering and Analyzing Novel Functions. *Methods in Enzymology* 497. pp. 539–579.
- Huang, L., 2009. *Genome*. Grady-McPherson. pp. 299.
- Hunter, R.L., Markert, C.L., 1957. Histochemical demonstration of enzymes separated by zone electrophoresis in starch gels. *Science* 125, 1294–1295.
- Jablonsky, J., Hagemann, M., Schwarz, D., Wolkenhauer, O., 2013. Phosphoglycerate mutases function as reverse regulated isoenzymes in *Synechococcus elongatus* PCC 7942. *PLoS One* 8, e58281.
- Jablonsky, J., Papacek, S., Hagemann, M., 2016. Different strategies of metabolic regulation in cyanobacteria: from transcriptional to biochemical control. *Sci. Rep.* 6, 33024.
- Kaneko, T., Sato, S., Kotani, H., Tanaka, A., Asamizu, E., Nakamura, Y., Miyajima, N., Hirose, M., Sugiura, M., Sasamoto S., et al. 1996. Sequence Analysis of the genome of the unicellular cyanobacterium *Synechocystis* sp. strain PCC6803. II. sequence determination of the entire genome and assignment of potential protein-coding regions. *DNA Res.* 3, 109–136.
- Koretke, K. K., Lupas, A. N., Warren, P. V., Rosenberg, M., and Brown, J. R. 2000. Evolution of two-component signal transduction. *Molecular biology and evolution*, 17(12): 1956–1970.

- Klemke, F., Baier, A., Knoop, H., Kern, R., Jablonsky, J., Beyer, G., Volkmer, T., Steuer, R., Lockau, W., and Hagemann, M. 2015. Identification of the light-independent phosphoserine pathway as an additional source of serine in the cyanobacterium *Synechocystis* sp. PCC 6803. *Microbiology* (Reading, England), 161(5): 1050–1060. <https://doi.org/10.1099/mic.0.000055>
- Koksharova, O., Schubert, M., Shestakov, S., Cerff, R., 1998. Genetic and biochemical evidence for distinct key functions of two highly divergent GAPDH genes in catabolic and anabolic carbon flow of the cyanobacterium *Synechocystis* sp. PCC 6803. *Plant Mol. Biol.* 36, 183–194.
- Lee, H.W., Roh, S.W., Shin, N.R., Lee, J., Whon, T.W., Jung, M.J., Yun, J.H., Kim, M.S., Hyun, D.W., Kim, D., Bae, J.W., 2013. *Blastopirellula reme* sp. nov., isolated from a dead ark clam. *Int. J. Syst. Evol. Microbiol.* 63, 2314–9.
- Martin, W., Brinkmann, H., Savona, C., Cerff, R., 1993. Evidence for a chimeric nature of nuclear genomes: eubacterial origin of eukaryotic glyceraldehyde-3-phosphate dehydrogenase genes. *Proc. Natl. Acad. Sci. USA* 90, 8692–8696.
- Marin, K., Kanesaki, Y., Los, D.A., Murata, N. Suzuki, I., Hagemann, M., 2004. Gene expression profiling reflects physiological processes in salt acclimation of *Synechocystis* Sp. Strain PCC 68031. *Plant Physiol.* 136, 3290–3300.
- Nakahara, K., Yamamoto, H., Miyake, C., Yokota, A., 2003. Purification and characterization of class-i and class-ii fructose-1,6-bisphosphate aldolases from the cyanobacterium *Synechocystis* sp. PCC 6803 *Plant Cell Physiol.* 44, 326–333.
- Neumann, N., Lee, K. and Forchhammer, K., 2022. On the role and regulation of glycogen catabolic isoenzymes in *Synechocystis* sp. PCC6803. *bioRxiv*. doi: <https://doi.org/10.1101/2022.11.21.517384>.
- Okada, K., Horii, E., Nagashima, Y. Mitsui, M., Matsuura, H., Fujiwara, S., Tsuzuki, M., 2015. Genes for a series of proteins that are involved in glucose catabolism are upregulated by the hik8-cascade in *Synechocystis* Sp. PCC 6803. *Planta* 241, 1453–1462.
- Ononye, S.N., Shi, W., Wali, V.B., Aktas, B., Jiang, T., Hatzis, C., Pusztai, L., 2014. Metabolic isoenzyme shifts in cancer as potential novel therapeutic targets. *Breast Cancer Res. Treat.* 148, 477–488.
- Orthwein, T., Scholl, J., Spät, P., Lucius, S., Koch, M., Macek, B., Hagemann, M., Forchhammer, K., 2021. The novel PII-interactor PirC identifies phosphoglycerate mutase as key control point of carbon storage metabolism in cyanobacteria. *Proc. Natl. Acad. Sci. U S A*. 118: e2019988118. <https://doi.org/10.1073/pnas.2019988118>
- Osanai, T., Shirai, T., Iijima, H., Nakaya, Y., Okamoto, M., Kondo, A., Hirai, M.Y., 2015. Genetic manipulation of a metabolic enzyme and a transcriptional regulator increasing succinate excretion from unicellular cyanobacterium. *Front. Microbiol.* 6, 1064.
- Parducci, R.E., Cabrera, R., Baez, M., Guixe, V., 2006. Evidence for a catalytic Mg<sup>2+</sup> ion and effect of phosphate on the activity of *Escherichia coli* phosphofructokinase-2: regulatory properties of a ribokinase family member. *Biochemistry* 45, 9291–9299.
- Patipong, T., Ngoenneta, S. Hondac, M., Hibino, T. Waditee-Sirisatthaa, R., Kageyamab, H., 2019. A class I fructose-1,6-bisphosphate aldolase is associated with salt stress tolerance in a halotolerant cyanobacterium *Halotheca* sp. PCC 7418. *Arc. Biochem. Biophysic.* 672,108059.
- Patron, N.J., Rogers, M.B., Keeling, P.J., 2004. Gene replacement of fructose-1,6-bisphosphate aldolase supports the hypothesis of a single photosynthetic ancestor of Chromalveolates. *Eukaryotic Cell* 3, 1169–1175.

- Rodrigues, J.S., Lindberg, P., 2020. Metabolic engineering of *Synechocystis* sp. PCC 6803 for improved bisabolene production. *Metabol. Eng. Commun.* 12, e00159.
- Romeo, T., Kumar, A., Preiss, J., 1988. Analysis of the *Escherichia coli* glycogen gene cluster suggests that catabolic enzymes are encoded among the biosynthetic genes. *Gene* 70, 363–376.
- Rutter, W.J., 1964. Evolution of aldolase. *Fed. Proc.* 23, 1248.
- Scandalios, J.G., 1969. Genetic control of multiple molecular forms of enzymes in plants: A review. *Biochem. Genet.* 3, 37–79.
- Schlesner, H., Rensmann, C., Tindall, B.J., Gade, D., Rabus, R., et al. 2004. Taxonomic heterogeneity within the Planctomycetales as derived by DNA-DNA hybridization, description of *Rhodopirellula baltica* gen. nov., sp. Nov., transfer of *Pirellula marina* to the genus *Blastopirellula* gen. nov. as *Blastopirellula marina* comb. Nov. and emended description of the genus *Pirellula*. *Int. J. Syst. Evol. Microbiol.* 54, 1567–1580.
- Siebers, B., Brinkmann, H, Dorr, C., Tjaden, B., Lilie, H., Van der Oost, J., Verhees, C.H., 2001. Archaeal fructose-1,6-bisphosphate aldolases constitute a new family of archaeal type class I aldolase. *J. Biol. Chem.* 276, 28710–28718.
- Singh, A.K., Sherman, L.A., 2005. Pleiotropic effect of a histidine kinase on carbohydrate metabolism in *Synechocystis* Sp. Strain pcc 6803 and its requirement for heterotrophic growth. *J. Bacteriol.* 187, 2368–2376.
- Shi, K., Zhang, Y., Zhou, Y., Liu, X., Zhu, G., Qin, B., Gao, G., 2017. Long-term MODIS observations of cyanobacterial dynamics in Lake Taihu: Responses to nutrient enrichment and meteorological factors. *Sci. Rep.* 40326
- Stoecker, D., Tillmann, U., Granéli, E., 2006. Phagotrophy in harmful algae Springer Berlin Heidelberg, New York pp. 177–187
- Subashchandrabose, S.R., Ramakrishnan, B., Megharaj, M., Venkateswarlu, K., Naidu, R. 2013. Mixotrophic cyanobacteria and microalgae as distinctive biological agents for organic pollutant degradation. *Environ. Int.* 51, 59–72
- Tabei, Y., Okada, K., Tsuzuki, M., 2007. Sll1330 controls the expression of glycolytic genes in *Synechocystis* sp. PCC 6803. *Biochem. Biophys. Res. Co.* 355, 1045–1050.
- Tabei, Y., Okada, K., Makita, N., Tsuzuki, M., 2009. Light-induced gene expression of fructose 1,6-bisphosphate aldolase during heterotrophic growth in a cyanobacterium, *Synechocystis* sp. PCC 6803. *FEBS J.* 276, 187–198.
- Tabei, Y., Okada, K., Horii, E., Mitsui, M., Nagashima, Y., Sakai, T., Yoshida, T., Kamiya, A., Fujiwara, S., Tsuzuki, M., 2012. Two regulatory networks mediated by light and glucose involved in glycolytic gene expression in cyanobacteria. *Plant & Cell Physiol.* 53, 1720–1727.
- Ungerer, J.L., Pratte, B.S., Thiel, T., 2008. Regulation of fructose transport and its effect on fructose toxicity in *Anabaena* spp. *J. Bacteriol.* 190, 8115–8125.
- Wang, H.L., Bradley, L.P.B.L., Burnap, R.L., 2004. Alterations in global patterns of gene expression in *Synechocystis* sp. PCC 6803 in response to inorganic carbon limitation and the inactivation of NdhR, a LysR Family Regulator. *J. Biol. Chem.* 279, 5739–5751.
- Yoo, S.H., Lee, B.H., Moon, Y., Spalding, M.H., Jane, J.L., 2014. Glycogen synthase isoforms in *Synechocystis* sp. PCC6803: identification of different roles to produce glycogen by targeted mutagenesis. *PLoS one.* 9, e91524. <https://doi.org/10.1371/journal.pone.0091524>.



- Yoshikawa, K., Hirasawa, T., Ogawa, K., Hidaka, Y., Nakajima, T., Furusawa, C., Shimizu, H., 2013. Integrated transcriptomic and metabolomic analysis of the central metabolism of *Synechocystis* sp. PCC 6803 under different trophic conditions. *Biotechnol. J.* 8, 571–580.
- Yoshikawa, K., Toya, Y., Shimizu, H., 2017. Metabolic engineering of *Synechocystis* sp. PCC 6803 for enhanced ethanol production based on flux balance analysis. *Bioprocess Biosyst. Eng.* 40, 791–796.
- Xiong, W., Lee, T.C., Rommelfanger, S., Gjersing, E., Cano, M., Maness, P.C., Ghirardi, M., Yu, J., 2015. Phosphoketolase pathway contributes to carbon metabolism in cyanobacteria. *Nat. Plants* 2, 15187.



## CHAPTER 2

### **A NEW INSIGHT INTO ROLE OF PHOSPHOKETOLASE PATHWAY IN *SYNECHOCYSTIS* SP. PCC 6803**

Bachhar, A., Jablonsky, J., 2020. A new insight into role of phosphoketolase pathway in *Synechocystis* sp. PCC 6803. *Sci. Rep.* 10, 22018.

Open access: This article is licensed under a Creative Commons Attribution 4.0 International License (CC By 4.0), which permits use, sharing, adaptation, distribution and reproduction in any medium or format, as long as you give appropriate credit to the original author(s).

My contribution in this work 50%.



# scientific reports



OPEN

## A new insight into role of phosphoketolase pathway in *Synechocystis* sp. PCC 6803

Anushree Bachhar & Jiri Jablonsky<sup>✉</sup>

Phosphoketolase (PKET) pathway is predominant in cyanobacteria (around 98%) but current opinion is that it is virtually inactive under autotrophic ambient CO<sub>2</sub> condition (AC-auto). This creates an evolutionary paradox due to the existence of PKET pathway in obligatory photoautotrophs. We aim to answer the paradox with the aid of bioinformatic analysis along with metabolic, transcriptomic, fluxomic and mutant data integrated into a multi-level kinetic model. We discussed the problems linked to neglected isozyme, *pket2* (*slr0529*) and inconsistencies towards the explanation of residual flux via PKET pathway in the case of silenced *pket1* (*slr0453*) in *Synechocystis* sp. PCC 6803. Our in silico analysis showed: (1) 17% flux reduction via RuBisCO for  $\Delta$ *pket1* under AC-auto, (2) 11.2–14.3% growth decrease for  $\Delta$ *pket2* in turbulent AC-auto, and (3) flux via PKET pathway reaching up to 252% of the flux via phosphoglycerate mutase under AC-auto. All results imply that PKET pathway plays a crucial role under AC-auto by mitigating the decarboxylation occurring in OPP pathway and conversion of pyruvate to acetyl CoA linked to EMP glycolysis under the carbon scarce environment. Finally, our model predicted that PKETs have low affinity to 57P as a substrate.

Metabolic engineering of cyanobacteria provides many options for producing valuable compounds, e.g., acetone from *Synechococcus elongatus* PCC 7942<sup>1</sup> and butanol from *Synechocystis* sp. strain PCC 6803<sup>2</sup>. However, certain metabolites or overproduction of intermediates can be lethal. There is also a possibility that required mutation(s) might be unstable or the target bacterium may even be able to maintain the flux distribution for optimal growth balance due to redundancies in the metabolic network, such as alternative pathways. The current dominant “trial and error” approach implies that our understanding of cellular metabolic regulatory mechanisms, including those involving isozymes, post-translational modifications or allosteric regulations, is secondary to achieve the desired effect/product. Integrating computational biology methods may help both to understand complex big data and to improve our understanding of cellular processes, improving potential biotechnological applications in the long term.

Cyanobacterium *Synechocystis* sp. strain PCC 6803 (hereafter referred to as *Synechocystis*) is one of the more complex prokaryotes, known for its metabolic plasticity<sup>3</sup>. All known glycolytic pathways that exist in nature are accommodated in its central carbon metabolism: the Embden–Meyerhof–Parnas (EMP) pathway, the oxidative pentose phosphate (OPP) pathway, the phosphoketolase (PKET) pathway and the Entner–Doudoroff (ED) pathway. However, our knowledge about regulatory roles of PKET in *Synechocystis* is still limited.

Phosphoketolase converts xylulose 5-phosphate to glyceraldehyde 3-phosphate and acetyl phosphate, or fructose 6-phosphate to erythrose 4-phosphate and acetyl phosphate, see Fig. 1. PKET is, based on current data (Uniprot, September 2020), present in around 98% of cyanobacteria, which makes it more common than phosphofruktokinase (around 72%) or ED pathway (around 64%) (Uniprot, September 2020). PKET is found mostly in gram negative bacteria, cyanobacteria, fungi and algae but not in higher plants. It is assumed that PKET pathway plays a role in heterotrophic conditions<sup>4</sup>, and it is known that deactivation of PKET pathway leads to 11.5% slower growth under autotrophic ambient CO<sub>2</sub> (AC-auto) condition<sup>5</sup>. Moreover, an engineered strain of *Synechocystis* with blocked glycogen synthesis and enabled xylose catabolism was reported with over 30% total carbon flux directed via PKET<sup>6</sup> under mixotrophic condition on xylose and CO<sub>2</sub>. Furthermore, overproduction of acetyl phosphate, caused by overexpression of *pket* (PKET gene), can negatively influence the pentose sugar metabolism<sup>7</sup> but may increase lipid synthesis<sup>8</sup>. Finally, recent <sup>13</sup>C labelling study concluded that there is virtually zero flux via PKET under AC-auto<sup>9</sup> in *Synechocystis*. This finding is in direct disagreement with the previous theoretical stoichiometric<sup>8</sup> and kinetic<sup>9</sup> studies which estimated the flux via PKET pathway to be 11.6% and

Institute of Complex Systems, FFPW, University of South Bohemia, CENAKVA, Zamek 136, 373 33 Nove Hradky, Czech Republic. ✉email: jiri.jablonsky@gmail.com

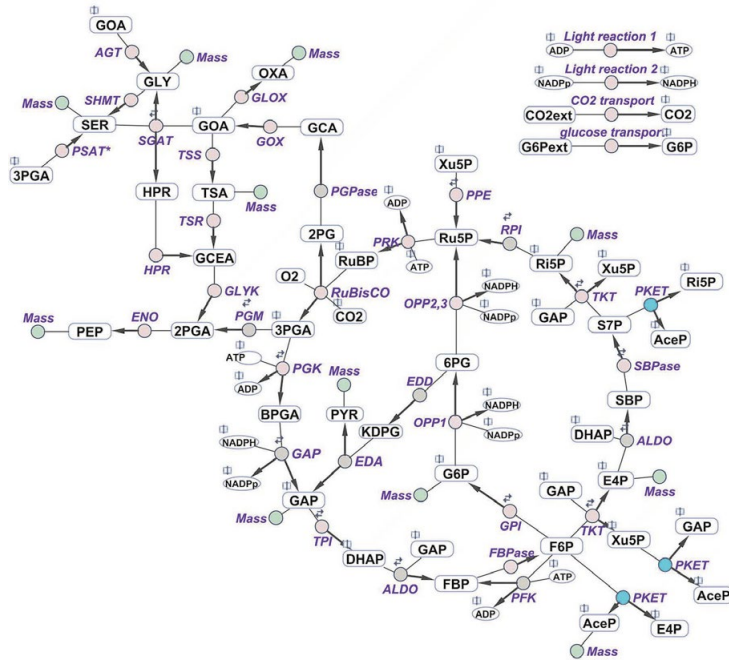


**Figure 1.** Schematic representation of the central carbon metabolism network, which was implemented in the multi-level kinetic model of *Synechocystis*. Blue indicates the reactions catalyzed by phosphoketolase. The model includes the Calvin-Benson cycle, glycogen synthesis (sink from glucose-6-phosphate), photosynthetic pathways, phosphoketolase pathway, glycolysis, the oxidative pentose pathway, Entner-Doudoroff pathway and sink reactions (representing the adjacent pathway and the calculation of biomass production). The reversibility of a particular reaction is indicated by two small arrows. Purple indicates the involved enzymes: *RuBisCO* ribulose-1,5-bisphosphate carboxylase oxygenase, *PGK* phosphoglycerate kinase, *GAP* glyceraldehyde-3-phosphate dehydrogenase, *TPI* triose-phosphate isomerase, *ALDO* aldolase, *FBPase* fructose-1,6 bisphosphatase, *PFK* phosphofructokinase, *TKT* transketolase, *SBPase* sedoheptulose-1,7 bisphosphatase, *RPI* phosphopentose isomerase, *PPE* phosphopentose epimerase, *PRK* phosphoribulokinase, *GPI* glucose-6-phosphate isomerase, *G6PD* glucose-6-phosphate dehydrogenase, *PGD* phosphogluconate dehydrogenase, *PGPase* phosphoglycolate phosphatase, *PKET* phosphoketolase, *GOX* glyoxylate oxidase, *SGAT* serineglyoxylate transaminase, *HPR* hydroxypyruvate reductase, *GLYK* glycerate kinase, *AGT* alanineglyoxylate transaminase, *TSS* tartronatesemialdehyde synthase, *TSR* tartronatesemialdehyde reductase, *SHMT* serine hydroxymethyltransferase, *GLOX* glyoxylate oxidase, *PSAT\** phosphoserine transaminase, *PGM* phosphoglycerate mutase, *ENO* enolase, *EDD* 6P-gluconate dehydratase, *EDA* 2-keto-3-deoxygluconate-6-phosphate aldolase (*EDD* and *EDA* are currently simplified into a single reaction in the model). Open book symbol indicates an involvement of metabolite in other reaction(s). The scheme was created in SimBiology toolbox of MATLAB 2010b (The MathWorks, Inc., Natick, Massachusetts, United States of America), <http://www.mathworks.com>.

5.3% of flux via *RuBisCO*, respectively. Thus, we have decided to investigate this issue and to review the flux via *PKET* pathway based on all available data.

Our study aims to provide answers to the following questions with the help of multi-level kinetic model of central carbon metabolism for *Synechocystis*: (1) if *PKET* pathway is present in cyanobacteria, especially in obligatory photoautotrophs, why it is inactive in autotrophic conditions during day, (2) what is the role of *PKET* and can we quantify its potential benefits and (3) does the role of *PKET* pathway change in different environmental conditions?

## Results and discussion

**One or two phosphoketolases in *Synechocystis*?** Existence of two PKETs was biochemically characterized in cyanobacteria so far only in *Nostoc/Anabena* PCC 7120 (*Nostoc*)<sup>10</sup> but our multiple sequence alignment showed 78% homology among PKETs in cyanobacteria with annotated PKET isozymes (see Supplement). Phylogenetic analysis indicated a significant spread of PKET isozymes, see Fig. 2, namely a clearly separated cluster for cyanobacteria, containing also *pket1* (*slr0453*) of *Synechocystis* and *pket1* (*all1483*) of *Nostoc*. Interestingly, the secondary PKETs of cyanobacteria, including *pket2* (*slr0529*) of *Synechocystis* and *pket2* (*alr1850*) of *Nostoc*, are clustered also with fungi, bacteria and algae, implying a possible horizontal gene transfer. The common feature of photosynthetic and non-photosynthetic species in this heterogeneous cluster is a complex metabolism, allowing to survive on organic source of carbon. Strikingly, PKET2, firstly mentioned in 2010<sup>11</sup>, was ignored in the metabolic studies despite the residual (approximately 10%) flux via PKET pathway in the case of silenced *pket1* under both mixotrophic<sup>11</sup> and autotrophic<sup>12</sup> condition. It was suggested that this residual flux is caused by the activity of phosphate acetyl-transferase (PTA) activity<sup>7</sup>. The problem with this explanation is that it considers only reactions towards TCA cycle, i.e., reversibility of PTA, even though the same residual flux was detected also towards glyceraldehyde-3-phosphate (GAP) synthesis<sup>4</sup>. Since GAP synthesis is not connected to PTA activity (Fig. 1), the proposed role of PTA on the residual flux via PKET pathway lacks any justification.

We propose that neglected PKET2 of *Synechocystis* is responsible for the residual flux via PKET pathway. Furthermore, to explain why PKET2 is not taking over in the case of silenced *pket1*, we assumed that PKET2 might be allosterically inhibited. This prediction is supported by the fact that bacterial PKETs, clustered with PKET2 in question (Fig. 2), can be inhibited by several metabolites, including phosphoenolpyruvate, oxaloacetate and glyoxylate<sup>12</sup>. Moreover, based on residual flux, required 90/10 ratio of activity for PKET1 and PKET2 is not unique for *Synechocystis*. We know at least one more example of allosterically inhibited isozymes with similar activity ratio, the aldolase 1 and 2. Ninety percent of total aldolase activity involves aldolase 1 (class II) whereas aldolase 2 (class I) supplies only 10% of total due to allosteric inhibition<sup>13</sup>. It can thus be speculated that, after *pket1* is silenced, PKET2 is behind the residual activity of PKET pathway and PKET2 contribution does not increase due to allosteric inhibition. However, despite other known cases among isozymes in *Synechocystis*, allosteric inhibition is only one of possible explanations and we cannot prioritize it or exclude other options such as post-translational modification or regulation by signalling cascade(s), etc.

We presented certain support for existence and role of PKET2. However, it is still unknown what, if any, are the benefits of secondary PKET in the metabolism or growth of *Synechocystis*. Fortunately, our method of multi-level kinetic modelling (see “Materials and methods”) is capable to quantify the impact of PKET2. We performed an *in silico* experiment in which growth behaviour of *Synechocystis* was simulated under turbulent environment mimicked by a random variation in gene expression, up to  $\pm 20\%$ . Two scenarios were tested, either one or two PKETs in the system; the flux via PKET pathway was same in both cases. Since it is unknown if either of F6P or Xu5P (Fig. 1) is preferred substrate for any specific growth condition, the fitted parameters for WT (i.e., 2 PKETs) could be biased. To avoid any mistake in judging the impact of single PKET in the system, we analysed two rather extreme cases (ninety percent of flux via PKET pathway occurs either via F6P branch or Xu5P branch) and balanced scenario (50% of flux occurs both via F6P branch and Xu5P branch). This analysis showed 11.2–14.3% higher growth in AC-auto in the case of 2 PKETs, see Fig. 3, regardless of low activity of PKET2. Furthermore, the negative impact of single PKET was highest for Xu5P as the preferred substrate and lowest for balanced distribution of substrates (Fig. 3). Interestingly, the impact of single PKET was positive but rather negligible under high CO<sub>2</sub> autotrophic condition (HC-auto) and ambient CO<sub>2</sub> mixotrophic condition (AC-mix), varying slightly in dependence of preferred substrate (Fig. 3). However, the statistical analysis for HC-auto and AC-mix indicated no significance for 2PKETs or a single PKET, i.e., second PKET can be viewed as expendable in these growth conditions.

In order to test the impact of PKET2 on growth in case of  $\Delta$ *pket1*, the activity of original PKET pathway was reduced by 90%, based on the reported value of residual flux for  $\Delta$ *pket1*. The simulated growth impact was –13.6%, see Table 1, which was very close to previously reported experimental value –11.5%<sup>11</sup>. We note that some changes in gene expression were probably induced in the  $\Delta$ *pket1* mutant but could not be considered in the simulation due to the lack of available data. Furthermore, we showed that  $\Delta$ *pket1* could be beneficial under HC-auto, see Table 1. Finally, the gene expressions of *pket1* and *pket2* were compared in the changing environment, see Table 2, and both were upregulated in AC-auto and downregulated in the in/organic carbon rich environment. All presented bioinformatical analyses and simulations lead to the following conclusions: (i) PKET2 is very likely to be present in *Synechocystis*, (ii) PKET2 has a positive impact on growth rate in turbulent, carbon scarce environment and (iii) PKET2 is currently the only explanation of the residual fluxes via PKET pathway in the case of silenced *pket1*, both towards TCA cycle and GAP synthesis.

**Flux contribution of phosphoketolase pathway in various scenarios.** The first attempt to assess the flux via PKET pathway in *Synechocystis* was made with the aid of stoichiometric model based on flux balance analysis, suggesting flux of 14.9 (11.6% of flux via RuBisCO)<sup>8</sup>. At the time, it was believed that the model accurately describe HC-auto due to very good agreement with labeling experiment performed in HC-auto<sup>14</sup>. However, it was suggested later that the majority of fluxes are scalable in response to a changing environment<sup>9</sup>. Thus, explaining the stoichiometric model, designed for AC-auto, nearly fitting the fluxomic data for HC-auto. The rescaled value for PKET flux under AC-auto from stoichiometric model is then 4.1. This value is more than double of our previous estimate (1.9, 5.3% of flux via RuBisCO)<sup>8</sup>. However, <sup>13</sup>C labeling experiment was recently performed for AC-auto which concluded virtually zero flux via PKET pathway<sup>7</sup>. This result implied that both theoretically estimated values of PKET flux were incorrect. The problems with such implication were: (1) stoichiometric modeling approach assumes the flux balance for maximal growth benefits so non-zero flux via

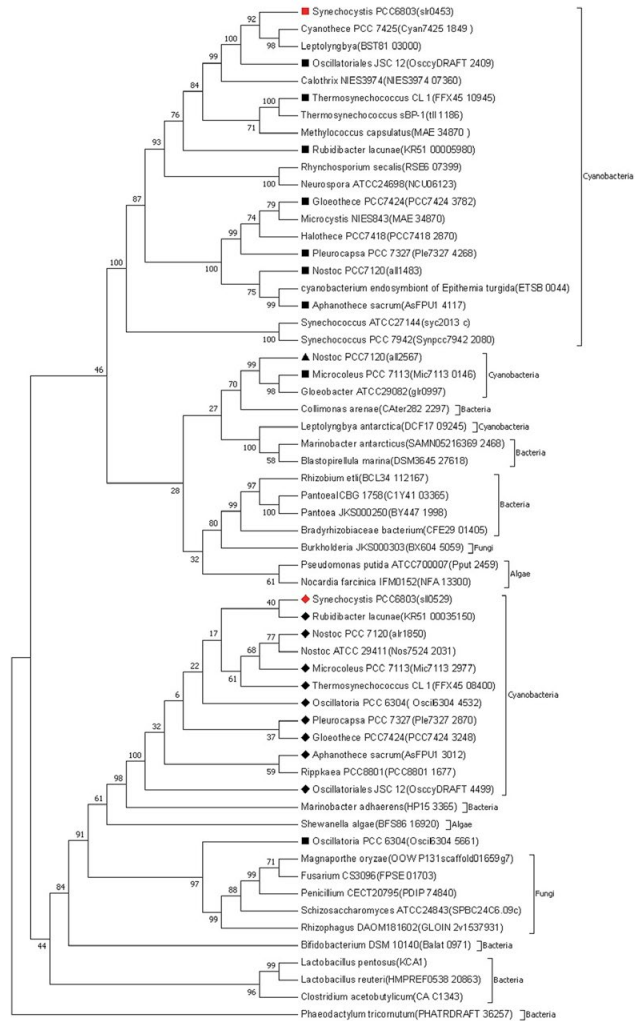


**Figure 2.** Phylogenetic tree created from the retrieved amino acid sequences of phosphoketolase (PKET) from sequence databases (Uniprot and NCBI) with MEGA 7 using Neighbour joining method (maximum bootstrap value of 500). The evolutionary distances were computed using the JTT matrix-based method. Square, diamond and triangle symbols are showing the first, second and third isozymes of PKET, respectively. Red colour is highlighting *Synechocystis*.



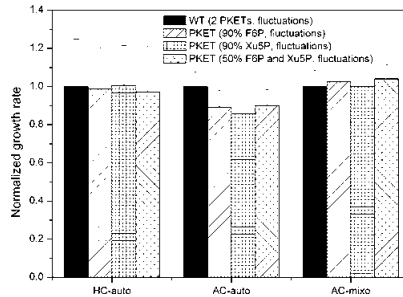


**Figure 3.** Comparing the impact of having one and two PKETs in the metabolism during simulated variation in gene expression in the different environments. AC-auto, HC-auto and AC-mixo denotes the growth conditions: ambient CO<sub>2</sub> autotrophic, high CO<sub>2</sub> autotrophic and ambient CO<sub>2</sub> mixotrophic state, respectively. WT (wild type) represent the scenario with 2 PKETs. Single PKET scenarios indicate the same flux via PKET pathway as WT, however, with 90% preference of particular substrate (F6P or Xu5P) and 50% preference for both substrates. Fluctuation means a simulation of changing environment by random, up to ± 20% variation in gene expression in the model. Each scenario was run 100-times; mean values and standard deviations are shown. We note that higher error bars for HC-auto indicates higher sensitivity towards changes in gene expression. Statistical analysis (paired t-test, 2 PKETs vs single PKET) showed no significance for HC-auto and AC-mixo (p > 0.05) but a great significance for AC-auto (p < 0.001).

|                           | HC-auto | AC-auto | AC-mixo |
|---------------------------|---------|---------|---------|
| Growth WT/ $\Delta$ pket1 | 0.89    | 1.13    | 1.04    |

**Table 1.** Impact of simulated silencing *pket1* on growth in various conditions. AC-auto, HC-auto and AC-mixo denotes the growth conditions, ambient CO<sub>2</sub> autotrophic, high CO<sub>2</sub> autotrophic and ambient CO<sub>2</sub> mixotrophic state, respectively.

|                        | AC-auto/HC-auto <sup>1</sup> | AC-auto/AC-mixo <sup>2</sup> |
|------------------------|------------------------------|------------------------------|
| <i>pket1</i> (str0453) | 1.35                         | 1.36                         |
| <i>pket2</i> (sl0529)  | 1.10                         | 1.21                         |

**Table 2.** Gene expression of phosphoketolases annotated for *Synechocystis*. Transcriptomic data were taken from<sup>16</sup> (1) and<sup>18</sup> (2). AC-auto, HC-auto and AC-mixo denotes the growth conditions, ambient CO<sub>2</sub> autotrophic, high CO<sub>2</sub> autotrophic and ambient CO<sub>2</sub> mixotrophic state, respectively.

PKET pathway indicates at least a potential growth benefit and (2) our previous kinetic model<sup>1</sup>, validated for different environmental conditions, also predicted non-zero flux via PKET pathway in order to improve the match between the experiments and simulations.

Therefore, we decided to elaborate the role and benefits of PKET pathway in detail. We tailored the flux via PKET1 and PKET2 to match 11.5% growth decrease under AC-auto for  $\Delta$ pket1<sup>1</sup>. The simulated flux via PKET pathway was 3.16 (7.2% of flux via RuBisCO) under AC-auto which strongly out-performed (up to 2.5-fold) the flux via phosphoglycerate mutase, the exit point of EMP glycolysis from Calvin-Benson cycle, see Fig. 4; we note the high upper bound for PGM in the original labeling study<sup>7</sup>. Since more accurate simulation actually increased the estimated flux via PKET pathway, we compared these values with original fluxes from labeling experiment<sup>7</sup>. The data from labeling experiment calculated a virtually non-existent flux via Xu5P branch (10<sup>-6</sup>) and high flux (16.86, 7.2% of flux via RuBisCO) via F6P branch of PKET pathway<sup>7</sup> which agrees with our predicted value perfectly. However, this result was not mentioned in their discussion, probably due to zero lower bound value for flux via both branches of PKET pathway, implying theoretically inactive PKET pathway. The lower bound of PKET flux might be explained only by reversibility of PTA. In the case of PTA flux, lower bound was 16.86 which was the same as calculated flux via F6P branch of PKET pathway. Since we have already rejected the reversibility

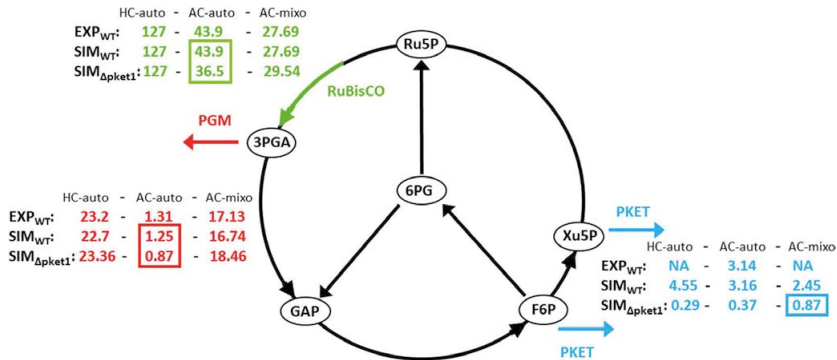


**Figure 4.** Experimental and estimated flux distribution in various environmental conditions. Green color indicates the flux via RuBisCO, blue color shows the flux via PKET (phosphoketolase) and red color highlights the flux via PGM (phosphoglycerate mutase). EXP<sub>WT</sub> and SIM<sub>WT</sub> indicates the experimental and simulated wild type values, respectively. SIM<sub>Δpket1</sub> shows the results for silenced *pket1*, while PKET2 remains active. Marked values indicates interesting values or their significant changes. Sources of experimental fluxomic data: HC-auto<sup>14</sup>, AC-auto<sup>7</sup> and AC-mixo<sup>18</sup>.

| Substrates of PKET | Growth in AC-auto |       |               | Data fit |
|--------------------|-------------------|-------|---------------|----------|
|                    | Mean              | SD    | Highest value |          |
| F6P and Xu5P       | 118.52            | 1.08  | 119.07        | 110.73   |
| F6P, Xu5P and S7P  | 100               | 13.48 | 113.69        | 110.73*  |

**Table 3.** In silico analysis of substrates dependent tuned PKET pathway for theoretical maximal growth under AC-auto in *Synechocystis*. Mean and SD represent the statistical data from parameter estimation. Highest growth value denotes the maximal theoretical growth for a particular set of substrates. Data fit indicates the estimated growth rate based on experimental data ( $\Delta pket1$ ). Asterisks signifies data fit for scenario with S7P allowed to be metabolized by PKETs but the best fit considered zero activity via S7P branch.

of PTA as the source of residual flux via PKET pathway (see the section above), we can conclude that the flux via PTA is mostly, if not fully, originated from PKET pathway.

Our flux analysis revealed other interesting information. First of all, silencing *pket1* has negative impact over all fluxes, especially via RuBisCO, under AC-auto, see Fig. 4. Hence, despite the carbon flux redirection after silencing *pket1*, less amount of carbon is available in the system due to decarboxylation in OPP and conversion of pyruvate to acetyl CoA linked to EMP glycolysis. This conclusion is further supported by the data from AC-mixo (Fig. 4) where we can see that silencing *pket1* has a positive effect on fluxes via RuBisCO and PGM, i.e., the flux redirection is beneficial and is not impaired by limited carbon resources. Finally, we can see that impact of silenced *pket1* on the residual flux is different under all environmental conditions; namely that the residual flux in AC-mixo is 35.5% of WT flux which could be due to significant change in metabolic network fluxes, substrates and inhibitors concentration in the presence of glucose, some of which are not considered in the model.

**Sedoheptulose-7P—an overlooked substrate of PKET?** Recently, sedoheptulose-7P (S7P) has been identified as a substrate of PKET in *E. coli* although with very low affinity ( $K_M = 68.1$  mM) and only 0.42% of total PKET activity maintained by S7P branch<sup>15</sup>. PKET breaks down S7P into ribose-5P and acetyl-P (Fig. 1). However, no information regarding S7P branch of PKET is available for cyanobacteria where it might play a more prominent role. Therefore, we designed an in silico experiment to predict the possible benefits of this pathway on growth by maximizing the expression of *pket1* and *pket2*. Our growth-based in silico analysis predicted that PKET pathway with S7P as one of substrates is once again beneficial only for AC-auto condition (data not shown). The target of our in silico experiment was to maximize the growth with any combination of the substrates (F6P, Xu5P and S7P) for PKETs. Firstly, the statistical analysis of results implies significantly higher variability in growth rate when S7P is metabolized via PKET pathway (Table 3). When the best fits were compared, 4.5% decline in growth was observed when S7P was metabolized by PKETs (Table 3). Thus, involvement of S7P

in PKET pathway is not providing any robustness to the system but rather has a destabilizing effect on the metabolic homeostasis; one of the possible explanations could be competition for S7P with transketolase. Although the estimated growth based on experimental data ( $\Delta pket1$ ) is the same for both scenarios (with or without S7P), the reason behind the same value is that parameter estimation routine applied zero flux via S7P branch of PKET pathway due to its lower efficiency. Thus, our model predicts that the affinity of PKETs towards S7P in cyanobacteria is very low, similarly as shown for *E. coli*<sup>15</sup>. Nevertheless, experimental verification is required as the role of S7P branch of PKET pathway might be more significant under certain stress conditions.

### Conclusions

We presented the following support for the existence and role of two PKETs in *Synechocystis*: (1) bacteria have PKETs that are regulated by allosteric inhibition<sup>14</sup> and *pket2* is in the cluster with bacteria (in contrast to *pket1*), opening the possibility for horizontal gene transfer; thus we can speculate that PKET2 is also allosterically inhibited by phosphoenolpyruvate, oxaloacetate or glyoxylate which provides currently the only explanation for the residual flux via PKET pathway in  $\Delta pket1$  and clarifies why PKET2 does not display any higher activity in such scenario; however, other alternative explanations such as post-translational modification cannot be currently excluded, (2) our in silico experiment of  $\Delta pket1$  mutant with active PKET2 showed the same impact on growth as reported previously in AC-auto for silenced *pket1* which was believed at the time to be a total inhibition of PKET pathway, (3) there are other known cases of allosteric inhibition in *Synechocystis*, including the proposed 90/10 flux contribution of isozymes, e.g., aldolase 1 and 2, and (4) we showed a clear benefit of having PKET2 in the central carbon metabolism of *Synechocystis*, namely, an 11.2–14.3% growth increase in the turbulent AC-auto. However, an experimental verification, if the product of gene *sl0529* (*pket2*) indeed has phosphoketolase activity, as well as what, if any, is the impact of phosphate acetyl-transferase on residual flux via PKET pathway, is needed. Similarly, here proposed allosteric regulation of PKET should be experimentally verified.

In addition to analysing the putative PKET2 isozyme, we have also focused on the flux distribution of PKET pathway under various conditions. We showed that PKET pathway could be the major carbon flux exit point from Calvin–Benson cycle in AC-auto, overcoming the flux via phosphoglycerate mutase by up to 252%. This finding is in direct disagreement with recent <sup>13</sup>C labelling experiment which revealed virtually no flux via PKET pathway under AC-auto. However, we have found a critical error in their analysis and their own labelling data supports our conclusion of the great importance of PKET pathway. Furthermore, we have shown that silencing *pket1* has a negative impact over all fluxes, including RuBisCO and PGM in AC-auto but not in HC-auto and AC-mix. We conclude that high flux via PKET pathway mitigates the decarboxylation occurring in OPP pathway and conversion of pyruvate to acetyl CoA linked to EMP glycolysis under AC-auto, i.e., in the carbon scarce environment. Finally, we have tested S7P as a substrate for PKETs as it was reported for *E. coli*. Our analysis predicted low efficiency of S7P branch of PKET pathway and low affinity towards S7P, similarly as shown for *E. coli*.

In the end, we did not analyse the role of PKET pathway under heterotrophic condition because its impact has already been shown and because heterotrophic condition is substantially more difficult to integrate into our light-on-only multi-state model. Our main goal was to address the purported negligible impact of PKET pathway in autotrophic condition; however, we plan to analyse the role of PKET in heterotrophic or photoheterotrophic conditions in the future, together with other isozymes within the central carbon metabolism of *Synechocystis*.

### Materials and methods

#### Sources of experimental data integrated into multi-level kinetic model.

##### Transcriptomic data

HC-auto to AC-auto<sup>16</sup>.  
AC-auto to AC-mix<sup>17</sup>.

##### <sup>13</sup>C labeling data

HC-auto<sup>14</sup>.  
AC-auto<sup>7</sup>.  
AC-mix<sup>18</sup>.

We note that, despite its not clearly stated in the original work as authors are talking only about photoautotrophic condition<sup>14</sup>, there is a line of evidence that this particular labeling experiment is describing HC-auto. Firstly, the growth rate of culture was 0.09 h<sup>-1</sup><sup>14</sup> which is higher rate than the one observed for 3% CO<sub>2</sub> enriched medium (0.06 h<sup>-1</sup>)<sup>7</sup>. Secondly, authors used a high concentration of bicarbonate in their study and demonstrated that level of photorespiration is very small under high CO<sub>2</sub> conditions<sup>14</sup>; study was performed under single environmental condition, i.e., HC-auto. Finally, we showed that majority of metabolic fluxes scales based on the level of carbon<sup>9</sup> which explains why most of fluxes are very similar for AC-auto and HC-auto after normalization. However, key exit fluxes, such as phosphoglycerate mutase, OPP or PKET pathway do not scale<sup>9</sup> which explains significant difference for exit fluxes between<sup>14</sup> and<sup>7</sup>, e.g., ratio between fluxes via RuBisCO and OPP is 7.8 for HC-auto<sup>14</sup> but 1.7 for AC-auto<sup>7</sup>.

## Metabolic data

HC-auto<sup>19–21</sup>,  
 AC-auto<sup>19,20</sup>,  
 AC-mixo<sup>17</sup>.

## Mutant data

$\Delta$ *pket1* mutant<sup>1</sup>.

**General information about the model.** The multi-level kinetic model for *Synechocystis* was developed and simulations were executed using the SimBiology toolbox, Optimization toolbox, Global optimization toolbox and Parallel toolbox of MATLAB (The MathWorks, Inc., Natick, Massachusetts, United States of America). The routine for parameter estimation was a hybrid genetic algorithm. The model for HC-auto is available in the Supplement in SBML format L2V4 compatible with MATLAB 2010b and higher. We recommend to open the model either in MATLAB or user friendly COPASI (free academic license). The weight factors (applied transcriptomic data) necessary to run the model in other conditions (AC-auto and AC-mixo) is provided in Supplement.

The scope of the model includes the following parts of central carbon metabolism: Calvin–Benson cycle, photosynthesis, all glycolytic pathways (Embden–Meyerhof–Parnas pathway, Entner–Doudoroff pathway, phosphoketolase pathway and oxidative pentose phosphate) and carbohydrate synthesis. These metabolic reactions were coupled to simplified light reactions and Ci and glucose uptake as the main input parameters. Biomass production is estimated as weighted sum of sink reactions<sup>9</sup>. This simplified approach allowed to estimate the CO<sub>2</sub> fixation and glucose uptake by comparing to relative experimental fluxes in all tested conditions as well as to keep the track of growth rate, matching the experimental levels from literature<sup>9</sup>. Moreover, the biomass in the model is assumed to be equal to the amount of fixed carbon, whereas nitrogen was not a limiting nutrient factor in the experimental setups<sup>1</sup>. The definition of biomass in the model is provided by following equation, based on the model content, in which upper index *s* stands for accumulation of respective metabolite in the sink (Fig. 1) and a particular coefficient corresponds to the amount of carbon atoms in the molecule:

$$\text{Mass} = 2*(\text{AceP}^s + \text{GLY}^s + \text{OXA}^s) + 3*(\text{PEP}^s + \text{PYR}^s + \text{GAP}^s + \text{SER}^s) + 4*\text{E4P}^s + 5*\text{Ri5P}^s + 6*\text{G6P}^s.$$

The model consists of 61 reactions, 48 metabolites and 214 kinetic parameters. The enzymatic reactions are described by Michaelis–Menten kinetics, except for the light reactions, Ci and glucose uptake, which are described by mass action kinetics. All reactions, except for the import of external carbon, are localized in a single compartment. The starting point of modelling was our previous model of *Synechocystis*<sup>1</sup>, which was modified and extended in order to describe AC-mixo condition. We note that the justification of using fold changes in the mRNA levels as a proxy between different environmental conditions, assuming a 1:1 ratio between a change in transcriptome and enzymatic amount, is provided in our previous study, including the support from experimental studies, can be found in our previous study<sup>1</sup>.

**Systems biology workflow.** The integration of various omics data occurs in several steps. In the first step, transcriptomic data from HC-auto to AC-auto and AC-auto to AC-mixo are included into the model in the form of mean values of measured mRNA changes as weight factors for each  $V_{\text{max}}$ . Then, we fit the experimental fluxomics and metabolic data from HC-auto. In this process of parameter estimation, we obtain a set of parameters which will be used in all following steps or trashed and search for new set will begin. If there is a match between simulation and experiment in HC-auto, metabolic and fluxomics data are saved (including the set of kinetic parameters). Then, we simulate a transition from HC-auto to AC-auto, i.e., applying the weight factors (mRNA), run the simulation for the steady state AC-auto, save the metabolic and fluxomic data and do the same for AC-auto to AC-mixo shift. At this point, we do semi-automated check for the reasonable match between simulated and experimental data for AC-auto and AC-mixo (growth levels, physiological range of key metabolites such as 3PGA, etc.), followed by manual curation of results. If acceptable match is found, the final step is a fine tuning of parameters and observing the changes in all three conditions. Manual tuning and curation of kinetic parameters at the different levels of parameter estimation and data integration is an essential part of modelling, because it provides a deeper understanding of system behavior and helps to detect errors in the algorithms, routines and model structure, e.g., when a new pathway is added.

We note that we shifted our priority from metabolic levels to fluxomic data as a key reference for match fitting. The main reason is that we are analyzing now 3 environmental conditions and planning to add more. However, there is no study providing metabolic data for the particular conditions of our interest and combining multiple metabolic data sets from different studies proved to be extremely challenging. We continue observing and analyzing the metabolic levels but in the case of parameter fitting, we currently only check if metabolic levels are in the physiological range and analyze the homeostatic stability of metabolites. Finally, simulation of fluctuating environment was done by applying up to  $\pm 20\%$  random variation in all  $V_{\text{max}}$  and  $k_i$  parameters, running it 100-times and calculating the mean value and standard deviation. Two scenarios, with one or two PKET, were tested, in all three environmental conditions.

More information about the method, parameter estimation and other details can be found in our previous study<sup>1</sup>. The first application of the method, the case study of phosphoglycerate mutase, discussed the potential of this method, e.g., the verification of gene annotation<sup>21</sup>.

Received: 23 July 2020; Accepted: 25 November 2020  
Published online: 16 December 2020

## References

- Chwa, J.-W., Kim, W. J., Sim, S. J., Um, Y. & Woo, H. M. Engineering of a modular and synthetic phosphoketolase pathway for photosynthetic production of acetone from CO<sub>2</sub> in *Synechococcus elongatus* PCC 7942 under light and aerobic condition. *Plant Biotechnol. J.* **14**, 1768–1776 (2016).
- Liu, X., Miao, R., Lindberg, P. & Lindblad, P. Modular engineering for efficient photosynthetic biosynthesis of 1-butanol from CO<sub>2</sub> in cyanobacteria. *Energy Environ. Sci.* **12**, 2765–2777 (2019).
- Xiong, W., Cano, M., Wang, B., Douchi, D. & Yu, J. The plasticity of cyanobacterial carbon metabolism. *Curr. Opin. Chem. Biol.* **41**, 12–19 (2017).
- Xiong, W. *et al.* Phosphoketolase pathway contributes to carbon metabolism in cyanobacteria. *Nat. Plants* **2**, 1–8 (2015).
- Liu, L. *et al.* Phosphoketolase pathway for xylose catabolism in *Clostridium acetobutylicum* revealed by <sup>13</sup>C metabolic flux analysis. *J. Bacteriol.* **194**, 5413–5422 (2012).
- Kim, J. *et al.* Flux balance analysis of primary metabolism in the diatom *Phaeodactylum tricornutum*. *Plant J. Cell Mol. Biol.* **85**, 161–176 (2016).
- Yu King Hing, N., Liang, F., Lindblad, P. & Morgan, J. A. Combining isotopically non-stationary metabolic flux analysis with proteomics to unravel the regulation of the Calvin–Benson–Bassham cycle in *Synechocystis* sp. PCC 6803. *Metab. Eng.* **56**, 77–84 (2019).
- Knoop, H. *et al.* Flux balance analysis of cyanobacterial metabolism: the metabolic network of *Synechocystis* sp. PCC 6803. *PLoS Comput. Biol.* **9**, e1003081 (2013).
- Jablonsky, J., Papacek, S. & Hagemann, M. Different strategies of metabolic regulation in cyanobacteria: from transcriptional to biochemical control. *Sci. Rep.* **6**, 33024 (2016).
- Moriyama, T., Tajima, N., Sekine, K. & Sato, N. Characterization of three putative xylose 5-phosphate/fructose 6-phosphate phosphoketolases in the cyanobacterium *Anabaena* sp. PCC 7120. *Biosci. Biotechnol. Biochem.* **79**, 767–774 (2015).
- Sánchez, B., Zúñiga, M., González-Candelas, F., de los Reyes-Gavilán, C. G. & Margolles, A. Bacterial and eukaryotic phosphoketolases: phylogeny, distribution and evolution. *J. Mol. Microbiol. Biotechnol.* **18**, 37–51 (2010).
- Glenn, K. & Smith, K. S. Allosteric regulation of *Lactobacillus plantarum* xylose 5-phosphate/fructose 6-phosphate phosphoketolase (Xfp). *J. Bacteriol.* **197**, 1157–1163 (2015).
- Nakahara, K., Yamamoto, H., Miyake, C. & Yokota, A. Purification and characterization of class-I and class-II fructose-1,6-bisphosphate aldolases from the cyanobacterium *Synechocystis* sp. PCC 6803. *Plant Cell Physiol.* **44**, 326–333 (2003).
- Young, J. D., Shastri, A. A., Stephanopoulos, G. & Morgan, J. A. Mapping photoautotrophic metabolism with isotopically nonstationary (<sup>13</sup>C) flux analysis. *Metab. Eng.* **13**, 656–665 (2011).
- Krüseemann, J. L. *et al.* Artificial pathway emergence in central metabolism from three recursive phosphoketolase reactions. *FEBS J.* **285**, 4367–4377 (2018).
- Hackenbarg, C. *et al.* Low-carbon acclimation in carboxysome-less and photorespiratory mutants of the cyanobacterium *Synechocystis* sp. strain PCC 6803. *Microbiol. Read. Engl.* **158**, 398–413 (2012).
- Yoshikawa, K. *et al.* Integrated transcriptomic and metabolomic analysis of the central metabolism of *Synechocystis* sp. PCC 6803 under different trophic conditions. *Biotechnol. J.* **8**, 571–580 (2013).
- Nakajima, T. *et al.* Integrated metabolic flux and omics analysis of *Synechocystis* sp. PCC 6803 under mixotrophic and photoheterotrophic conditions. *Plant Cell Physiol.* **55**, 1605–1612 (2014).
- Eisenhut, M. *et al.* Metabolome phenotyping of inorganic carbon limitation in cells of the wild type and photorespiratory mutants of the *Cyanobacterium* *Synechocystis* sp. strain PCC 6803. *Plant Physiol.* **148**, 2109–2120 (2008).
- Schwarz, D., Orf, L., Kopka, J. & Hagemann, M. Effects of inorganic carbon limitation on the metabolome of the *Synechocystis* sp. PCC 6803 mutant defective in *glnB* encoding the central regulator PII of cyanobacterial C/N acclimation. *Metabolites* **4**, 232–247 (2014).
- Dempo, Y., Ohta, E., Nakayama, Y., Bamba, T. & Fukusaki, E. Molar-based targeted metabolic profiling of cyanobacterial strains with potential for biological production. *Metabolites* **4**, 499–516 (2014).
- Jablonsky, J., Hagemann, M., Schwarz, D. & Wolkenhauer, O. Phosphoglycerate mutases function as reverse regulated isoenzymes in *Synechococcus elongatus* PCC 7942. *PLoS ONE* **8**, e58281 (2013).

## Acknowledgements

This work was supported by the Ministry of Education, Youth and Sports of the Czech Republic—projects CENAKVA (LM2018099) and the CENAKVA Centre Development (No. CZ.1.05/2.1.00/19.0380).

## Author contributions

Jointly discussed ideas and concepts: J.J. and A.B. The modeling was done by: J.J. Bioinformatic analysis was done by: A.B. The manuscript was written by A.B. and J.J.

## Competing interests

The authors declare no competing interests.

## Additional information

**Supplementary Information** The online version contains supplementary material available at <https://doi.org/10.1038/s41598-020-78475-z>.

**Correspondence** and requests for materials should be addressed to J.J.

**Reprints and permissions information** is available at [www.nature.com/reprints](http://www.nature.com/reprints).

**Publisher's note** Springer Nature remains neutral with regard to jurisdictional claims in published maps and institutional affiliations.

[www.nature.com/scientificreports/](http://www.nature.com/scientificreports/)



**Open Access** This article is licensed under a Creative Commons Attribution 4.0 International License, which permits use, sharing, adaptation, distribution and reproduction in any medium or format, as long as you give appropriate credit to the original author(s) and the source, provide a link to the Creative Commons licence, and indicate if changes were made. The images or other third party material in this article are included in the article's Creative Commons licence, unless indicated otherwise in a credit line to the material. If material is not included in the article's Creative Commons licence and your intended use is not permitted by statutory regulation or exceeds the permitted use, you will need to obtain permission directly from the copyright holder. To view a copy of this licence, visit <http://creativecommons.org/licenses/by/4.0/>.

© The Author(s) 2020

## CHAPTER 3

### **ENTNER-DOUDOROFF PATHWAY IN *SYNECHOCYSTIS* PCC 6803: PROPOSED REGULATORY ROLES AND ENZYME MULTIFUNCTIONALITIES**

Bachhar, A., Jablonsky, J., 2022. Entner-Doudoroff pathway in *Synechocystis* PCC 6803: Proposed regulatory roles and enzyme multifunctionalities. *Front. Microbiol.* 13, 967545.

Open access: This article is licensed under a Creative Commons Attribution 4.0 International License (CC By 4.0), which permits use, sharing, adaptation, distribution and reproduction in any medium or format, as long as you give appropriate credit to the original author(s).

My contribution in this work 50%.







OPEN ACCESS

EDITED BY  
Weiwen Zhang,  
Tianjin University, China

REVIEWED BY  
Maurycy Daroch,  
Peking University, China  
Jun Ni,  
Shanghai Jiao Tong University, China  
Wenqiang Yang,  
Institute of Botany (CAS), China

\*CORRESPONDENCE  
Jiri Jablonsky  
jiri.jablonsky@gmail.com

SPECIALTY SECTION  
This article was submitted to  
Microbial Physiology and Metabolism,  
a section of the journal  
Frontiers in Microbiology

RECEIVED 04 July 2022  
ACCEPTED 25 July 2022  
PUBLISHED 16 August 2022

CITATION  
Bachhar A and Jablonsky J (2022)  
Entner-Doudoroff pathway  
in *Synechocystis* PCC 6803: Proposed  
regulatory roles and enzyme  
multifunctionalities.  
*Front. Microbiol.* 13:967545.  
doi: 10.3389/fmicb.2022.967545

COPYRIGHT  
© 2022 Bachhar and Jablonsky. This is  
an open-access article distributed  
under the terms of the [Creative  
Commons Attribution License \(CC BY\)](#).  
The use, distribution or reproduction in  
other forums is permitted, provided  
the original author(s) and the copyright  
owner(s) are credited and that the  
original publication in this journal is  
cited, in accordance with accepted  
academic practice. No use, distribution  
or reproduction is permitted which  
does not comply with these terms.

# Entner-Doudoroff pathway in *Synechocystis* PCC 6803: Proposed regulatory roles and enzyme multifunctionalities

Anushree Bachhar and Jiri Jablonsky\*

Institute of Complex Systems, FFPW, University of South Bohemia, CENAKVA, Nove Hradky, Czechia

The Entner-Doudoroff pathway (ED-P) was established in 2016 as the fourth glycolytic pathway in *Synechocystis* sp. PCC 6803. ED-P consists of two reactions, the first catalyzed by 6-phosphogluconate dehydratase (EDD), the second by keto3-deoxygluconate-6-phosphate aldolase/4-hydroxy-2-oxoglutarate aldolase (EDA). ED-P was previously concluded to be a widespread (~92%) pathway among cyanobacteria, but current bioinformatic analysis estimated the occurrence of ED-P to be either scarce (~1%) or uncommon (~47%), depending if dihydroxy-acid dehydratase (ilvD) also functions as EDD (currently assumed). Thus, the biochemical characterization of ilvD is a task pending to resolve this uncertainty. Next, we have provided new insights into several single and double glycolytic mutants based on kinetic model of central carbon metabolism of *Synechocystis*. The model predicted that silencing 6-phosphogluconate dehydrogenase (*gnd*) could be coupled with ~90% down-regulation of G6P-dehydrogenase, also limiting the metabolic flux via ED-P. Furthermore, our metabolic flux estimation implied that growth impairment linked to silenced EDA under mixotrophic conditions is not caused by diminished carbon flux via ED-P but rather by a missing mechanism related to the role of EDA in metabolism. We proposed two possible, mutually non-exclusive explanations: (i)  $\Delta eda$  leads to disrupted carbon catabolite repression, regulated by 2-keto3-deoxygluconate-6-phosphate (ED-P intermediate), and (ii) EDA catalyzes the interconversion between glyoxylate and 4-hydroxy-2-oxoglutarate + pyruvate in the proximity of TCA cycle, possibly effecting the levels of 2-oxoglutarate under  $\Delta eda$ . We have also proposed a new pathway from EDA toward proline, which could explain the proline accumulation under  $\Delta eda$ . In addition, the presented *in silico* method provides an alternative to

$^{13}\text{C}$  metabolic flux analysis for marginal metabolic pathways around/below the threshold of ultrasensitive LC-MS. Finally, our *in silico* analysis provided alternative explanations for the role of ED-P in *Synechocystis* while identifying some severe uncertainties.

## KEYWORDS

Entner-Doudoroff pathway, kinetic model, metabolic regulation, glycolysis, cyanobacteria

## Introduction

*Synechocystis* sp. PCC 6803 (*Synechocystis*) is a model cyanobacterial organism with complex carbon metabolism, reported to contain all known glycolytic routes found so far in cyanobacteria: (i) Embden-Meyerhof-Parnas pathway (EMP-P), (ii) oxidative pentose phosphate pathway (OPP-P), (iii) lately characterized (Xiong et al., 2015) phosphoketolase pathway (PKET-P) and (iv) recently identified and quantified (Chen et al., 2016; Makowka et al., 2020) Entner-Doudoroff pathway (ED-P). These four glycolytic pathways, doing a similar job, could be seen as contra-productive, like having a substantial number of isozymes. Nevertheless, the cellular resources are not being wasted, as all these “redundancies” allow enhanced robustness of metabolism, including adaptability to the changing environment (Xiong et al., 2017) and reduction of total protein cost (Jablonsky et al., 2016). This metabolic plasticity found in *Synechocystis* is clearly an evolutionary advantage under turbulent environmental conditions but makes the understanding of metabolic regulation rather challenging.

Entner-Doudoroff pathway (ED-P) is the shortest glycolytic route, consisting of only two reactions. The first one is catalyzed by 6-phosphogluconate dehydratase (EDD, *slr0452*, currently annotated as *ilvD* – dihydroxy-acid dehydratase), producing 2-keto3-deoxygluconate-6-phosphate (KDPG). The second reaction is catalyzed by keto3-deoxygluconate-6-phosphate aldolase (EDA, *sllo107*), producing pyruvate and glyceraldehyde 3-phosphate (Figure 1, blue). It should be noted that while only phosphorylated ED-P has been reported in *Synechocystis* (Chen et al., 2016), there are multiple branches of ED-P (namely phosphorylated, semi-phosphorylated, and non-phosphorylated) that can co-exist in a single organism as shown for *Sulfolobus solfataricus* (Figueiredo et al., 2017). More details about the different branches of ED-P and the enzymes involved can be found in a recently published comprehensive review (Kopp et al., 2020).

The protein cost of ED-P is 72% less while providing one less ATP (Flamholz et al., 2013) in comparison to EMP-P. Further, ED-P provides less NADPH than OPP-P but is more carbon-efficient (Asplund-Samuelsson and Hudson, 2021). Significant growth impairment was reported for EDA knockout ( $\Delta eda$ ),

both under autotrophic and mixotrophic conditions, up to 18% and 57% (Makowka et al., 2020), respectively. However, the exact factors behind observed growth impairment are somewhat unclear. The current lack of information on ED-P is partially due to unknown metabolic flux and the neglected possible signaling role of KDPG, identified in other organisms (Fuhrman et al., 1998; Kim et al., 2009). Therefore, we aim to address the current issues related to ED-P with the help of *in silico* analysis.

## Materials and methods

### Bioinformatic analysis: Standard and alternative calculation

To quantify the occurrence of each known glycolytic pathway, we chose four enzymes specific to those pathways based on their position and essentiality within the metabolic network: (i) 6-phosphogluconate dehydrogenase (GND) for OPP pathway, (ii) phosphoketolase (PKET) for PKET pathway, (iii) keto3-deoxygluconate-6-phosphate aldolase (EDA) for ED pathway and (iv) phosphofructokinase (PFK) for upper EMP pathway. The raw data for the occurrence of the marker enzymes were collected from UniProt (Supplementary file 1)<sup>1</sup> and later on verified using NCBI<sup>2</sup> and KEGG<sup>3</sup> databases. The collected data were then curated by discarding repetitive and discontinued amino acid sequences. In the case of isoenzymes, only one of them was counted. Finally, the percentage of occurrence of each enzyme was calculated against the list of total species of cyanobacteria found to date (Supplementary file 1). Along with the standard approach, an alternative approach was also employed to remove the influence of the heterogeneity in the size of different genera and marker occurrence within a particular genus. The alternative approach for the occurrence of enzyme markers was calculated as the sum of the first positive hits from each genus, divided by the sum of the first positive

1 <https://www.uniprot.org>

2 <https://www.ncbi.nlm.nih.gov/protein>

3 <https://www.genome.jp/kegg>

and first negative hits for each genus. An example of alternative calculation: based on our database ([Supplementary file 1](#)), the genus *Anabena* has 11 species, 10 of them with PFK. Thus, the particular result for *Anabena* will increase the numerator by one and the denominator by two in the alternative calculation for PFK among cyanobacteria.

## Sources of experimental data for kinetic parameters estimation

<sup>13</sup>C labeling data for autotrophic growth ([Hing et al., 2019](#)).

<sup>13</sup>C labeling data for mixotrophic growth ([Nakajima et al., 2014](#)).

## General information about the model

The multi-level kinetic model for *Synechocystis* was developed and simulations were executed using the SimBiology, Optimization, Global optimization and Parallel computing toolboxes of MATLAB (MathWorks, Inc., Natick, Massachusetts, United States of America). The routine for parameter estimation was a hybrid genetic algorithm. The model versions for tested growth conditions ([Supplementary files 5, 6](#)) are available in the SBML format L2V4, compatible with MATLAB 2010b–2014.

The scope of the model includes the following parts of central carbon metabolism: Calvin-Benson cycle, photorespiration, all glycolytic pathways (Embden–Meyerhof–Parnas pathway, Entner–Doudoroff pathway, phosphoketolase pathway and oxidative pentose phosphate) with simplified carbohydrate and biomass synthesis (weighted sum of sink reactions). These metabolic reactions were coupled with simplified light reactions,  $C_i$  and glucose uptake as the primary input parameters. This model is an updated version of the previous model employed for the analysis of PKET pathway ([Bachhar and Jablonsky, 2020](#)). The current model consists of 60 reactions, 49 metabolites and 199 kinetic parameters. The enzymatic reactions were described by Michaelis-Menten kinetics with an exception for the light reactions,  $C_i$  and glucose uptake (mass action kinetics). The list of all parameters within the model can be found in [Supplementary file 2](#).

## General information about the model

The constraint of model parameters occurred in several steps. Firstly, the original model of *Synechocystis* without ED-P ([Jablonsky et al., 2016](#)) was fitted on available fluxomic data from cells grown autotrophically at high  $CO_2$ . Then, we applied transcriptomic data as weight factors for each estimated  $V_{max}$  in simulated shifts to autotrophic ambient  $CO_2$ , followed

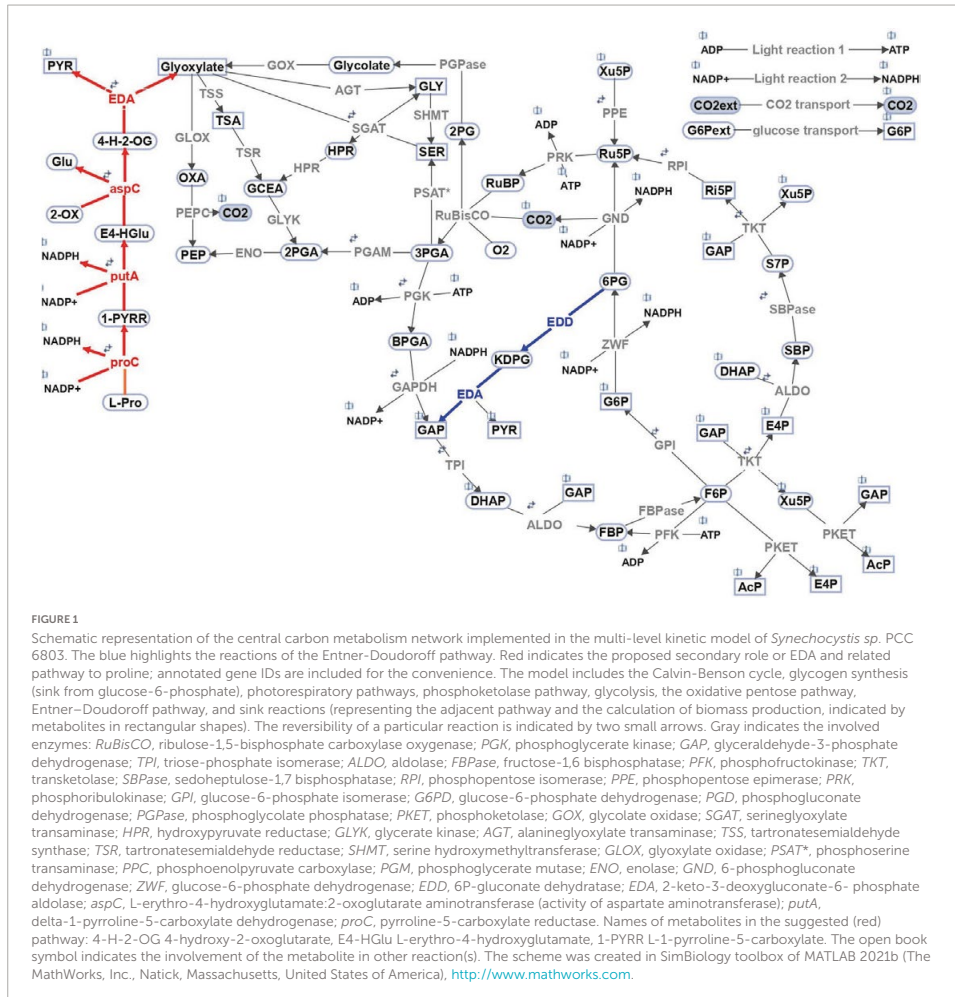
by mixotrophic ambient  $CO_2$ . Thus, we were searching for a single set of kinetic parameters describing all growth conditions. However, we are currently able to describe only autotrophic growth conditions (ambient and high  $CO_2$ ) with a single set of parameters; mixotrophic growth conditions are verified separately to respective fluxomic data. The justification and broader description of this part of our Methodology can be found in our previous work ([Jablonsky et al., 2016](#)).

Next, we have implemented a simplified, single reaction version of ED-P within the highly constrained model and fitted the flux *via* ED-P to match the reported levels of growth impairment. Additional constraining of parameter space was achieved by matching reported growth changes for single and double mutants from all glycolytic pathways, including silenced *eda* (keto3-deoxygluconate-6-phosphate aldolase), which represented blocked ED-P. After a confirmation that the metabolic fluxes available *via* ED-P cannot explain the reported level of growth impairment under mixotrophic conditions, we have incorporated a full version of ED-P (EDA and EDD) and tested the impact of accumulation and possible excretion of KDPG (intermediate of ED-P) as well as other scenarios under autotrophic conditions. Since all these scenarios are based on carbon availability which plays a marginal role under mixotrophic conditions, we proposed that the missing link, allowing us to explain the experimental data, is the signaling role of KDPG (carbon catabolite repression). We did not perform any simulations based on the signaling role of KDPG as the growth impairment caused by  $\Delta eda$  provides a sufficient description only of its impact, but new experimental data are needed to determine the kinetics of the signaling process. The current version of the model assumes a very low level of KDPG for WT, based on reported undetectable levels ([Will et al., 2019](#); [Schulze et al., 2022](#)).

## Results and discussion

### Occurrence of glycolytic pathways in cyanobacteria: Standard vs. alternative view

Cyanobacteria possess four glycolytic pathways, which play an essential role in metabolic adaptation and can even alternate with each other ([Xiong et al., 2017](#)). Previously, ED-P was concluded to be a widespread pathway in cyanobacteria, almost twice as common as upper EMP-P ([Chen et al., 2016](#)). However, our current bioinformatic analyses of all glycolytic pathways showed a very different result ([Table 1](#)). This discrepancy was probably caused by the influx of new species into the databases. Current data implies that the occurrence of EDD/ilvD (see the explanation below) in cyanobacteria is approximately 92% ([Table 1](#)) which is comparable to PKET and GND occurrences. Nevertheless, the occurrence of ED-P (based on EDA) drops



to 46.9% (Table 1), which is only half of the previous value (Chen et al., 2016). We note that the occurrence of EDA calculated in November 2015 (Chen et al., 2016) matches the occurrence for EDD/ilvD in 2021 (Table 1). Thus, ED-P goes down from one of the most common (Chen et al., 2016) to the rarest glycolytic pathway among cyanobacteria. Finally, going back to EDD, the previous (Chen et al., 2016) and our calculation of its occurrence is based on an assumption of dual functionality of EDD and ilvD (dihydroxy-acid dehydratase) in a single enzyme EDD/ilvD (Chen et al., 2016) but the corresponding gene is annotated to express

ilvD only. However, there is less than 50% similarity of ilvD (*Synechocystis*) toward EDD in *E. coli* (k 12) or *Pseudomonas* while ilvD from *E. coli* and *Pseudomonas* showed between 55 and 65% similarity with ilvD from *Synechocystis*, respectively. Currently, there are only four cyanobacteria annotated with a native (single functioning) EDD (Supplementary file 4). This fact may imply two origins of EDD among cyanobacteria, either associated with ilvD as assumed before (Chen et al., 2016) (4.2.1.9) or standalone enzyme (4.2.1.12), which would imply that ED-P is extremely rare (below 1% occurrence, Table 1) among cyanobacteria.

TABLE 1 Occurrence of marker enzymes among cyanobacteria [%].

| Pathway           | upper EMP |      | ED       |     | PKET | OPP  |
|-------------------|-----------|------|----------|-----|------|------|
|                   | PFK       | EDA  | EDD/ilvD | EDD | PKET | GND  |
| Chen et al., 2016 | 52.0      | NA   | 92.0     | NA  | NA   | NA   |
| 2021 standard     | 64.1      | 46.9 | 91.9     | 0.7 | 81.6 | 89.3 |
| 2021 alternative  | 70.3      | 65.2 | 80.1     | 3.6 | 89.6 | 90   |

The key enzymes were selected based on their position and role within a particular glycolytic pathway: upper Embden-Meyerhof-Parnas pathway – PFK, phosphoketolase pathway – PKET, oxidative pentose phosphate pathway – GND and Entner-Doudoroff pathway – EDA. EDD is shown either as a native enzyme or as the dual function enzyme annotated as dihydroxy-acid dehydratase (ilvD), involved in the synthesis of valine and isoleucine (Chen et al., 2016). The percentages were calculated based on the total species of cyanobacteria identified in Uniprot and the number of cyanobacteria identified with the annotated enzyme.

In the case of *Synechocystis*, there is no mention of gluconate as a substrate for ilvD in recent biochemical analysis (Zhang et al., 2020). Nevertheless, a product of EDD, KDPG, has been detected in a single study (Chen et al., 2016) while determined to be undetectable in others (Will et al., 2019; Schulze et al., 2022). The situation is further complicated by an approximately 30-fold difference in 6-phosphogluconate (a substrate of EDD) level under autotrophic vs. mixotrophic conditions (Yoshikawa et al., 2013), which might be the reason for the elusiveness of KDPG in metabolic profiling. However, KDPG was previously detected not only for WT but also for silenced *zwf* (glucose-6-phosphate dehydrogenase) (Chen et al., 2016). At that time, it was suspected that ZWF was not the only source of 6-phosphogluconate (Chen et al., 2016), but no evidence was found to support it. The possible remaining explanations for detected KDPG are rather questionable: (i) silencing *zwf* has either low efficiency or gets repaired fast; however, no accumulation of 6-phosphogluconate was reported for  $\Delta zwf$  (Makowka et al., 2020) or (ii) EDA conducts reversible reaction and thus can produce a significant amount of KDPG from pyruvate and glyceraldehyde 3-phosphate without a functional EDD. All these questions and uncertainties show that more experiments are needed to verify the status of ED-P not only in *Synechocystis* but generally in cyanobacteria. For the sake of further analysis, we will operate with EDA as a marker enzyme for ED-P occurrence.

Another point one should consider in any bioinformatic analysis is substantial heterogeneity in the number of species per genus as well as in the occurrence of marker enzymes within a particular genus, e.g., genus *Prochlorococcus* does not contain either PKET or PFK (Supplementary file 1). Therefore, we also present an alternative bioinformatic analysis of the occurrence of glycolytic marker enzymes, which shifts the focus from occurrence among species toward occurrence among the genera (see Methodology). This alternative calculation showed an approximate 18% and 11% change in the occurrence of EDA and EDD, respectively, in comparison to the standard calculation (Table 1). A lower level of correction could also be observed for PFK and PKET in contrast to minor change for GND (Table 1). Interestingly, the alternative calculation did not

change the ranking in the occurrence of glycolytic enzymes but lowered the occurrence of EDD/ilvD among cyanobacteria. This finding contradicts the known essentiality of ilvD for amino acid synthesis (Leyval et al., 2003; Kim and Lee, 2006). The cumulated bioinformatic data (Supplementary file 1) indicate that difference between the standard and alternative analysis is caused by a higher amount of negative occurrence of EDD/ilvD, primarily due to the single species genera (only one species identified in the genus). This problem could be due to the lack of experimental characterization and annotation of the enzyme-specific genes for those species. Currently, we cannot say what the possible implications of this finding are, but ED-P remains to be one of the most overlooked pathways in cyanobacteria. Finally, ED-P is known to regulate organic carbon intake in other species such as *Pseudomonas* (Daddaoua et al., 2009), so one could speculate that ED-P is found mostly or only in mixotrophic cyanobacteria. However, this is not the case as EDA is missing in many mixotrophic species, e.g., genera *Microcystis* and *Moorea*, yet could be found in obligatory photoautotrophs, e.g., genus *Prochlorococcus*. The observed low occurrence of ED-P, as well as the missing link to any growth conditions, open a question regarding its evolutionary importance among cyanobacteria. The distribution of EDA, EDD/ilvD and EDD in cyanobacteria, as well as the other glycolytic markers, is provided in Supplementary file 1.

Furthermore, the alternative approach grouped the upper EMP and ED pathways on one side (around 70%, Table 1) and OPP and PKET pathways on the other side (around 90%, Table 1). To detect a possible correlation, we searched for the occurrence of combinations of any two glycolytic pathways among cyanobacteria. The highest positive correlation was found between OPP and PKET pathways (84.8%, Table 2), further supporting our recent finding of the higher importance of PKET pathway (Bachhar and Jablonsky, 2020). Surprisingly, the lowest correlation was found between upper EMP and ED-P which also corresponds with single marker presence of EDA vs other markers (around 44%) (Table 2). Also, the number of cyanobacterial species without either of these pathways is, on average, three times higher than other combinations of glycolytic pathways. Approximately 40% of cyanobacteria is

“alternating” between upper EMP and ED-P (Table 2), e.g., *Calothrix desertica* PCC 7102 does not have any annotated *pfk* but has by two EDD/ilvD isozymes, DSM106972\_077550 and DSM106972\_030530 (Supplementary file 3). Having two EDD isozymes could increase the flux via ED-P, which may compensate for the incomplete upper EMP (Will et al., 2019) (Figure 1). On the other hand, genera *Microcystis*, *Moorea* and *Symploca*, known for their production of important secondary metabolites (Linington et al., 2008; Engene et al., 2012; Pimentel and Giani, 2014), do not have annotated ED-P (UniPathway) but contain more than one PFK isozyme (UniProt). Finally, ED-P is the least preferred to supplement any other glycolytic pathways (Table 2). This result further questions the role and benefits of ED-P in cyanobacteria; hence we decided to run a comprehensive analysis based on mutants from all four glycolytic pathways for model cyanobacterium *Synechocystis*.

## Glycolytic mutants and their impact on growth

The growth impact for all single and some of the double mutants of glycolytic pathways have been studied in recent years (Xiong et al., 2015; Chen et al., 2016; Bachhar and Jablonsky, 2020; Makowka et al., 2020). Thus, our initial step was to mimic the reported growth impairments related to ED-P as well as for other glycolytic pathways and their combinations. The model was constrained not only by previously reported growth impairments found for different mutants but also by fluxomic data (WTs only). These constraints significantly limit the parameter space as the model was required to match all available data simultaneously. Finally, gathering data from all mutants of enzyme markers and their combinations provided a more accurate analysis rather than focusing only on the mutant of EDA.

First, let us have a look at the results of single mutants under autotrophic (AC-auto) conditions. Simulated  $\Delta eda$  and double mutant of PFK1,2 ( $\Delta pfk$ ) followed the reported mean growth impacts (around -2%) (Makowka et al., 2020), see Table 3. Whereas for  $\Delta pket$  (double mutant of PKET1 and PKET2), no experimental data are available, but previously reported 11% growth impairment for  $\Delta pket1$  (Xiong et al., 2015) is in line with the simulated 14% growth loss for  $\Delta pket$ ; this result is based on predicted supremacy of PKET1 (Bachhar and Jablonsky, 2020). Additionally, *in silico* silencing of GND ( $\Delta gnd$ ) leads to a massive 43% growth increase under AC-auto and a significant carbon flux redistribution within the central carbon metabolism (Figure 2,  $\Delta gnd$ ), which is in disagreement with previously reported statistically insignificant impact (around + 2%) in comparison to WT (Chen et al., 2016; Makowka et al., 2020). The predicted growth increase, triggered by  $\Delta gnd$ , is mostly a consequence of reduced decarboxylation via OPP-P. Such discrepancy of the predicted vs. reported growth, not resolved by

model parameters tuning, can be explained only by a conclusion that silencing *gnd* is coupled with other changes in metabolic regulation, so far not considered in the model. After testing various scenarios, the easiest and most reasonable way to negate this massive *in silico* growth increase is to couple silencing *gnd* with >90% down-regulation of G6P-dehydrogenase (*zwf*). We denoted this scenario as  $\Delta gnd^*$  (asterisk differentiates from simple *in silico* *gnd* mutant discussed above) and the flux values and growth impact for  $\Delta gnd^*$  are shown in Figure 2 and Table 3, respectively. Very significant down-regulation of *zwf* as a consequence of  $\Delta gnd$  was reported previously for *Gluconobacter oxydans* (Richhardt et al., 2012), which supports our model prediction related to the real impact of silencing *gnd* in *Synechocystis*. An important consequence of *zwf* inhibition is a significant reduction in the production of 6-phosphogluconate, which is the key substrate for ED-P (Figure 1). When we accumulate all the effects of *in silico*  $\Delta gnd^*$ , i.e.,  $\Delta gnd$ , down-regulated *zwf* and limited EDD, the result is in agreement with the previous experimental value for what is believed to be simply  $\Delta gnd$  (Makowka et al., 2020) (Table 3).

Secondly, the double mutants under AC-auto implied some significant growth impairment which demands a closer look. The highest simulated negative growth impact was found for double mutant  $\Delta gnd^* \Delta pket$ , i.e., 49.5% (Table 3). This prediction is not surprising based on the fact that GND and PKET were the only two tested glycolytic markers not missing together in any analyzed cyanobacteria (Table 2), emphasizing the essential role of PKET-P and OPP-P under AC-auto. Moreover, this double mutant is close to the triple mutant ( $\Delta gnd \Delta pket \Delta eda$ ) due to the above predicted and discussed the real impact of  $\Delta gnd^*$ , which was greatly limiting the flux via ED-P (Figure 2). Another significant predicted growth impairment was found for  $\Delta eda \Delta pket$  (29.6%, Table 3), which is not a simple addition of respective single mutants as it surpasses the cumulative impact of both single mutants almost by 20%. This implies that blocking both glycolytic pathways protecting against decarboxylation via OPP-P and EMP-P might have an additional negative influence on the sustainability of the Calvin-Benson cycle, at least in the model.

Finally, the model failed to match the reported (~60%) growth impairment (Makowka et al., 2020) for  $\Delta eda \Delta gnd$  under autotrophic conditions (Table 3). If we consider our prediction of what the meaning of  $\Delta gnd$  is, i.e.,  $\Delta gnd^*$ , one may expect an accumulation of 6-phosphogluconate due to some degree still functioning ZWF. Inhibition of sugar-phosphate metabolism by 6-phosphogluconate was already emphasized for other species (Richhardt et al., 2012) and its accumulation was confirmed for  $\Delta eda \Delta gnd$  in *Synechocystis* (Makowka et al., 2020). Other co-explanations of significant growth impairment could be i) partial accumulation of KDPG due to functioning EDD, although possibly inhibited by  $\Delta eda$  and ii) other metabolic functions of EDA, which are further discussed in the next section. However, an experimental verification for the

TABLE 2 Occurrence of marker enzyme couples among cyanobacteria [%].

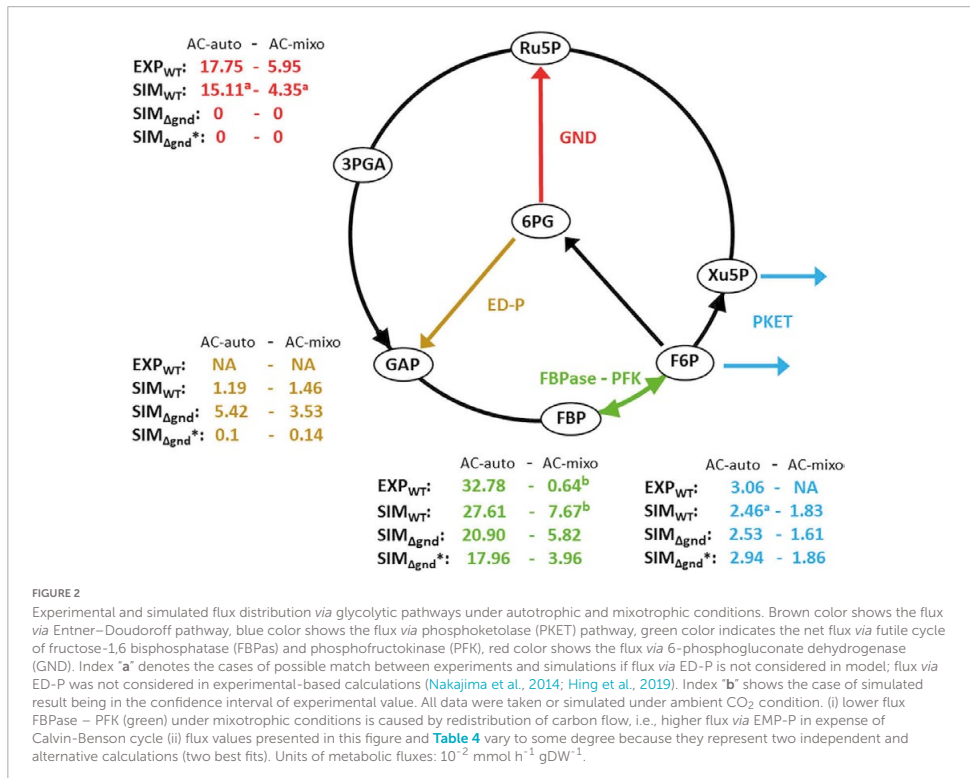
| Occurrence | PFK vs. EDA | GND vs. PKET | PFK vs. GND | PFK vs. PKET | PKET vs. EDA | EDA vs. GND |
|------------|-------------|--------------|-------------|--------------|--------------|-------------|
| ++         | 39.7        | 84.79        | 67.72       | 65.86        | 47.31        | 49.72       |
| -          | 19.48       | 0            | 1.67        | 8.35         | 8.35         | 2.23        |
| +-         | 40.82       | 15.21        | 30.61       | 25.79        | 44.34        | 48.05       |

"+-" denotes the presence of one of the markers within a particular couple, regardless of their order. "++" and "--" indicate both present and both absent, respectively (all data are available in [Supplementary file 1](#)). The percentages were calculated based on the total species of cyanobacteria found (UniProt, 2021) against the number of cyanobacteria with marker enzyme. ED pathway consists of only two enzymes, EDD and EDA, and thus the less occurring enzyme should be the marker. Due to extremely low occurrence of native EDD among cyanobacteria (around 100-fold difference vs. other markers) and the fact of *ilvD* functioning as EDD is the current opinion (Chen et al., 2016), we considered EDA (less common than *ilvD*) as the marker enzyme for ED-P in this analysis.

TABLE 3 Simulated growth rate changes (%) caused by single and double mutants of marker glycolytic enzymes under autotrophic and mixotrophic conditions.

|                | $\Delta pfk$ | $\Delta eda$ | $\Delta gnd^*$ | $\Delta pkt$ |
|----------------|--------------|--------------|----------------|--------------|
| $\Delta pfk$   | -1.8 -0.2    | -11.2        | 3.2            | -14.5        |
| $\Delta eda$   | -5.4         | -1.3 -11.0   | 0              | -29.6        |
| $\Delta gnd^*$ | 2.9          | 5.4          | 5.9 1.7        | -49.5        |
| $\Delta pkt$   | 1.5          | -1.0         | 6.1            | 0.5 -14.0    |

Roman font indicates autotrophic and bold shows mixotrophic results. Asterisk denotes  $\Delta gnd$ , including the assumed inhibition of *zwf*.  $\Delta pfk$  and  $\Delta pkt$  indicate double mutants of isozymes. The results were rounded to the first decimal place. The available experimental values are shown and discussed in the text.



role of 6-phosphogluconate accumulation, level of KDPG and preferably also fluxomic data for these mutants are needed.

Next, we focused on growth data for AC-mixo. Due to the unavailability of experimental data for  $\Delta$ pket and for most of the double mutants, it is difficult to discuss the results of simulations. However, the highest growth impairment caused by  $\Delta$ eda $\Delta$ pfk (5.4%, **Table 3**) can be justified easily as both EDA and PFK supports the flux *via* the dominant glycolytic route under AC-mixo, EMP glycolysis (Nakajima et al., 2014). In the case of  $\Delta$ gnd\*, the simulated 5.9% growth increase (**Table 3**) is in agreement with the recently reported value (Makowka et al., 2020). The only serious discrepancy between experiments and simulations for single mutant was found for  $\Delta$ eda; the predicted growth impairment under AC-mixo is around 1.3% (**Table 3**) which is in contrast to previously reported up to 57% (Makowka et al., 2020) growth impairment. The possible explanation of growth impairment caused by  $\Delta$ eda is elaborated in the next section.

Lastly, one can observe a relatively lower *in silico* flux *via* OPP-P (**Figure 2**) for WT compared to the experimental results (**Figure 2**). However, for  $\Delta$ eda, the model matches the reported flux *via* OPP-P (as well as *via* PKET-P) (WT) (**Figure 2** vs. **Table 4**). Since ED-P and OPP-P are closely connected (**Figure 1**) and ED-P was either not considered in the previous fluxomic analyses (Nakajima et al., 2014), or the flux *via* ED-P was not detected and assumed too low (Schulze et al., 2022). Thus, our simulation offers both an alternative solution and a possible revision of the available fluxomic data.

## Two components of growth impairment caused by $\Delta$ eda

Besides the reported mean growth impairment, there are also time-series data (Chen et al., 2016), (Makowka et al., 2020) for  $\Delta$ eda, which can shed new light on the role of EDA. However, the model is able to mimic only the last day of the time-series experiment under both conditions (**Figures 3A** day 5, **3B** day 7). When we take a closer look at gaps between experimental and simulated results under AC-auto, the maximal difference is ~2-fold (**Figure 3B**, day 4). Such difference could be eliminated by tuning parameters within the model, followed by a justifiable explanation of the physiological meaning behind an observed change in metabolic fluxes triggered by  $\Delta$ eda. On the other hand, the maximal difference under AC-mixo is ~50-fold (**Figure 3A**, day 2) and clearly diminishes by the end of the experiment (Makowka et al., 2020). Since the simulated growth impairment (1.3%) under AC-mixo is the maximum possible value achievable by the model within given constraints (fluxomic and mutant growth data), an essential function of ED-P is missing in the model. By comparing experimental and simulated results, two classes of effects could be distinguished in the growth impairment, one class

not reflected whereas the other one included in the model. Since the un-reflected class diminishes over time, we call it a “temporal component.” The second class of effects is based only on metabolic flux differences between WT and  $\Delta$ eda, which could be stable unless the mutation is reversed; thus we call it a “permanent component.” Our model predicted that the permanent component is negligible under AC-mixo (**Figure 3A**) but is comparable with the impact of the temporal component under AC-auto (**Figure 3B**). Since the permanent component is related to metabolic flux *via* ED-P, its observed significant variation under AC-auto and AC-mixo could be explained either by a major change in flux *via* ED-P in one of the growth conditions or by carbon scarcity (auto- vs. mixotrophic).

The flux *via* ED-P has been so far unknown due to difficulties in measuring labeled metabolites produced by ED-P, i.e., pyruvate and glyceraldehyde-phosphate, as more prominent metabolic pathways (Calvin-Benson cycle and EMP glycolysis) produce them in higher quantities. By looking at metabolic fluxes estimated by our model, the flux *via* ED-P is slightly higher under mixotrophic conditions (**Figure 2**) and  $\Delta$ eda leads to an expected increase of flux *via* GND (**Table 4**). Thus, ED-P is almost unaffected by the major flux redistribution triggered by autotrophic and mixotrophic conditions (**Table 4**). Hence, we could conclude that the key factor influencing the permanent component variability is carbon scarcity. A connection between ED-P and carbon scarcity is by  $\Delta$ eda enhanced decarboxylation (**Figure 1**) under AC-auto, which was hypothesized previously (Makowka et al., 2020).

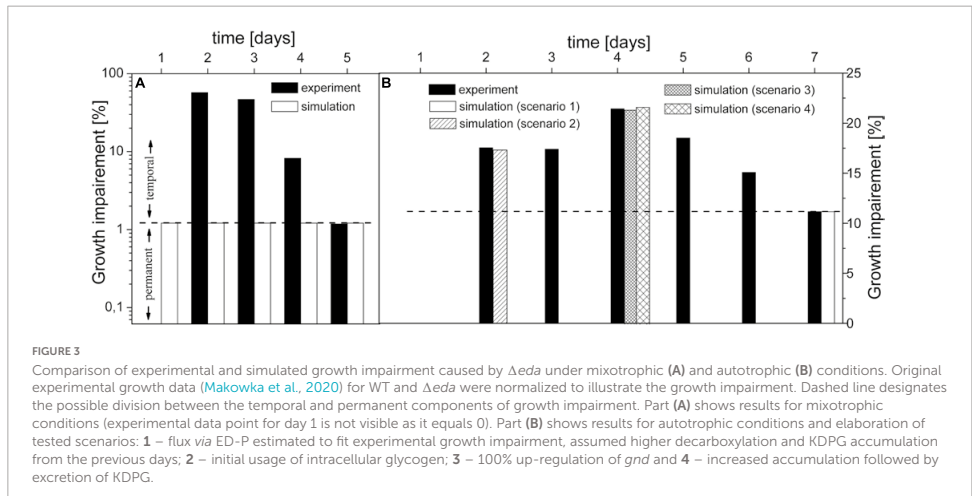
Now, the question remains is the origin behind the temporal component of growth impairment, which is not reflected in the model. If we start with AC-auto, we could assume that cultures used in growth experiments (Makowka et al., 2020) have started from a dormant state which explains zero growth impairment (Doello et al., 2018) on day 1 (Makowka et al., 2020) (**Figures 3A,B**). Thus, we hypothesize that both WT and  $\Delta$ eda initially utilized stored glycogen to restore the metabolism (Doello et al., 2018). It has been determined that the rate of glycogen depletion is several-fold slower for  $\Delta$ eda compared to WT under AC-auto (Makowka et al., 2020). So, we can speculate that glycogen lasted under  $\Delta$ eda till the end of day 3 (**Figure 3B**). As glycogen is processed mainly *via* OPP-P and ED-P (Doello et al., 2018), silencing *eda* would increase the flux *via* OPP-P, further enhancing the decarboxylation for the first three days. Our simulations indicated that *in silico* addition of glycogen amplifies the growth impairment (**Figure 3B**, scenario 2), but it is clear now that decarboxylation level based on the current activity of *gnd* (*sl0329*) itself could not explain the sudden boost in growth impairment on day 4 (presumably the day of depleted glycogen). The required increase in GND activity (~100% upregulation; **Figure 3B**, scenario 3) could be explained by posttranslational modification as predicted before for *Synechococcus* PCC 7942 (Jablonsky et al., 2016). The other potential explanation, besides the upregulation of *gnd*, is an



TABLE 4 Comparison of experimental and simulated metabolic fluxes.

| Enzymatic reaction        | Mixotrophic         |              |              | Autotrophic         |              |              |
|---------------------------|---------------------|--------------|--------------|---------------------|--------------|--------------|
|                           | <sup>13</sup> C exp | simulation   |              | <sup>13</sup> C exp | simulation   |              |
|                           | fit                 | WT           | $\Delta$ eda | fit                 | WT           | $\Delta$ eda |
| ext.G6P → G6P             | 9.12                | 8.97         | 0.00%        | 0                   | 0            | 0            |
| <u>KDPG → PYR + GAP</u>   | NA                  | 1.50         | -100%        | NA                  | 1.33         | -100%        |
| G6P → 6PG                 | 6.36                | <b>6.15</b>  | < ± 5%       | 17.75               | <b>16.15</b> | < ± 5%       |
| 6PG → Ru5P                | 6.36                | <b>4.65</b>  | 22.63%       | 17.75               | <b>14.82</b> | 9.74%        |
| 3PGA ↔ 2PGA               | 19.62               | 17.96        | 5.57%        | 1.27                | <b>1.11</b>  | < ± 5%       |
| 2PGA → PEP                | 19.62               | 17.96        | 5.57%        | 1.27                | <b>1.11</b>  | < ± 5%       |
| F6P ↔ G6P                 | -0.52               | <b>-0.92</b> | < ± 5%       | 18.36               | <b>49.26</b> | < ± 5%       |
| 3PGA ↔ BPGA               | 42.17               | <b>41.08</b> | < ± 5%       | 83.76               | <b>84.74</b> | < ± 5%       |
| BPGA ↔ GAP                | 42.17               | <b>41.08</b> | < ± 5%       | 83.76               | <b>84.74</b> | < ± 5%       |
| GAP ↔ DHAP                | 16.69               | <b>17.07</b> | < ± 5%       | 39.78               | <b>38.68</b> | < ± 5%       |
| F6P + GAP ↔ E4P + Xu5P    | 8.95                | <b>9.36</b>  | < ± 5%       | 11.04               | <b>10.52</b> | < ± 5%       |
| DHAP + E4P ↔ SBP          | 16.01               | <b>9.14</b>  | < ± 5%       | 0.00                | <b>11.12</b> | < ± 5%       |
| SBP ↔ S7P                 | 16.01               | <b>9.14</b>  | < ± 5%       | 6.98                | <b>11.12</b> | < ± 5%       |
| S7P + GAP ↔ Ri5P + Xu5P   | 8.26                | <b>9.14</b>  | < ± 5%       | 6.98                | <b>11.12</b> | < ± 5%       |
| Ri5P ↔ Ru5P               | 7.57                | 8.59         | < ± 5%       | 6.76                | <b>10.39</b> | -5.27%       |
| Xu5P ↔ Ru5P               | 17.04               | <b>17.06</b> | < ± 5%       | 11.04               | <b>19.71</b> | -5.80%       |
| Ru5P → RuBP               | 31.15               | <b>30.31</b> | < ± 5%       | 42.77               | <b>44.93</b> | < ± 5%       |
| F6P/Xu5P → E4P/GAP + AceP | NA                  | 1.46         | < ± 5%       | 3.06                | <b>2.55</b>  | 16.94%       |

Reaction catalyzed by EDA is in underlined. Simulated fluxes (WT and  $\Delta$ eda) correspond to day 5 for mixotrophic and day 7 for autotrophic growth experiments (<sup>13</sup>C exp), respectively, for each particular end of experiments (Makowka et al., 2020). The bold font highlight the simulated values within the experimental lower and upper bounds, for mixotrophic (Nakajima et al., 2014) and autotrophic (Hing et al., 2019) conditions. We note that flux values presented in Figure 2 and this table vary to some degree because they represent two independent and alternative calculations (two best fits). Units of metabolic fluxes: 10<sup>-2</sup> mmol h<sup>-1</sup> gDW<sup>-1</sup>.



accumulation of KDPG produced by EDD under  $\Delta$ eda. The flux via ED-P under AC-auto (WT) is less than 2% of flux via glyceraldehyde-3-phosphate dehydrogenase (GAP in Figure 1 and Table 4). Hence, the slow accumulation of KDPG, although

enhanced by glycogen, may take several days to activate at least a partial biochemical inhibition of EDD. Also, KDPG has been reported to be bacteriostatic at higher concentrations in *E.coli* (Fuhrman et al., 1998), thus *Synechocystis* may need a

mechanism to prevent or limit its accumulation, possibly by excreting KDPG (Fuhrman et al., 1998). This prediction could explain the peak in growth impairment at day 4 (Figure 3B, scenario 3) caused by additional loss of carbon due to KDPG excretion, along with decarboxylation. Lastly, we can speculate that reaching the final level of reported growth impairment (day 7) takes up to 2 days due to continuous metabolic adaptation in response to changes in intracellular concentration of KDPG and enhanced decarboxylation via OPP-P.

In the case of mixotrophic conditions, none of the mechanisms within the model or from the tested scenarios could explain the temporal component – carbon loss due to decarboxylation and possible KDPG excretion under  $\Delta eda$ ; these mechanisms do not have a significant impact on growth rate due to abundance of carbon, in contrast to AC-auto. Therefore, we propose that the substantial difference between the growth rate of WT and  $\Delta eda$  (Figure 3A) under AC-mix should be seen as a simple growth delay since the temporal component diminishes by the fifth day of the experiment (Makowka et al., 2020) where both samples growth autotrophically due to depleted glucose. A possible explanation for delayed growth could be the suppressed carbon catabolite repression mechanism (Deutscher, 2008), responsible for rapid sensing and utilization of organic carbon, which is under normal circumstances (WT) controlled by the metabolic level of KDPG. Thus, too low (temporal product-inhibition of EDD) or too high (bacteriostatic) levels of KDPG caused by  $\Delta eda$  is slowing down the utilization of organic carbon in *Synechocystis*, explaining the temporal component of growth impairment under AC-mix. The role of KDPG in carbon catabolite repression was reported in other organisms (Kim et al., 2009; Campilongo et al., 2017). However, such role of KDPG in cyanobacteria needs to be experimentally verified.

There is another possibility or rather a speculation on how to explain the temporal component under mixotrophic conditions and that is the other functionality of EDA, so far not analyzed in *Synechocystis*. Based on the current annotation (although experimental verification is still needed), EDA should catalyze the interconversion of 4-hydroxy-2-oxoglutarate and pyruvate from glyoxylate (KEGG), see Figure 1 (red). On the other hand, either glyoxylate or 4-hydroxy-2-oxoglutarate (+ L-erythro-4-hydroxyglutamate) could be converted into 2-oxoglutarate. 2-oxoglutarate is known to have a signaling role in glucose metabolism in both prokaryotes (Daniel and Danchin, 1986) and eukaryotes (Dang et al., 2009) and is also a signaling molecule regulating the activity of TCA cycle in *Synechocystis* (Orthwein et al., 2021). Although the impact of  $\Delta eda$  on the metabolism of 2-oxoglutarate is unknown, it regulates the glucose uptake (Doucette et al., 2011) and has a very significant impact on surrounding compounds such as proline in *Synechocystis* (Lucius et al., 2021). In order to explain the buildup of proline, we propose a pathway, fully annotated for *Synechocystis* (Uniprot), from proline to pyruvate

and glyoxylate, producing two molecules of NADPH (Figure 1, red) which supports previously speculated link among proline, NADPH and  $\Delta eda$  (Lucius et al., 2021). Furthermore, our assumptions related to  $\Delta eda$  leading to bacteriostasis linked to an accumulation of KDPG might be alternatively explained by an accumulation of 2-oxoglutarate which was reported to reduce the growth rate in *E. coli* (Bren et al., 2016). We did not simulate any of these options as we currently do not have experimental data needed and thus, such simulations would not be reliable.

Finally, a new labeling experiment has been published recently. This study (Schulze et al., 2022) compared WT and  $\Delta eda$ , however, the authors could not detect any flux via ED-P. The possible explanations are: i) a minor flux via ED-P, as suggested in our own flux estimation, ii) significant flux under certain conditions, such as fluctuating light (Schulze et al., 2022), which may explain previously reported significant level of KDPG (Chen et al., 2016), otherwise undetectable (Will et al., 2019; Schulze et al., 2022); we note that 10% fluctuations in light (i.e., ATP and NADPH regeneration in the model) did not influence our flux estimations (data not shown) for  $\Delta eda$ , or iii) ED-P is missing in *Synechocystis*. Furthermore,  $\Delta eda$  was reported to deactivate OPP shunt (Schulze et al., 2022), which disagrees with our model prediction purely based on the metabolic flux via ED-P. Thus,  $\Delta eda$  mediated deactivation of OPP could support either of the presented hypotheses, i.e., role of KDPG in carbon catabolite repression or the other role of EDA in the proximity of TCA cycle might play a role in regulating OPP as neither of these scenarios are in the model. The complexity of the whole problem makes it very difficult to understand, from the multifunctionality of EDA, uncertainty related to *ilvD* functionality as EDD and KDPG metabolism, the unclear identity of metabolite(s) behind the temporal component of growth impairment under both discussed conditions, to metabolic plasticity of the central carbon metabolism of *Synechocystis*. Therefore, a thorough experimental and theoretical analysis is required to shed more light on the depths of *Synechocystis* metabolism.

## Data availability statement

The original contributions presented in the study are included in the article/Supplementary material, further inquiries can be directed to the corresponding author. The list of names, IDs and UniProt links of specific genes or enzymes mentioned or analysed in our work, is summarized in Supplementary file 7 (Table 3).

## Author contributions

JJ and AB jointly discussed ideas and concepts and wrote the manuscript. JJ was done modeling. AB was done bioinformatic

analysis. Both authors contributed to the article and approved the submitted version.

claim that may be made by its manufacturer, is not guaranteed or endorsed by the publisher.

## Funding

This study was financially supported by the Ministry of Education, Youth and Sports of the Czech Republic – project CENAKVA (LM2018099), by the European Regional Development Fund in the frame of the project ImageHeadstart (ATCZ215) in the Interreg V-A Austria-Czech Republic programme, and University of South Bohemia - project GAJU 066/2021/Z.

## Conflict of interest

The authors declare that the research was conducted in the absence of any commercial or financial relationships that could be construed as a potential conflict of interest.

## Publisher's note

All claims expressed in this article are solely those of the authors and do not necessarily represent those of their affiliated organizations, or those of the publisher, the editors and the reviewers. Any product that may be evaluated in this article, or

## Supplementary material

The Supplementary Material for this article can be found online at: <https://www.frontiersin.org/articles/10.3389/fmicb.2022.967545/full#supplementary-material>

### SUPPLEMENTARY FILE 1 (TABLE 1)

Occurrence of marker enzymes among cyanobacteria.

### SUPPLEMENTARY FILE 2 (TABLE 2)

List of kinetic parameters employed in the simulations. Data for autotrophic and mixotrophic conditions.

### SUPPLEMENTARY FILE 3 (DATA SHEET 1)

Pair wise sequence alignment of annotated EDD isoenzymes (UNIPROT) of *Calothrix desertica*. Tool used: EMBOSS Matcher.

### SUPPLEMENTARY FILE 4 (DATA SHEET 2)

Amino acid sequences for native EDD (6-phosphogluconate dehydratase) found among cyanobacteria.

### SUPPLEMENTARY FILE 5 (DATA SHEET 3)

Kinetic model of central carbon metabolism of *Synechocystis* sp. PCC 6803 under autotrophic conditions. Model description can be found in the section "General information about the model".

### SUPPLEMENTARY FILE 6 (DATA SHEET 4)

Kinetic model of central carbon metabolism of *Synechocystis* sp. PCC 6803 under mixotrophic conditions. Model description can be found in the section "General information about the model".

### SUPPLEMENTARY FILE 7 (TABLE 3)

List of names, IDs and UniProt links of specific genes or enzymes mentioned or analysed in our work.

## References

- Asplund-Samuelsson, J., and Hudson, E. P. (2021). Wide range of metabolic adaptations to the acquisition of the Calvin cycle revealed by comparison of microbial genomes. *PLoS Comput. Biol.* 17:e1008742. doi: 10.1371/journal.pcbi.1008742
- Bachhar, A., and Jablonsky, J. (2020). A new insight into role of phosphoketolase pathway in *Synechocystis* sp. PCC 6803. *Sci. Rep.* 10:22018. doi: 10.1038/s41598-020-78475-z
- Bren, A., Park, J. O., Towbin, B. D., Dekel, E., Rabinowitz, J. D., and Alon, U. (2016). Glucose becomes one of the worst carbon sources for *E. coli* on poor nitrogen sources due to suboptimal levels of cAMP. *Sci. Rep.* 6:24834. doi: 10.1038/srep24834
- Campilongo, R., Fung, R., Little, R., Grenga, L., Trampari, E., Pepe, S., et al. (2017). One ligand, two regulators and three binding sites: How KDPG controls primary carbon metabolism in *Pseudomonas*. *PLoS Genet.* 13:e1006839. doi: 10.1371/journal.pgen.1006839
- Chen, X., Schreiber, K., Appel, J., Makowka, A., Fährnich, B., Roettger, M., et al. (2016). The Entner-Doudoroff pathway is an overlooked glycolytic route in cyanobacteria and plants. *Proc. Natl. Acad. Sci. U.S.A.* 113, 5441–5446. doi: 10.1073/pnas.1521916113
- Daddaoua, A., Krell, T., and Ramos, J.-L. (2009). Regulation of glucose metabolism in *Pseudomonas*: The phosphorylative branch and Entner-Doudoroff enzymes are regulated by a repressor containing a sugar isomerase domain\*. *J. Biol. Chem.* 284, 21360–21368. doi: 10.1074/jbc.M109.014555
- Dang, L., White, D. W., Gross, S., Bennett, B. D., Bittinger, M. A., Driggers, E. M., et al. (2009). Cancer-associated IDH1 mutations produce 2-hydroxyglutarate. *Nature* 462, 739–744. doi: 10.1038/nature08617
- Daniel, J., and Danchin, A. (1986). 2-Ketoglutarate as a possible regulatory metabolite involved in cyclic AMP-dependent catabolite repression in *Escherichia coli* K12. *Biochimie* 68, 303–310. doi: 10.1016/s0300-9084(86)80027-x
- Deutscher, J. (2008). The mechanisms of carbon catabolite repression in bacteria. *Curr. Opin. Microbiol.* 11, 87–93. doi: 10.1016/j.mib.2008.02.007
- Doello, S., Klotz, A., Makowka, A., Gutekunst, K., and Forchhammer, K. (2018). A specific glycogen mobilization strategy enables rapid awakening of dormant cyanobacteria from chlorosis. *Plant Physiol.* 177, 594–603. doi: 10.1104/pp.18.00297
- Doucette, C. D., Schwab, D. J., Wingreen, N. S., and Rabinowitz, J. D. (2011).  $\alpha$ -ketoglutarate coordinates carbon and nitrogen utilization via enzyme I inhibition. *Nat. Chem. Biol.* 7, 894–901. doi: 10.1038/nchembio.685
- Engene, N., Rottacker, E. C., Kaštvský, J., Byrum, T., Choi, H., Ellisman, M. H., et al. (2012). *Moorea producens* gen. nov., sp. nov. and *Moorea bouillonii* comb. nov., tropical marine cyanobacteria rich in bioactive secondary metabolites. *Int. J. Syst. Evol. Microbiol.* 62, 1171–1178. doi: 10.1099/ijs.0.033761-0
- Figueiredo, A. S., Kouril, T., Esser, D., Haferkamp, P., Wieloch, P., Schomburg, D., et al. (2017). Systems biology of the modified branched Entner-Doudoroff pathway in *Sulfolobus solfataricus*. *PLoS One* 12:e0180331. doi: 10.1371/journal.pone.0180331
- Flamholz, A., Noor, E., Bar-Even, A., Liebermeister, W., and Milo, R. (2013). Glycolytic strategy as a tradeoff between energy yield and protein cost. *Proc. Natl. Acad. Sci. U.S.A.* 110, 10059–10044. doi: 10.1073/pnas.1215283110
- Fuhrman, L. K., Wanken, A., Nickerson, K. W., and Conway, T. (1998). Rapid accumulation of intracellular 2-keto-3-deoxy-6-phosphogluconate in an

- Entner-Doudoroff aldolase mutant results in bacteriostasis. *FEMS Microbiol. Lett.* 159, 261–266. doi: 10.1111/j.1574-6968.1998.tb12870.x
- Hing, N. Y. K., Liang, F., Lindblad, P., and Morgan, J. A. (2019). Combining isotopically non-stationary metabolic flux analysis with proteomics to unravel the regulation of the Calvin-Benson-Bassham cycle in *Synechocystis* sp. PCC 6803. *Metab. Eng.* 56, 77–84. doi: 10.1016/j.ymben.2019.08.014
- Jablonsky, J., Papacek, S., and Hagemann, M. (2016). Different strategies of metabolic regulation in cyanobacteria: From transcriptional to biochemical control. *Sci. Rep.* 6:33024. doi: 10.1038/srep33024
- Kim, J., Yeom, J., Jeon, C. O., and Park, W. (2009). Intracellular 2-keto-3-deoxy-6-phosphogluconate is the signal for carbon catabolite repression of phenylacetic acid metabolism in *Pseudomonas putida* KT2440. *Microbiology* 155, 2420–2428. doi: 10.1099/mic.0.027060-0
- Kim, S., and Lee, S. B. (2006). Catalytic promiscuity in dihydroxy-acid dehydratase from the thermoacidophilic archaeon *Sulfolobus solfataricus*. *J. Biochem.* 139, 591–596. doi: 10.1093/jb/mvj057
- Kopp, D., Bergquist, P. L., and Sunna, A. (2020). Enzymology of alternative carbohydrate catabolic pathways. *Catalysts* 10:1231. doi: 10.3390/catal10111231
- Leyval, D., Uy, D., Delaunay, S., Goergen, J. L., and Engasser, J. M. (2003). Characterisation of the enzyme activities involved in the valine biosynthetic pathway in a valine-producing strain of *Corynebacterium glutamicum*. *J. Biotechnol.* 104, 241–252. doi: 10.1016/S0168-1656(03)00162-7
- Linington, R. G., Edwards, D. J., Shuman, C. F., McPhail, K. L., Matainaho, T., and Gerwick, W. H. (2008). Symplocamide A, a potent cytotoxin and chymotrypsin inhibitor from the marine cyanobacterium *Symploca* sp. *J. Nat. Prod.* 71, 22–27. doi: 10.1021/np070280x
- Lucius, S., Makowka, A., Michl, K., Gutekunst, K., and Hagemann, M. (2021). The Entner-Doudoroff pathway contributes to glycogen breakdown during high to low CO<sub>2</sub> Shifts in the cyanobacterium *Synechocystis* sp. PCC 6803. *Front. Plant Sci.* 12:787943. doi: 10.3389/fpls.2021.787943
- Makowka, A., Nichelmann, L., Schulze, D., Spengler, K., Wittmann, C., Forchhammer, K., et al. (2020). Glycolytic shunts replenish the Calvin-Benson-Bassham cycle as anaplerotic reactions in cyanobacteria. *Mol. Plant* 13, 471–482. doi: 10.1016/j.molp.2020.02.002
- Nakajima, T., Kajihata, S., Yoshikawa, K., Matsuda, F., Furusawa, C., Hirasawa, T., et al. (2014). Integrated metabolic flux and omics analysis of *Synechocystis* sp. PCC 6803 under mixotrophic and photoheterotrophic conditions. *Plant Cell Physiol.* 55, 1605–1612. doi: 10.1093/pcpp/pcu091
- Orthwein, T., Scholl, J., Spaet, P., Lucius, S., Koch, M., Macek, B., et al. (2021). The novel P-II-interactor PiC identifies phosphoglycerate mutase as key control point of carbon storage metabolism in cyanobacteria. *Proc. Natl. Acad. Sci. U.S.A.* 118:e2019988118. doi: 10.1073/pnas.2019988118
- Pimentel, J. S. M., and Giani, A. (2014). Microcystin production and regulation under nutrient stress conditions in toxic microcystin strains. *Appl. Environ. Microbiol.* 80, 5836–5843. doi: 10.1128/AEM.01009-14
- Richhardt, J., Bringer, S., and Bott, M. (2012). Mutational analysis of the pentose phosphate and Entner-Doudoroff pathways in *Gluconobacter oxydans* reveals improved growth of a  $\Delta$ edd  $\Delta$ eda mutant on mannitol. *Appl. Environ. Microbiol.* 78, 6975–6986. doi: 10.1128/AEM.01166-12
- Schulze, D., Kohlstedt, M., Becker, J., Cahoreau, E., Peyriga, L., Makowka, A., et al. (2022). GC/MS-based <sup>13</sup>C metabolic flux analysis resolves the parallel and cyclic photomixotrophic metabolism of *Synechocystis* sp. PCC 6803 and selected deletion mutants including the Entner-Doudoroff and phosphoketolase pathways. *Microb. Cell Fact.* 21:69. doi: 10.1186/s12934-022-01790-9
- Will, S. E., Henke, P., Boedeker, C., Huang, S., Brinkmann, H., Rohde, M., et al. (2019). Day and night: Metabolic profiles and evolutionary relationships of six axenic non-marine cyanobacteria. *Genome Biol. Evol.* 11, 270–294. doi: 10.1093/gbe/evy275
- Xiong, W., Cano, M., Wang, B., Douchi, D., and Yu, J. (2017). The plasticity of cyanobacterial carbon metabolism. *Curr. Opin. Chem. Biol.* 41, 12–19. doi: 10.1016/j.cbpa.2017.09.004
- Xiong, W., Lee, T.-C., Rommelfanger, S., Gjersing, E., Cano, M., Maness, P.-C., et al. (2015). Phosphoketolase pathway contributes to carbon metabolism in cyanobacteria. *Nat. Plants* 2:15187. doi: 10.1038/nplants.2015.187
- Yoshikawa, K., Hirasawa, T., Ogawa, K., Hidaka, Y., Nakajima, T., Furusawa, C., et al. (2013). Integrated transcriptomic and metabolomic analysis of the central metabolism of *Synechocystis* sp. PCC 6803 under different trophic conditions. *Biotechnol. J.* 8, 571–580. doi: 10.1002/biot.201200235
- Zhang, P., MacTavish, B. S., Yang, G., Chen, M., Roh, J., Newsome, K. R., et al. (2020). Cyanobacterial dihydroxy-acid dehydratases are a promising growth inhibition target. *ACS Chem. Biol.* 15, 2281–2288. doi: 10.1021/acscchembio.0c00507

## **CHAPTER 4**

**GENERAL DISCUSSION**

**ENGLISH SUMMARY**

**CZECH SUMMARY**

**ACKNOWLEDGEMENTS**

**LIST OF PUBLICATIONS**

**TRAINING AND SUPERVISION PLAN DURING THE STUDY**

***CURRICULUM VITAE***



---

## 4.1. General discussion

---

There are various modelling approaches used in biochemistry, but the most common ones are: agent-based modelling, cellular automata, structural modelling, stoichiometric modelling and kinetic modelling. If our knowledge about the system is good enough, i.e., opposite to “black box”, and the goal is to describe the dynamics of the system, the standard approach is to choose either the kinetic or stoichiometric modelling. For the purpose of studying isozymes, we chose kinetic modelling as the stoichiometric model cannot distinguish the metabolic flux via different isoforms. Kinetic models developed for describing biochemical pathways, are based on chosen kinetics, most common ones are mass action law or Michaelis-Menten, but even general methods such as power law kinetics (Vera, et al., 2007) are also used. If it is not sure which kinetics is suitable for a given system, there are certain guidelines. For instance, according to Cleland classification (Cleland, 1963), enzymatic reactions could be distinguished in four degrees: 1) simple one with a minimum number of parameters (usually mass action law), e.g., for description of basic reactions such as isomerization or dehydration; we use this approach also for more complex reactions in the cases of unavailability of suitable experimental data; 2) more complex reactions with regulatory mechanisms, e.g., post-translational modifications, but without allosteric properties, common approach employed here is Michaelis-Menten kinetics, 3) allosteric regulation and role of effectors – typically used for enzymes with subunits (oligomeric structure), where the dynamics of the reaction is following sigmoidal pattern and thus Michaelis-Menten kinetics should be replaced by other concepts, e.g., by Monod-Wyman-Changeux equation (Monod, et al., 1965), 4) enzymatic reaction catalysed by enzyme occurring in different states, e.g., pH dependency, requiring multiple equations.

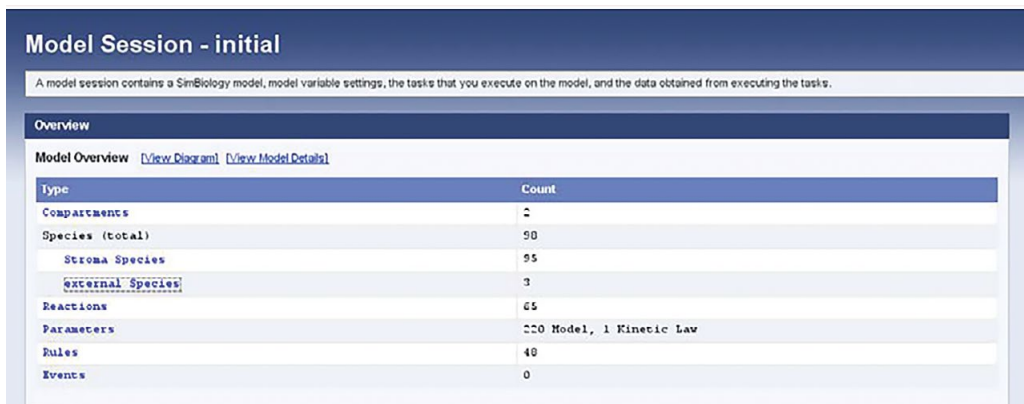
In addition, all kinetic models employ kinetic parameters, which could be obtained experimentally, usually from *in vitro* experiments, or could be estimated based on multi-omics data. However, despite the simple or complex description of the system, the final model is always a simplification of the real system, neglecting some or many features. Common issues with kinetic models in biochemistry are neglected pathways, assumed constant levels of certain metabolites, overlooked compartments, dependencies of parameters on physical properties (pH, temperature, ...), synthesis/degradation of enzymes, level(s) of regulation (signalling pathways, allosteric regulation, ...) and many more.

If we know all these issues, the question arises why don't we make a “perfect” kinetic model, considering everything known according to the state of art. The reasons are usually two: 1) lack of experimental data for all system parameters due to labour and financial constraints and 2) considering all features of the studied system would dramatically increase the number of parameters needed in the model, which might decrease the accuracy and timely manner of providing the results. Thus, we must make a compromise and accept some simplifications and make speculations, which should have only minimal impact on the phenomenon we are studying.

Since my target organism is model cyanobacterium *Synechocystis* PCC 6803, I will briefly discuss its features relevant for model integration. *Synechocystis* is presumed to have all four known glycolytic pathways exist in nature: Embden-Meyerhof-Parnas pathway (EMP-P), oxidative pentose phosphate pathway (OPP-P), phosphoketolase pathway (PKET-P) and Entner-Doudoroff pathway (ED-P). The efficient enzyme regulation found within the central carbon metabolism of *Synechocystis* provides it with rapid adaptation capabilities, which helps to survive under most growth conditions. Since the whole genome sequencing of *Synechocystis* (Kaneko et al., 1996), multiple enzymes and isoenzymes have been predicted with complex functionalities. It is already established that isoenzymes provide significant

protection against environmental stress. However, the extent of enzyme functions and their regulatory roles are yet to be fully understood. Recent studies showed that *Synechocystis* can survive without any significant growth loss if both phosphofructokinase isoenzymes are silenced (Makowka et al., 2020). Even silencing a whole glycolytic pathway, e.g. lower EMP/ED pathway, does not affect the growth behaviour of *Synechocystis* significantly (Chen et al., 2016; Makowka et al., 2020). The aims of the current study are to predict i) the specific roles of isoenzymes under different conditions, ii) the possible connection between glycolytic pathway regulation in the presence of different carbon sources (organic vs inorganic).

The initial step of isozyme analysis is to identify the distribution of enzyme/isozyme among the genera, followed by checking if the enzyme sequence is thoroughly conserved or possesses significant heterogeneity among species to species of cyanobacteria. The raw data sets are downloaded from Uniprot (<https://www.uniprot.org>), KEGG (<https://www.genome.jp/kegg/>) and NCBI (<https://www.ncbi.nlm.nih.gov/>). If the status of a potential enzyme is confirmed, the omics data is acquired either from different research articles as well as from different databases ex. For amino acid and enzyme activities confirmation: BRENDA enzyme database (<https://www.brenda-enzymes.org/>), Uniprot, NCBI, for gene expression data: original research articles and Cyanoexpress (<http://cyanoexpress.sysbiolab.eu/>) databases are referred. The curated data is later incorporated into the simbiology model (Fig. 4.1.) for further analysis.



| Type             | Count                    |
|------------------|--------------------------|
| Compartments     | 2                        |
| Species (total)  | 90                       |
| Stroma Species   | 95                       |
| External Species | 3                        |
| Reactions        | 65                       |
| Parameters       | 220 Model, 1 Kinetic Law |
| Rules            | 40                       |
| Events           | 0                        |

**Figure 4.1.** Components of the model in the Simbiology toolbox under the Matlab platform for simulations. Stroma species consist of metabolites. External species: source of external carbon (ex.  $CO_2$ , glucose/fructose).

However, the options of UI on Simbiology does not allow complex analyses, such as covering various growth conditions or single/double enzyme mutants in silico experiments In order to predict the mechanism(s) that is providing the observed protection against growth loss in *Synechocystis*, it was necessary to write scripts in programming language of Matlab; an example is shown on Fig 4.2.



```

%% MUTANTS
if cc==2 % %ED-P off

    X = sbioselect(model, 'Name', 'V_EDglyc'); set (X, 'Value', 0);
    X = sbioselect(model, 'Name', 'V_Sink_G6P');
    Y = get (X, 'Value'); set (X, 'Value', Y*1.05);
end

if cc==3 %ED-P off    + GND PTM test
    X = sbioselect(model, 'Name', 'V_EDglyc'); set (X, 'Value', 0);
    X = sbioselect(model, 'Name', 'V_Sink_G6P');
    Y = get (X, 'Value'); set (X, 'Value', Y*1.05);
    X = sbioselect(model, 'Name', 'V_PPP2');
    Y = get (X, 'Value'); set (X, 'Value', Y*2);
end

if cc==4 %GND (OPP2) off
    X = sbioselect(model, 'Name', 'V_PPP2'); set (X, 'Value', 0);
    X = sbioselect(model, 'Name', 'V_PPP1');
    Y = get (X, 'Value'); set (X, 'Value', Y*0.1);
    X = sbioselect(model, 'Name', 'V_EDglyc');
    Y = get (X, 'Value'); set (X, 'Value', Y*0.01);
    X = sbioselect(model, 'Name', 'V_Sink_Ri5P');
    Y = get (X, 'Value'); set (X, 'Value', Y*0.11);
    X = sbioselect(model, 'Name', 'V_Sink_G6P');
    Y = get (X, 'Value'); set (X, 'Value', Y*0.035);
end

```

**Figure 4.2.** An example of code employed for the simulations analysing the isozymes functionalities in Simbiology, Matlab. This part of code shows the inner portion of FOR loop cycle running on index *cc*. This index decides which mutant is currently run in the simulation, i.e., if *cc* = 1, only the wild-type simulation is executed, if *cc* = 1 and 2, the wild-type and mutant 1 (deactivated Entner-Doudoroff pathway) scenarios are simulated. That way, we can compare the results of wild type and various mutations altogether.

---

#### 4.2. General information about the model

---

The scope of the model of *Synechocystis* includes the following parts of central carbon metabolism: Calvin-Benson-Bassham cycle, photorespiration, all glycolytic pathways (Embden-Meyerhof-Parnas pathway, Entner-Doudoroff pathway, phosphoketolase pathway and oxidative pentose phosphate pathway) with simplified carbohydrate and biomass synthesis (weighted sum of sink reactions). These metabolic reactions were coupled with simplified light reactions, inorganic carbon (Ci) and glucose uptake as the primary input parameters. The current model consists of 60 reactions, 49 metabolites and 199 kinetic parameters. The enzymatic reactions were described by Michaelis-Menten kinetics with an exception for the light reactions, Ci and glucose uptake (mass action kinetics). The list of all parameters within the model for autotrophic conditions is shown on Table 4.1. and the list of initial concentrations is shown on Table 4.2.

**Table 4.1.** List of kinetic parameters employed for model of central carbon metabolism for *Synechocystis* PCC 6803 under autotrophic conditions. The parameters were fitted on fluxomics data from (Hing et al., 2019). The full extent of data could be found in Bachhar and Jablonsky (2020). (Abbreviations: 3PGA – 3-phosphoglycerate, BPGA – bisphosphoglycerate, GAP – glyceraldehyde 3-phosphate, DHAP – dihydroxyacetone phosphate, E4P – erythrose 4-phosphate, Xu5P – xylulose 5-phosphate, Ri5P – ribose 5-phosphate, Ru5P – ribulose 5-phosphate, RuBP – ribulose bisphosphate, G6P – glucose 6-phosphate, F6P – fructose 6-phosphate, FBP – fructose 1,6-bisphosphate, S7P- sedoheptulose 7-phosphate, SBP – sedoheptulose-1,7-bisphosphate, Pi – inorganic phosphate, 2PG – 2-phosphoglycolate, GCA – glycolate, GOA – glyoxylate, GLY – glycine, SER – serine, HPR – hydroxypyruvate, 2PGA – 2-phosphoglycerate, PEP – phosphoenolpyruvate, KDPG – 2-keto3-deoxygluconate-6-phosphate. M – Mol · liter<sup>-1</sup>; kf – reaction rate constant; V – maximum velocity, KM – Michaelis-Menten constant; KE – equilibrium constant; KI – inhibition constant)

\*(Rest of the parameters with K as initials are Michaelis-Menten constant)

| reaction (mass action law kinetics)      | k <sub>f</sub> HC-auto | k <sub>f</sub> AC-auto | units                      |
|--|------------------------|------------------------|----------------------------|
| ADP + Pi → ATP                           | 0.16                   | 0.25                   | s <sup>-1</sup>            |
| NADPp → NADPH                            | 0.58                   | 0.21                   | s <sup>-1</sup>            |
| extCO <sub>2</sub> → CO <sub>2</sub>     | 1.9                    | 0.141                  | s <sup>-1</sup>            |
| reaction (Michaelis-Menten kinetics)     | Parameter name         | Parameter value        | units                      |
| RuBP + CO <sub>2</sub> → 2*3PGA          | V1                     | 0.952                  | mM · s <sup>-1</sup>       |
| RuBisCO                                  | KM12                   | 0.22                   | mM                         |
|  | KI11                   | 0.84                   | mM                         |
|  | KI14                   | 0.9                    | mM                         |
|  | KM13                   | 0.02                   | mM                         |
|  | KM11                   | 0.0115                 | mM                         |
|  | KI13                   | 0.075                  | mM                         |
|  | KI15                   | 0.07                   | mM                         |
|  | KI12                   | 0.04                   | mM                         |
| <b>3PGA + ATP → BPGA + ADP</b>           | <b>V2</b>              | <b>1.724</b>           | <b>mM · s<sup>-1</sup></b> |
| phosphoglycerate kinase                  | KM2_BPGA               | 0.107                  | mM                         |
|  | KE2                    | 0.00616                | □                          |
|  | KM2_ATP                | 1.99                   | mM                         |
|  | KM2_PGA                | 1.21                   | mM                         |
|  | KM2_ADP                | 0.24                   | mM                         |
| <b>BPGA + NADPH ↔ GAP + NADPp + Pi</b>   | <b>V3</b>              | <b>0.423</b>           | <b>mM · s<sup>-1</sup></b> |
| glyceraldehyde 3-phosphate dehydrogenase | KM32                   | 0.1                    | mM                         |
|  | KM31                   | 0.004                  | mM                         |
| <b>GAP ↔ DHAP</b>                        | <b>V4</b>              | <b>0.0784</b>          | <b>mM · s<sup>-1</sup></b> |
| triose phosphate isomerase               | KE4                    | 0.598                  | □                          |
|  | KM4_GAP                | 0.37                   | mM                         |
|  | KM4_DHAP               | 0.76                   | mM                         |
| <b>GAP + DHAP ↔ FBP</b>                  | <b>V5</b>              | <b>2.69</b>            | <b>mM · s<sup>-1</sup></b> |
| aldolase 1                               | KE5                    | 3.58                   | □                          |
|  | KM5_8_DHAP             | 0.12                   | mM                         |
|  | KM5_8_E4P              | 0.57                   | mM                         |
|  | KM5_8_GAP              | 1.79                   | mM                         |

|                                  |             |              |                            |
|----------------------------------|-------------|--------------|----------------------------|
|                                  | KM5_8_SBP   | 2.03         | mM                         |
|                                  | KM5_8_FBP   | 1.38         | mM                         |
| <b>GAP + DHAP ↔ FBP</b>          | <b>V5b</b>  | <b>1.62</b>  | <b>mM · s<sup>-1</sup></b> |
| aldolase 2                       | KM5_8b_SBP  | 1.73         | mM                         |
|                                  | KM5_8b_GAP  | 2.37         | mM                         |
|                                  | KM5_8b_FBP  | 1.77         | mM                         |
|                                  | KM5_8b_E4P  | 0.158        | mM                         |
|                                  | KM5_8b_DHAP | 0.64         | mM                         |
|                                  | KE5         | 3.58         | □                          |
| <b>FBP → F6P + Pi</b>            | <b>V6</b>   | <b>1.72</b>  | <b>mM · s<sup>-1</sup></b> |
| fructose-1,6-bisphosphatase      | KM61        | 7.82         | mM                         |
|                                  | KI61        | 0.7          | mM                         |
|                                  | KI62        | 12           | mM                         |
| <b>F6P + GAP ↔ E4P + Xu5P</b>    | <b>V7</b>   | <b>1.75</b>  | <b>mM · s<sup>-1</sup></b> |
| transketolase                    | KE7         | 0.509        | □                          |
|                                  | KM7_10_Ri5P | 0.53         | mM                         |
|                                  | KM7_10_S7P  | 2            | mM                         |
|                                  | KM7_10_F6P  | 1.23         | mM                         |
|                                  | KM7_10_E4P  | 1.36         | mM                         |
|                                  | KM7_10_GAP  | 1.05         | mM                         |
|                                  | KM7_10_Xu5P | 0.068        | mM                         |
| <b>DHAP + E4P ↔ SBP</b>          | <b>V8</b>   | <b>2.36</b>  | <b>mM · s<sup>-1</sup></b> |
| aldolase 1                       | KE8         | 1.75         | □                          |
|                                  | KM5_8_DHAP  | 0.12         | mM                         |
|                                  | KM5_8_E4P   | 0.57         | mM                         |
|                                  | KM5_8_GAP   | 1.79         | mM                         |
|                                  | KM5_8_SBP   | 2.03         | mM                         |
|                                  | KM5_8_FBP   | 1.38         | mM                         |
| <b>DHAP + E4P ↔ SBP</b>          | <b>V8b</b>  | <b>0.972</b> | <b>mM · s<sup>-1</sup></b> |
| aldolase 2                       | KM5_8b_SBP  | 1.73         | mM                         |
|                                  | KM5_8b_GAP  | 2.37         | mM                         |
|                                  | KM5_8b_FBP  | 1.77         | mM                         |
|                                  | KM5_8b_E4P  | 0.158        | mM                         |
|                                  | KM5_8b_DHAP | 0.64         | mM                         |
|                                  | KE8         | 1.75         | □                          |
| <b>SBP → S7P + Pi</b>            | <b>V9</b>   | <b>1.81</b>  | <b>mM · s<sup>-1</sup></b> |
| sedoheptulose-1,7 bisphosphatase | KM9_FBP     | 1.71         | mM                         |
|                                  | KM9_SBP     | 0.11         | mM                         |
| <b>S7P + GAP ↔ Ri5P + Xu5P</b>   | <b>V10</b>  | <b>0.55</b>  | <b>mM · s<sup>-1</sup></b> |
| transketolase                    | KE10        | 0.576        | □                          |
|                                  | KM7_10_Ri5P | 0.53         | mM                         |
|                                  | KM7_10_S7P  | 2            | mM                         |
|                                  | KM7_10_F6P  | 1.23         | mM                         |
|                                  | KM7_10_E4P  | 1.36         | mM                         |
|                                  | KM7_10_GAP  | 1.05         | mM                         |
|                                  | KM7_10_Xu5P | 0.068        | mM                         |

|  |                     |               |                            |
|--|---------------------|---------------|----------------------------|
| <b>Ri5P ↔ Ru5P</b>                       | <b>V11</b>          | <b>0.96</b>   | <b>mM · s<sup>-1</sup></b> |
| phosphopentose isomerase                 | KE11                | 2.4           | □                          |
|  | KM11_Ri5P           | 0.1           | mM                         |
|  | KM11_Ru5P           | 1.1           | mM                         |
| <b>Xu5P ↔ Ru5P</b>                       | <b>V12</b>          | <b>0.469</b>  | <b>mM · s<sup>-1</sup></b> |
| phosphopentose epimerase                 | KE12                | 0.477         | □                          |
|  | KM12_Ru5P           | 0.439         | mM                         |
|  | KM12_Xu5P           | 0.6           | mM                         |
| <b>Ru5P + ATP → RuBP + ADP</b>           | <b>V13</b>          | <b>0.425</b>  | <b>mM · s<sup>-1</sup></b> |
| phosphoribulokinase                      | KM132               | 0.05          | mM                         |
|  | KM131               | 0.05          | mM                         |
|  | KI135               | 0.4           | mM                         |
|  | KI134               | 2.5           | mM                         |
|  | KI133               | 4             | mM                         |
|  | KI132               | 0.7           | mM                         |
|  | KI131               | 2             | mM                         |
| <b>F6P → FBP</b>                         | <b>V_PFK</b>        | <b>1.91</b>   | <b>mM · s<sup>-1</sup></b> |
| phosphofructokinase 1                    | KM_F6P_PFK          | 11.84         | mM                         |
|  | KM_ATP_PFK          | 15.87         | mM                         |
| <b>F6P → FBP</b>                         | <b>V_PFK_beta</b>   | <b>0.196</b>  | <b>mM · s<sup>-1</sup></b> |
| phosphofructokinase 2                    | KM_ATP_PFK_beta     | 9.38          | mM                         |
|  | KM_F6P_PFK_beta     | 6.43          | mM                         |
| <b>GAP + NADPp + Pi ↔ BPGA + NADPH</b>   | <b>Vgap_dehyd</b>   | <b>1.077</b>  | <b>mM · s<sup>-1</sup></b> |
| glyceraldehyde 3-phosphate dehydrogenase | Kpga                | 0.357         | mM                         |
|  | Knadpp              | 2             | mM                         |
|  | Knadph              | 0.927         | mM                         |
|  | Kgap                | 1             | mM                         |
| <b>3PGA ↔ 2PGA</b>                       | <b>Vf_PGM_alpha</b> | <b>0.268</b>  | <b>mM · s<sup>-1</sup></b> |
| phosphoglycerate mutase 1                | Kms_PGM_alpha       | 0.189         | mM                         |
|  | Kmp_PGM_alpha       | 0.74          | mM                         |
|  | Keq_PGM             | 0.71          | □                          |
| <b>3PGA ↔ 2PGA</b>                       | <b>Vf_PGM_beta</b>  | <b>0.55</b>   | <b>mM · s<sup>-1</sup></b> |
| phosphoglycerate mutase 2                | Kms_PGM_beta        | 0.277         | mM                         |
|  | Kmp_PGM_beta        | 0.05          | mM                         |
|  | Keq_PGM             | 0.71          | □                          |
| <b>3PGA ↔ 2PGA</b>                       | <b>Vf_PGM_gama</b>  | <b>0.0115</b> | <b>mM · s<sup>-1</sup></b> |
| phosphoglycerate mutase 3                | Kms_PGM_gama        | 2.58          | mM                         |
|  | Kmp_PGM_gama        | 0.6           | mM                         |
|  | Keq_PGM             | 0.71          | □                          |
| <b>2PGA ↔ PEP</b>                        | <b>Vf_enol</b>      | <b>0.826</b>  | <b>mM · s<sup>-1</sup></b> |
| enolase                                  | Keq_enol            | 0.866         | □                          |
|  | Kms_enol            | 0.525         | mM                         |
|  | Kmp_enol            | 0.279         | mM                         |

|  |                      |                 |                            |
|--|----------------------|-----------------|----------------------------|
| <b>RuBP + O<sub>2</sub> → 2PG + 3PGA</b> | <b>V_PP1</b>         | <b>0.048</b>    | <b>mM · s<sup>-1</sup></b> |
| RuBisCO                                  | KM12                 | 0.22            | mM                         |
|  | KI11                 | 0.84            | mM                         |
|  | KI14                 | 0.9             | mM                         |
|  | KM13                 | 0.02            | mM                         |
|  | KM11                 | 0.0115          | mM                         |
|  | KI13                 | 0.075           | mM                         |
|  | KI15                 | 0.07            | mM                         |
|  | KI12                 | 0.04            | mM                         |
| <b>2PG → GCA</b>                         | <b>V_PP2a</b>        | <b>0.000588</b> | <b>mM · s<sup>-1</sup></b> |
| phosphoglycolate phosphatase 1           | Km112a               | 3               | mM                         |
|  | KI1122               | 2.55            | mM                         |
|  | KI1121               | 94              | mM                         |
| <b>2PG → GCA</b>                         | <b>V_PP2b</b>        | <b>0.00039</b>  | <b>mM · s<sup>-1</sup></b> |
| phosphoglycolate phosphatase 2           | Km112b               | 0.1             | mM                         |
|  | KI1122               | 2.55            | mM                         |
|  | KI1121               | 94              | mM                         |
| <b>2PG → GCA</b>                         | <b>V_PP2c</b>        | <b>0.001</b>    | <b>mM · s<sup>-1</sup></b> |
| phosphoglycolate phosphatase 3           | Km112c               | 0.5             | mM                         |
|  | KI1122               | 2.55            | mM                         |
|  | KI1121               | 94              | mM                         |
| <b>GCA → GOA</b>                         | <b>V_PP3</b>         | <b>0.0042</b>   | <b>mM · s<sup>-1</sup></b> |
| glycolate oxidase                        | Km121                | 0.1             | mM                         |
| <b>GOA + SER ↔ HPR + GLY</b>             | <b>V_PP4</b>         | <b>0.18</b>     | <b>mM · s<sup>-1</sup></b> |
| serineglyoxylate transaminase            | KI124                | 2               | mM                         |
|  | Km1242               | 1.7             | mM                         |
|  | KE124                | 607             | □                          |
|  | Km1241               | 0.15            | mM                         |
| <b>2*GLY → SER</b>                       | <b>V_PP5</b>         | <b>0.002</b>    | <b>mM · s<sup>-1</sup></b> |
| serine hydroxymethyltransferase          | K1 (local parameter) | 6               | mM                         |
| <b>HPR → GCEA</b>                        | <b>V_PP6</b>         | <b>0.004</b>    | <b>mM · s<sup>-1</sup></b> |
| hydroxypyruvate reductase                | KI123                | 12              | mM                         |
|  | KE123                | 250000          | □                          |
|  | Km1231               | 0.09            | mM                         |
| <b>GCEA + ATP → 2PGA + ADP</b>           | <b>V_PP7</b>         | <b>0.013</b>    | <b>mM · s<sup>-1</sup></b> |
| glycerate kinase                         | KI113                | 0.36            | mM                         |
|  | Km1131               | 0.21            | mM                         |
|  | Km1132               | 0.25            | mM                         |
|  | KE113                | 300             | □                          |
| <b>GOA → OXA</b>                         | <b>V_OXA1</b>        | <b>0.096</b>    | <b>mM · s<sup>-1</sup></b> |
| glyoxylate oxidase                       | K_OXA1               | 2               | mM                         |
| <b>GOA → TSA</b>                         | <b>V_TSA1</b>        | <b>0.01</b>     | <b>mM · s<sup>-1</sup></b> |
| tartronate semialdehyde synthase         | K_TSA1               | 0.1             | mM                         |
| <b>TSA → GCEA</b>                        | <b>V_TSA3</b>        | <b>0.1</b>      | <b>mM · s<sup>-1</sup></b> |
| tartronate semialdehyde reductase        | K_TSA3               | 0.1             | mM                         |

|   |                    |                 |                            |
|---|--------------------|-----------------|----------------------------|
| <b>3PGA → SER</b>                         | <b>V_synth_SER</b> | <b>0.00024</b>  | <b>mM · s<sup>-1</sup></b> |
| simplified phosphoserine transaminase     | K_synth_SER        | 2               | mM                         |
| <b>GOA ↔ GLY</b>                          | <b>V_GLY_syn</b>   | <b>0.1</b>      | <b>mM · s<sup>-1</sup></b> |
| glycine transaminase                      | K_GOA              | 0.1             | mM                         |
| <b>F6P ↔ G6P</b>                          | <b>V_SS1</b>       | <b>0.62</b>     | <b>mM · s<sup>-1</sup></b> |
| glucose-6-phosphate isomerase             | KE_SS1             | 3               | □                          |
|   | KM_F6P_SS1         | 1               | mM                         |
|   | KM_G6P_SS1         | 1               | mM                         |
| <b>G6P → P6G</b>                          | <b>V_PP1</b>       | <b>0.54</b>     | <b>mM · s<sup>-1</sup></b> |
| glucose-6-phosphate dehydrogenase         | Kmp_PP1            | 0.1             | mM                         |
|   | Kms_PP1            | 2               | mM                         |
| <b>P6G + NADPp → Ru5P + NADPH</b>         | <b>V_PP2</b>       | <b>0.3</b>      | <b>mM · s<sup>-1</sup></b> |
| phosphogluconate dehydrogenase            | Kms_p6g_ppp2       | 1.2             | mM                         |
|   | Kms_nadpp_ppp2     | 1               | mM                         |
| <b>F6P → E4P + AceP</b>                   | <b>V_PKET1a</b>    | <b>0.875</b>    | <b>mM · s<sup>-1</sup></b> |
| phosphoketolase 1                         | KM_PKET1a_Xu5P     | 1.25            | mM                         |
|   | KM_PKET1a_GAP      | 0.0011          | mM                         |
|   | KM_PKET1a_F6P      | 0.195           | mM                         |
|   | KM_PKET1a_E4P      | 0.7             | mM                         |
|   | KM_PKET1a_AceP     | 1.76            | mM                         |
|   | Keq_PKETa          | 0.289           | □                          |
| <b>Xu5P → GAP + AceP</b>                  | <b>V_PKET1b</b>    | <b>0.034</b>    | <b>mM · s<sup>-1</sup></b> |
| phosphoketolase 2                         | KM_PKET1b_E4P      | 0.97            | mM                         |
|   | KM_PKET1b_F6P      | 0.073           | mM                         |
|   | KM_PKET1b_GAP      | 0.126           | mM                         |
|   | KM_PKET1b_Xu5P     | 0.315           | mM                         |
|   | KM_PKET1b_AceP     | 0.674           | mM                         |
|   | Keq_PKETb          | 0.47            | □                          |
| <b>F6P → E4P + AceP</b>                   | <b>V_PKET2a</b>    | <b>0.000069</b> | <b>mM · s<sup>-1</sup></b> |
| phosphoketolase 1                         | KM_PKET2a_Xu5P     | 0.66            | mM                         |
|   | KM_PKET2a_GAP      | 1.21            | mM                         |
|   | KM_PKET2a_F6P      | 0.21            | mM                         |
|   | KM_PKET2a_E4P      | 0.56            | mM                         |
|   | KM_PKET2a_AceP     | 0.347           | mM                         |
|   | Keq_PKETa          | 0.289           | □                          |
| <b>Xu5P → GAP + AceP</b>                  | <b>V_PKET2b</b>    | <b>0.00535</b>  | <b>mM · s<sup>-1</sup></b> |
| phosphoketolase 2                         | KM_PKET2b_Xu5P     | 0.79            | mM                         |
|   | KM_PKET2b_GAP      | 0.051           | mM                         |
|   | KM_PKET2b_F6P      | 0.71            | mM                         |
|   | KM_PKET2b_E4P      | 0.0014          | mM                         |
|   | KM_PKET2b_AceP     | 0.7             | mM                         |
|   | Keq_PKETb          | 0.47            | □                          |
| <b>P6G → KDPG</b>                         | <b>V_edd</b>       | <b>0.0059</b>   | <b>mM · s<sup>-1</sup></b> |
| 6-phosphogluconate dehydratase            | Km_edd_P6G         | 1               | mM                         |
|   | KI_KDPG            | 1.5             | mM                         |
| <b>KDPG ↔ GAP + PYR</b>                   | <b>V_eda</b>       | <b>0.1</b>      | <b>mM · s<sup>-1</sup></b> |
| keto3-deoxygluconate-6-phosphate aldolase | Km_eda_KDPG        | 1               | mM                         |

The metabolic model was constrained in several steps. The original model of *Synechocystis* (Jablonsky et al., 2016) was without PKET pathway and ED-P. After verification of incorporation of these two pathways, the model was fitted based on available fluxomic data from cells grown autotrophically at high CO<sub>2</sub>. Then, transcriptomic data was applied as weight factors for each estimated Vmax. The model was simulated to shift from high CO<sub>2</sub> to ambient CO<sub>2</sub> autotrophic, followed by ambient CO<sub>2</sub> mixotrophic conditions. The goal is to identify a single set of kinetic parameters which could explain/fit all the growth conditions. However, the current set of parameters can only describe autotrophic growth conditions (ambient and high CO<sub>2</sub>). For verification of data from mixotrophic growth conditions, fluxomic data for mixotrophy were used.

**Table 4.2.** Initial concentrations of the metabolites within the model of *Synechocystis* for high CO<sub>2</sub> autotrophic conditions. 3PGA – 3-phosphoglycerate, BPGA – bisphosphoglycerate, GAP – glyceraldehyde 3-phosphate, DHAP – dihydroxyacetone phosphate, E4P – erythrose 4-phosphate, Xu5P – xylulose 5-phosphate, Ri5P – ribose 5-phosphate, Ru5P – ribulose 5-phosphate, RuBP – ribulose biphosphate, G6P – glucose 6-phosphate, F6P – fructose 6-phosphate, FBP – fructose 1,6-biphosphate, S7P – sedoheptulose 7-phosphate, SBP – sedoheptulose-1,7-biphosphate, Pi – inorganic phosphate, 2PG – 2-phosphoglycolate, GCA – glycolate, GOA – glyoxylate, GLY – glycine, SER – serine, HPR – hydroxypyruvate, 2PGA – 2-phosphoglycerate, PEP – phosphoenolpyruvate, KDPG – 2-keto-3-deoxygluconate-6-phosphate. (M: Mol/liter)

| Initial concentration |       | Initial concentration |       |
|-----------------------|-------|-----------------------|-------|
|                       | mM    |                       | mM    |
| 3PGA                  | 2.310 | Pi (constant)         | 5.000 |
| BPGA                  | 0.003 | 2PG                   | 0.640 |
| GAP                   | 0.930 | GCA                   | 0.019 |
| DHAP                  | 0.108 | GOA                   | 0.004 |
| E4P                   | 0.026 | GLY                   | 0.830 |
| Xu5P                  | 0.160 | SER                   | 0.360 |
| Ri5P                  | 0.022 | HPR                   | 0.003 |
| Ru5P                  | 0.046 | 2PGA                  | 1.530 |
| RuBP                  | 0.033 | PEP                   | 1.260 |
| G6P                   | 0.102 | KDPG                  | 0.000 |
| F6P                   | 0.130 | NADPH                 | 0.196 |
| FBP                   | 0.320 | NADP+                 | 0.220 |
| S7P                   | 0.840 | ADP                   | 0.270 |
| SBP                   | 0.001 | ATP                   | 1.150 |

A significant benefit of using a biochemical/kinetic model-based approach is its prediction power which extends from identifying a potential inhibitory metabolic regulation (Bachhar and Jablonsky, 2020) to calculating extreme low flux (Bachhar and Jablonsky, 2022) via a metabolic pathway that cannot be calculated with fluxomic-based experiments (Schulze et al., 2022) or even to create and analyse different growth scenarios which is difficult to achieve with experiments. However, due to the unavailability of preliminary multi-omics data for all enzymes, the kinetic model-based approaches are sometimes found to be difficult to create. Thus, an integrated experiment-model based approach could easily overcome these issues and should be a future standard.

---

### 4.3. Conclusion

---

My doctoral research program has given me an opportunity to study the metabolic profiles and regulations within the model cyanobacterium *Synechocystis* PCC 6803 from various perspectives and growth conditions. I have analysed all four known glycolytic pathways in *Synechocystis*, namely the flux redistribution for glycolytic mutants as well as for wild type under changing environment. In particular, I have focused on neglected phosphoketolase glycolytic pathway and role of isoenzymes within (Bachhar and Jablonsky, 2020). The flux via PKET-P could be above 250% of the flux via EMP glycolysis under autotrophic ambient CO<sub>2</sub> conditions, we predicted that role of PKET-P under other growth conditions is rather negligible. In the case of PKET 1, we estimated 17% flux reduction via RuBisCO for  $\Delta pket1$  under ambient CO<sub>2</sub> autotrophic conditions. In addition, we have provided data supporting the existence of putative PKET 2 isozyme and simulated 11.2–14.3% growth decrease for  $\Delta pket2$  in turbulent environment.

Finally, the major impact of my work on research of cyanobacteria are our conclusions related to the Entner-Doudoroff pathway, its regulation and enzymatic multi functionalities (Bachhar and Jablonsky, 2022). These results have a potential to reshape our understanding about ED-P and role of its enzyme in *Synechocystis*. The current bioinformatic analysis indicated a significant rarity of ED-P distribution among cyanobacteria. We also provided a possible explanation behind significant impact of ED-P mutants of *Synechocystis*, estimated the flux via ED-P, and analysed the impact of single and double-pathway glycolytic mutants and their impact on metabolic plasticity in *Synechocystis*.

The current issue with the experimental studies is to be able (time, money, data reproducibility, man-power...) to create a set of data that considers all the metabolic interactions and enzyme multi-functionalities, followed by processing the datasets generated from these experiments. With the aid of the biochemical kinetic model, these issues could be partially answered in form of faster data integrations and predictions for analysed scenarios. However, the main constraint with model-based studies is the availability of data that could be incorporated into the model. This issue of data could be fixed by designing the preliminary experiments based on the model data requirement. It could be hoped that with future experiment-model-based integrated studies, the issues with both model and experiments could be significantly minimized.



## Reference

- Bachhar, A., Jablonsky, J. 2020. A new insight into role of phosphoketolase pathway in *Synechocystis* sp. PCC 6803. *Sci. Rep.* 10, 22018.
- Bachhar, A., Jablonsky, J. 2022. Entner-Doudoroff pathway in *Synechocystis* PCC 6803: Proposed regulatory roles and enzyme multifunctionalities. *Front. Microbiol.* 13,967545.
- Chen, X., Schreiber, K., Appel, J., Makowka, A., Fähnrich, B., Roettger, M., et al., 2016. The Entner-Doudoroff pathway is an overlooked glycolytic route in cyanobacteria and plants. *Proc. Natl. Acad. Sci. U.S.A.* 113, 5441–5446.
- Cleland, W., 1963. The kinetics of enzyme-catalyzed reactions with two or more substrates and products. I. Nomenclature and rate equations. *Biochim. Biophys. Acta*, 67, 104–137.
- Hing, Yu King N., Liang, F., Lindblad, P., Morgan, 2019. Combining isotopically non-stationary metabolic flux analysis with proteomics to unravel the regulation of the Calvin-Benson-Bassham cycle in *Synechocystis* sp. PCC 6803. *Metabol. Engineerin*, 56, 77–84.
- Jablonsky, J., Papacek, S., Hagemann, M., 2016. Different strategies of metabolic regulation in cyanobacteria: From transcriptional to biochemical control. *Sci. Rep.* 6, 33024.
- Kaneko, T., Sato, S., Kotani, H., Tanaka, A., Asamizu, E., Nakamura, Y., Miyajima, N., Hirose, M., Sugiura, M., Sasamoto S., et al., 1996. Sequence analysis of the genome of the unicellular cyanobacterium *Synechocystis* sp. strain PCC6803. II. Sequence Determination of the Entire Genome and Assignment of Potential Protein-coding Regions. *DNA Res.*3, 109–136.
- Makowka, A., Nichelmann, L., Schulze, D., Spengler, K., Wittmann, C., Forchhammer, K., et al., 2020. Glycolytic shunts replenish the Calvin-Benson-Bassham cycle as anaplerotic reactions in cyanobacteria. *Mol. Plant* 13, 471–482.
- Monod, J., Wyman, J., Changeux, J., 1965. On the nature of allosteric transitions: a plausible model. *J. Mol. Biol.* 12, 88–118.
- Schulze, D., Kohlstedt, M., Becker, J., Cahoreau, E., Peyriga, L., Makowka, A., et al. 2022. GC/MS-based <sup>13</sup>C metabolic flux analysis resolves the parallel and cyclic photomixotrophic metabolism of *Synechocystis* sp. PCC 6803 and selected deletion mutants including the Entner-Doudoroff and phosphoketolase pathways. *Microb. Cell Fact.* 21, 69.
- Vera, J., Balsa-Canto, E., Wellstead, P., Banga, J.R., Wolkenhauer, O., 2007. Power-law models of signal transduction pathways. *Cell. Signal.* 19, 1531–1541. <https://doi.org/10.1016/j.cellsig.2007.01.029>

## English summary

## Role of isoenzymes in metabolic regulation of cyanobacteria

Anushree Bachhar

Model cyanobacterium *Synechocystis* PCC 6803 is one of the most studied species of cyanobacteria, having a significant impact in biotechnology, which explains why it is also known as “green *E. coli*”. Experimental studies could provide *in vitro* characterization of isozymes but cannot provide accurate information about a particular isozyme despite the single/multiple mutant studies. The reasons behind this issues are: i) single knock-out is likely to be compensated by remaining isozyme(s), ii) deactivation of all isozymes does not count for unknown multi functionalities or redirection towards alternative pathways and metabolic plasticity of *Synechocystis*. I aimed to decipher some of the regulatory mechanisms within the metabolism of *Synechocystis* with the aid of kinetic model, integrating fluxomic, metabolic and transcriptomic data from literature.

In the first half of my PhD research, I have focused on the impact of the mostly ignored glycolytic phosphoketolase pathway (PKET-P). In particular, we have shown that carbon flux via PKET-P could be above 250% of the flux via Embden-Meyerhof-Parnas glycolysis under autotrophic conditions ambient CO<sub>2</sub>, thus playing a crucial role by mitigating the decarboxylation, i.e., carbon loss, occurring in other glycolytic pathways. We predicted that role of PKET-P under other light conditions is rather negligible. In addition, we supported the existence of putative PKET 2 isozyme and quantified the following results under autotrophic conditions ambient CO<sub>2</sub>: 1) 17% flux reduction via RuBisCO for  $\Delta pket1$  and 2) 11.2–14.3% growth decrease for  $\Delta pket2$  in turbulent environment.

In the second half of my research work, I have focused on the recently confirmed glycolytic route in *Synechocystis*, the Entner-Doudoroff pathway (ED-P). ED-P was previously concluded to be a very common (~92%) pathway among cyanobacteria, but my bioinformatic analysis declassified its occurrence to be below 50% among cyanobacteria (as per current annotation). Interestingly, we have also identified plausible isozymes within ED-P for some cyanobacteria. In the case of *Synechocystis*, we provided the first estimation of flux via ED-P based on the growth impairment data which cannot be currently detected by 13C labelling experiments due to current detection limits of mass-spectrometry. Nevertheless, we have identified too many uncertainties (enzyme multifunctionalities and identity issues) that it become difficult to annotate or predict the extent of possible metabolic and regulatory functions of ED-P in *Synechocystis*.

Currently, I am studying the roles of ribose phosphate isomerase isozymes in *Synechocystis*. Finally, we plan to extend the model towards TCA cycle followed by amino acid metabolism, but this work will be already outside of my doctoral research.

## Czech summary

## Úloha izoenzymů v regulaci metabolismu sinic

Anushree Bachhar

Modelová sinice *Synechocystis* PCC 6803 je jedním z nejstudovanějších druhů sinic, která má významný vliv na biotechnologie, což vysvětluje, proč je také známá jako „zelená *E. coli*“. Experimentální studie by mohly poskytnout in vitro charakterizaci isoenzymů, ale nemohou poskytnout přesné informace o konkrétním izoenzymu, a to navzdory studiím s jedním či více mutanty. Důvody, které stojí za těmito problémy, jsou: i) jediný „knock-out“ je pravděpodobně kompenzován zbývajícím izoenzymem (izoenzymy), ii) deaktivace všech izoenzymů nepočítá s neznámou multifunkčností nebo přesměrováním na alternativní dráhy a metabolickou plasticitou *Synechocystis*. Mým cílem bylo rozluštit některé regulační mechanismy v rámci metabolismu *Synechocystis* pomocí kinetického modelu, integrujícího fluxomické, metabolické a transkriptomické údaje z literatury.

V první polovině svého doktorského výzkumu jsem se zaměřila na vliv většinou opomíjené glykolytické fosfoketolázové dráhy (PKET-P). Zejména jsme ukázali, že tok uhlíku přes PKET-P může být vyšší než 250% toku přes Embden-Meyerhof-Parnasovu glykolýzu za autotrofních podmínek a běžné úrovně  $\text{CO}_2$ , a hrát tak klíčovou roli tím, že zmírňuje dekarboxylaci, tj. ztráty uhlíku, ke kterým dochází v ostatních glykolytických drahách. Předpověděli jsme, že role PKET-P za jiných světelných podmínek je spíše zanedbatelná. Kromě toho jsme podpořili existenci předpokládaného izoenzymu PKET 2 a kvantifikovali následující výsledky za autotrofních podmínek a běžné úrovně  $\text{CO}_2$ : 1) 17% snížení toku prostřednictvím RuBisCO pro  $\Delta pket1$  a 2) 11,2–14,3% snížení růstu pro  $\Delta pket2$  v turbulentním prostředí.

V druhé polovině své výzkumné práce jsem se zaměřila na nedávno potvrzenou glykolytickou dráhu u *Synechocystis*, Entner-Doudoroffovu dráhu (ED-P). ED-P byla dříve považována za velmi běžnou (~92%) dráhu mezi sinicemi, ale moje bioinformatická analýza deklasovala její výskyt mezi sinicemi na méně než 50% (podle současné anotace). Zajímavé je, že jsme také identifikovali pravděpodobné izoenzymy v rámci ED-P u některých sinic. V případě *Synechocystis* jsme poskytli první odhad toku prostřednictvím ED-P na základě údajů o snížení růstu, kterou v současné době nelze zjistit pomocí experimentů se značeným  $^{13}\text{C}$  kvůli detekčním limitům hmotnostní spektrometrie. Nicméně jsme zjistili příliš mnoho nejasností (multifunkčnost a otázky identity enzymů), takže je obtížné anotovat nebo předpovědět rozsah možných metabolických a regulačních funkcí ED-P v *Synechocystis*.

V současné době se zabývám studiem rolí izoenzymů ribózafosfát izomerázy v *Synechocystis*. V neposlední řadě plánujeme rozšíření modelu směrem k citrátovému cyklu s následným metabolismem aminokyselin, ale tato práce bude již mimo můj doktorský výzkum.

**Acknowledgement**

I would like to express my sincere gratitude to my supervisor Dr. Jiri Jablonsky for his guidance throughout the journey of my doctoral study as well as shaping my skills for a better understanding of science and research.

I would also like to thank the members of our Institute of Complex Systems, Nove Hradky for providing profound support throughout my study and stay.

Last but not least, I want to acknowledge the support I have received from family as well as my best friends Avra and Rai. Without their encouragement, I would have come to this point in my education and life.

I also appreciate the financial support from the following projects that funded the research discussed in this dissertation:

This study was financially supported by the Ministry of Education, Youth and Sports of the Czech Republic – project **CENAKVA** (LM2018099)

University of South Bohemia in České Budějovice – project **GAJU** (Cisar) 114/2022/Z

University of South Bohemia in České Budějovice – project **GAJU** (Anushree Bachhar) 066/2021/Z

## List of publications

### Peer-reviewed journals with IF

**Bachhar, A.,** Jablonsky, J., 2022. Entner-Doudoroff pathway in *Synechocystis* PCC 6803: Proposed regulatory roles and enzyme multifunctionalities. *Front. Microbiol.* 13: 967545. doi: 10.3389/fmicb.2022.967545. (IF 2021 = 6.064)

**Bachhar, A.,** Jablonsky, J., 2020. A new insight into role of phosphoketolase pathway in *Synechocystis* sp. PCC 6803. *Sci. Rep.* 10: 22018. doi: 10.1038/s41598-020-78475-z. (IF 2020 = 4.380)

### Peer-reviewed journals without IF

**Bachhar, A.,** Bhaskar, H., Pathrose, B., Shylaja, M.R., 2019. Resistance to acaricides in *Tetranychus truncatus* ehara on vegetables. *Ind. J. Entomol.* 81: 130–133. <http://dx.doi.org/10.5958/0974-8172.2019.00018.X>

### Training and supervision plan during the study

|  |                                    |                           |
|--|------------------------------------|---------------------------|
| <b>Name</b>  | Anushree Bachhar                   |                           |
| <b>Ph.D. research period</b>   | 1/05/2019–31/03/2023               |                           |
| <b>Department</b>  | Institute of Complex Systems, FFPW |                           |
| <b>Supervisor</b>  | Jiri Jablonsky, Ph.D.              |                           |
| <b>Ph.D. Courses</b>   |                                    | <b>Year</b>               |
| Applied hydrobiology   |                                    | 2019                      |
| Basics of scientific communication   |                                    | 2020                      |
| Ecology of still and running waters  |                                    | 2021                      |
| Toxicology focused on aquatic organisms  |                                    | 2021                      |
| Bioinformatics   |                                    | 2021                      |
| Cycles of elements in aquatic ecosystems and their catchments                                  |                                    | 2021                      |
| English language   |                                    | 2021                      |
| Omics methods and data analyses  |                                    | 2021                      |
| Czech language for foreigners A  |                                    | 2022                      |
| <b>Scientific seminars</b>   |                                    | <b>Year</b>               |
| Ph.D. seminar 1  |                                    | 2020                      |
| Ph.D. seminar 2  |                                    | 2021                      |
| Ph.D. seminar 3  |                                    | 2021                      |
| Ph.D. seminar 4  |                                    | 2022                      |
| <b>Research internship during my Ph.D.</b>   |                                    | <b>Time</b>               |
| University of Rostock, Department of Plant Physiology, Rostock Germany                         |                                    | 10.01.2022<br>–30.06.2022 |
| <b>International conferences</b>   |                                    | <b>Year</b>               |
| 22 <sup>nd</sup> EMBL PhD Symposium: The Roaring 20s: A New Decade for Life Sciences (virtual) |                                    | 2020                      |
| EMBL Symposium: Multiomics to Mechanisms: Challenges in Data Integration. (virtual)            |                                    | 2021                      |

## Curriculum vitae

### PERSONAL INFORMATION

**Name:** Anushree Bachhar  
**Born:** 23<sup>rd</sup> January, 1993, Kolkata, India  
**Nationality:** Indian  
**Languages:** English, Bengali, Hindi  
**Address:** Zamek 136, Nove Hrad, Czech Republic  
**E-mail:** shreea.bachhar@gmail.com  
**Telephone:** +420 777237921  
**Website:** <https://www.researchgate.net/profile/Anushree-Bachhar-2>



### EDUCATION

**2019–present** University of South Bohemia; Ph.D. (Protection of Aquatic Ecosystems)  
**2016–2018** Kerala Agricultural University; M.Sc. Ag. Plant Biotechnology  
**2012–2016** Banaras Hindu University; B.Sc. Agriculture

### AFFILIATION AND WORK EXPERIENCE

**2022** Research internship  
 University of Rostock, Department of Plant Physiology, Rostock Germany  
**2019–2023** Doctoral Researcher  
 University of South Bohemia in Ceske Budejovice, FFPW, Institute of complex systems, Czech Republic  
**2016–2018** Student  
 Kerala Agricultural University, Dept. of Biotechnology, CPBMB  
**2012–2016** Student  
 Banaras Hindu University, Institute of Agricultural Sciences (IAS, BHU)

### RESEARCH INTERESTS

Systems biology, Metabolic modeling, Biochemical modelling, stoichiometric modeling, bioinformatics, Genomics, Transcriptomics, Proteomics, Metabolomics, Single cell omics, Cell biology, Xenobiotics, Bacteria, Cyanobacteria, Enzyme technology, Isoenzymes, Photosynthesis, Metabolic regulation, Photosystem II, Chlorophyll fluorescence, Regulation of glycolysis in cancer

### METHODS

Metabolic modeling, Biochemical modelling, Kinetic modelling, DNA Isolation (Plant, Spider Mites) Enzyme Isolation, Enzyme Activity Analysis, PCR Amplification In-Silico Analysis of Sequences Bioinformatics, Western Blotting, Immunological Techniques, Microbiology, Cell culture, Plant Tissue Culture

**Awards:** Department of Plant Biotechnology Fellowship 2016 (Post Graduation)  
**Projects:** Xenobiotic and signalling role of 2-keto-3-deoxy-6-phosphogluconate on cyanobacteria (066/2021/Z)